Interfilament Interactions in the Cytoskeleton : Single Filament Measurements and Mechanical Consequences

by

Jagesh V. Shah

B. A. Sc. Computer Engineering (1992)
University of Waterloo

S. M. Electrical Engineering and Computer Science (1995)
Massachusetts Institute of Technology

Submitted to the Harvard-MIT Division of Health Sciences and Technology
in Partial Fulfillment of the Requirements for the Degree of
Doctor of Philosophy in Medical Engineering

at the

Massachusetts Institute of Technology

May 1999

Signature of Author .....
Harvard-MIT Division of Health Sciences and Technology
27th of May 1999

Certified by .....
Paul A. Janmey
Associate Professor of Medicine
Brigham and Women's Hospital
Harvard Medical School
Thesis Supervisor

Accepted by .....
Martha Gray
J. W. Kieckhefer Associate Professor of Electrical Engineering
Co-Director, Harvard-MIT Division of Health Sciences and Technology

INTERFILAMENT INTERACTIONS IN THE CYTOSKELETON :
Single Filament Measurements and Mechanical Consequences

by

JAGESH V. SHAH

Submitted to the Harvard-MIT Division of Health Sciences and Technology
on the 27th of May 1999 in Partial Fulfillment of the Requirements for the Degree of
Doctor of Philosophy in Medical Engineering

ABSTRACT

The eucaryotic cytoskeleton is composed of three major filament systems : actin filaments, microtubules and intermediate filaments, and is responsible for the mechanical properties of the cell, the intracellular transport network and the organization of the cytoplasm. Previous studies have focussed on the role of a single filament systems in isolation. In this thesis, the role of inter-filament system interactions in the cytoskeleton is investigated. Interfilament interactions are classified by the physical mechanism responsible - steric constraints, passive binding or active, force-generating sliding attachments. Steric constraints result from filaments being unable to pass through each other. Passive binding is provided by molecules that can bind two filaments together. Active interactions are provided by mechanoenzymes that bind two filaments together and transduce chemical energy into the mechanical translocation of one filament along the other. For each physical mechanism in vitro experimental evidence for a specific interfilament interaction is demonstrated and putative cellular roles are discussed.

The steric interactions between microtubules and actin filaments are explored through the direct visualization of microtubule diffusion, or reptation, in a network of actin filaments. The presence of the actin network results in a sigmoidal dependence of diffusion on filament length for the microtubule switching from low diffusivity to high diffusivity at ~15 μm . This sigmoidal dependence is not predicted by current polymer theories and the underlying mechanism remains to be defined. The pronounced effect of steric constraints on MT diffusivity implicates their role in the spatial organization of microtubules and actin filaments in the cell.

Passive crosslinking is demonstrated by the direct binding of a c-terminal peptide of a vimentin-type intermediate filament to actin filaments and was investigated by biochemical and light scattering techniques. The interaction between full-length vimentin and actin filaments, presumably mediated by the c-terminus in part, is demonstrated by unique material properties of a mixture of the filaments that are unlike either filament system alone. The composite material properties demonstrates the role of passive interfilament binding in cellular mechanics.

Active sliding attachments between neuronal intermediate filaments, or neurofilaments, and microtubules are shown to be mediated by kinesin and dynein microtubule motor proteins. Fluorescently labelled native neurofilaments are observed to translocate bidirectionally along purified microtubules. The motility is due to the dynein/dynactin motor complex and at least one kinesin-like protein. The bidirectional nature of the motility supports a hypothesis whereby the axonal transport of neurofilaments in neurons proceeds by fast bidirectional saltatory motions which result the observed net slow plus-ended velocity.

Steric constraints, passive binding and active crosslinking provide a set of physical principles by which to classify interfilament interactions both between and within filament systems in the cytoskeleton.

Thesis Supervisor : Paul A. Janmey

Title : Associate Professor of Medicine, Brigham and Women's Hospital, Harvard Medical School

Table of contents

List of figures

List of tables

Acknowledgements

I came to Paul's lab with no biology experience ... nothing ... nada ... never pipetted ... wouldn't know an actin filament from an ebola virus. My partial transformation from an electrical engineer to biophysicist/biochemist is really a testament not to my bumbling and fumbling about, but to those who always had the time and patience to explain a protocol or demonstrate an instrument or just talk science all afternoon - thanks to you all for your help and insight.

To Josef who was my babysitter when I arrived at the lab ... "don't you know not to let the kids play with drill presses" - thanks for your patience. To Jay who made the world simpler through his calm and patient demeanor and elegant experiments. To Phil where 'caveats abound', and who always reminded me, and correctly so, "that life's usually more complicated than you think". To Lisa, who taught me the black magic of immunoblots and neuroscience (just kidding about the blots). To Louise and Sarah, my poor bench-mates who saw the caffeine-induced euphoria, the sleep deprived mania and were the recipients of mountains of unsolicited advice - to them I owe some of my sanity. To Adarsh, who unfortunately is a Red Wings fan but at least likes hockey - thanks for making my last few months fun. To Gabriel, from whom a learned a great deal and none of it about science. To Walter, Toshi and Rocky - thanks for the advice, albeit many of your wise words were often wasted on a novice like me. To David, the undergraduate, who realized early on that automated meant that he did it instead of me. To Klaus and Jan, the theorists, who explained and repeatedly explained the most fundamental of principles without a second thought. To my committee members, Maha, Frank and Ken who had infinite patience with my irreverence. Although seemingly immutable, I did listen and I did learn - thank you for your guidance.

To Jean-François, well what does one say about the jolliest scientist you've ever met, he who can make neurofilaments, tend to his garden, turn his compost (actually I did that) and bottle wine (hey, I did that too !) all in one day - your visits here, although thoroughly exhausting, were some of the most exciting times I had as a grad student. Thanks for your inspiration, patience and long emails in which I can still find gems.

To Paul, who dared to take on a scientific infant and helped me develop by making mistakes (oh ... the desmin prep) sending me to France regularly (vive les houches !), generally running amuck in the lab and introducing me to single malt scotch (thank you reverend I'll have another !). I honestly cannot imagine having been better suited to anyone else as an advisor. Thanks for everything and let me know when the Fisheries University of Nova Scotia offer comes through. Few graduate students can say they were having so much fun they didn't want to leave - I'd certainly be one of them.

To those who supported me when I actually left the lab. To Dan, Ravi and Leon, roommates who never could understand why I worked long days but were always available for an extended hallway chat. To the Boston crew with whom much steam was blown off - thanks for taking me in all those many years ago. To those in T.O., my home no matter where I am, thanks for keeping in touch and having faith even when I was absent.

To my in-laws, thanks for the questions, the advice, the FOOD and the electronic virus updates, especially around thesis writing time, thanks for bringing me into your family. To my parents, the people who honestly made me what I am today and in the future - I know it was a long time ... thanks for hanging in. To my sister Nisha, who will always be chronologically younger but much wiser than I. And finally, to the one person who had to endure it all, the late nights at lab, the early mornings from the late nights ... the downs when the experiments failed and the ups when they temporarily worked. To my wife, Sangeeta, who I met the first day at MIT and who has changed my life ever since. Thanks for making it all worth it, thanks for making it fun.

Chapter 1

Background

Biological cells have evolved to perform many complex processes for an independent existence. Cells must generate energy, forage for nutrients, divide and resist environmental stressors. To carry out these processes, the cell has the ability to generate a tremendous variety of molecules. Historically, the study of these molecules has usually ascribed one function to each molecule. However, an increasing number of molecules have become associated with a variety of functions. This versatility of function is demonstrated by the proteins which make up the cellular skeleton, or cytoskeleton. The cytoskeleton is responsible for the mechanical properties of the cell, intracellular transport and spatial organization of the cytoplasm and internal organelles. These functions are carried out in eucaryotic cells through a network three filament systems : actin microfilaments, microtubules and intermediate filaments.

Actin microfilaments (f-actin) are linear, helical filaments formed of a 42 kilodalton (kDa) globular monomer unit (g-actin). F-actin is approximately 7 nm in diameter and is dynamic, having a fast-growing (barbed) end and a slow-growing (pointed) end (figure 1-1A). F-actin is found predominantly at the cortex of cells where it is crosslinked by actin-crosslinking proteins such as filamin-like proteins(39, 134, 141) and plays a major role in maintaining cell shape. In addition, f-actin is concentrated at the leading edge of motile cells where the polymerization of actin is the basis for protrusive activity. F-actin can also support an energy-dependent translocation along its contour mediated by the myosin family of motor proteins. Through the hydrolysis of adenosine triphosphate (ATP) myosin can move along actin filament from the pointed to the barbed end thereby forming part of the intracellular transport system(78, 100) and the cellular contraction apparatus.

Microtubules (MTs) are tubular structures formed from a heterodimeric α–β tubulin monomer unit (~100 kDa). The MT outer diameter is approximately 25 nm. Like f-actin, MTs are dynamic and have a fast growing (plus) end and a slow growing (minus) end (figure 1-1B). Microtubules are arranged radially in most non-dividing cells emanating from a perinuclear area designated the microtubule organizing centre (MTOC) and extending out toward the cell periphery. MTs, like f-actin, can support a energy-dependent translocation mediated by motor proteins such as kinesin and dynein. Members of the kinesin family primarily move towards the plus end of MTs, whereas dynein motors move towards the minus end. The radial array of MTs in interphase cells, in concert with MT motor proteins, form the intracellular network responsible for transport of materials. The MT array also forms the substrate for the spatial organization of intracellular organelles such as mitochondria, the golgi apparatus and the endoplasmic reticulum. The MT transport network

has become highly specialized in neurons where the microtubules form long polarized bundles which connect the cell body and synaptic region of the cell through the axon. Transport of vesicular cargoes and cytoskeletal elements proceeds along the axonal microtubules both away from and towards the cell body. In dividing cells, MTs and MT motors form a specialized structure called the mitotic spindle which is essential in arranging the chromosomes and distributing them to each of the daughter cells.

Intermediate filaments (IFs) form a family of structurally related proteins that are differentially expressed in various tissues. All cytoplasmic intermediate filaments form linear filaments of 10 nm diameter (figure 1-1C). IFs are dynamic, like microtubules and f-actin, but exchange monomer units from along the filament length, not only the ends. Intermediate filaments are assembled from anti-parallel dimeric subunits which have no polarity, thus IFs have no polarity(46). Each specialized tissue has a specific IF protein expressed, such as vimentin in mesenchymal and hematopoietic tissues, desmin in muscle tissue, neurofilaments in neural tissue and keratins in epithelial tissues. The distribution of IFs in each cell type is predominantly perinuclear and extends from the nuclear membrane to the plasma membrane. In neurons, neuronal IFs, or neurofilaments (NFs), form aligned bundles filling the interior of the axonal and dendritic compartments. IFs play an important role in the maintenance of cellular and tissue integrity, especially in cells and tissues which are exposed to mechanical stress(32). No motor molecule has been identified for IFs.

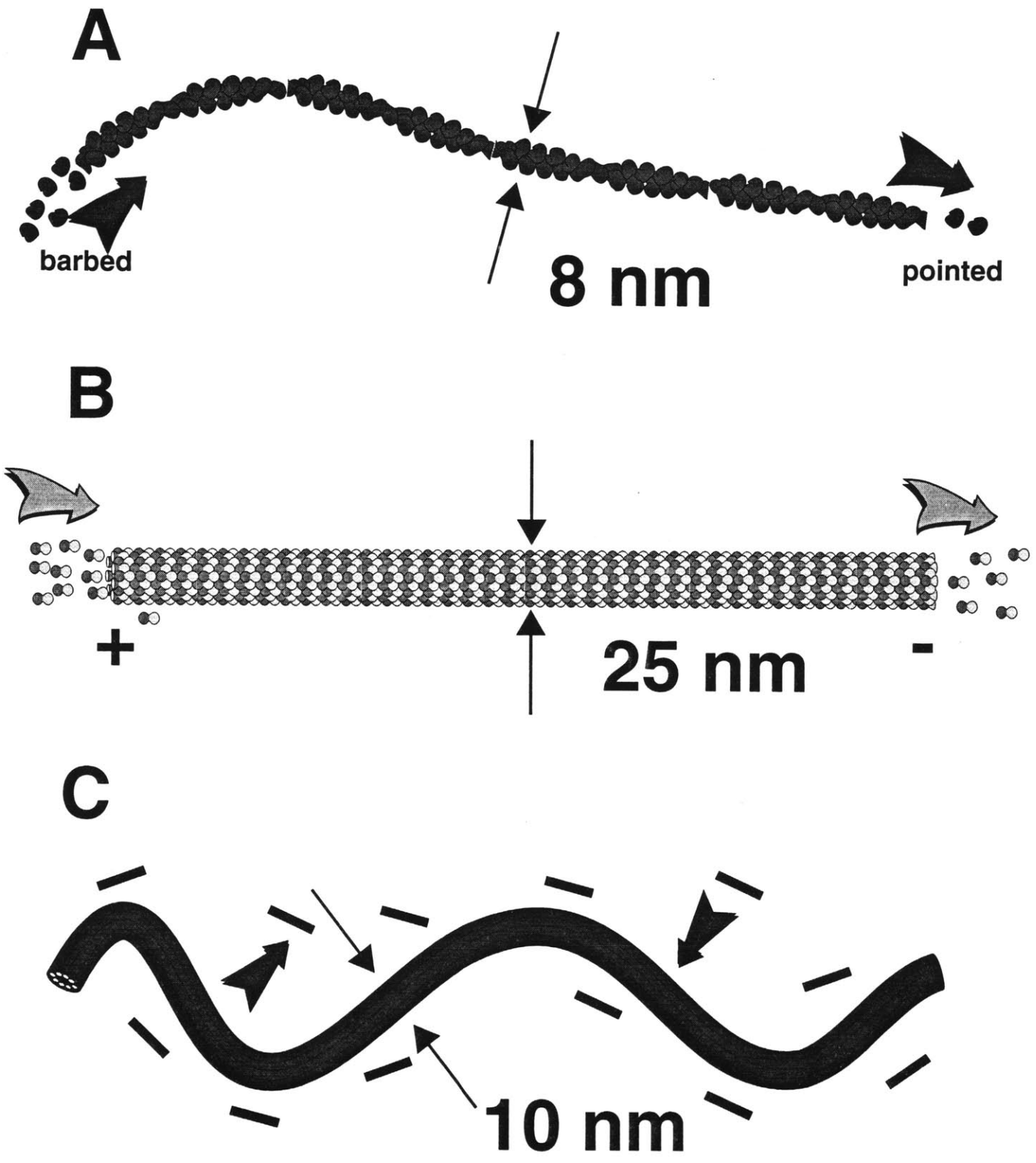

Figure 1-1 : **Filamentous constituents of the cytoskeleton.**
A, actin filament, **B**, microtubule, **C**, intermediate filament.

1.1 Understanding the role of each cytoskeletal filament system

The cytoskeletal filament systems have been studied extensively for their cellular roles in mechanics, transport and organization. Previous work, as described below, has studied the cytoskeletal systems individually. This thesis describes and demonstrates interactions between the filament systems which themselves give rise to new functions of the cytoskeleton.

1.1.1 Mechanics

To understand mechanics of the cytoskeletal elements in isolation, the monomeric constituents of the cytoskeleton have been purified(83, 135, 147, 150) and networks of a single filament type reconstituted in vitro. These in vitro networks are then subjected to a variety of mechanical deformations to determine the properties of the network.

The study of material deformation and flow is called rheology. Many rheological techniques have been utilized for the characterization of in vitro cytoskeletal networks : falling ball viscometry(92), osmometry(61) and dynamic shear deformation(67, 127). Janmey and colleagues have used dynamic oscillatory measurements to characterize the viscoelastic properties of all three cytoskeletal filaments in vitro(64).

Viscoelastic materials, such as cytoskeletal networks, have properties of both elastic solids and viscous liquids, that is they store and dissipate energy upon deformation. The relative contribution of viscous versus elastic responses defines the material properties. Models of viscoelastic behaviour are based on energy relaxation (or dissipation) modes(27). Each material has a characteristic energy relaxation spectrum which determines the energy dissipated at each time scale (including infinite which represents an elastic contribution). From the relaxation spectrum and the time profile of the mechanical deformation (strain), the internal tension (stress) generated within the material can be calculated. Strain is the non-dimensional change in shape imposed on the material and is measured in percent. Stress is a measure of the resistance to the imposed deformation and is measured in force per unit area.

For polymer networks, such as those in the cytoskeleton, the molecular nature of relaxation modes are a result of isolated polymer relaxation as seen in dilute solution or through diffusive, or reptative, modes in polymer networks. Through these relaxation modes the polymers assume a new conformation in the solution or network to dissipate the energy added by the deformation. The nature of energy storing, or elastic, mechanisms in polymer networks is well understood for synthetic networks(27, 28) , but is the subject of a number of recent investigations for cytoskeletal networks(59, 77, 91, 102, 126).

Rheological measurements probe the response of a material to an imposed stress or strain to identify the characteristic relaxation spectrum. For static measurements, i.e. where time dependent material behaviour is not taken into account, a sudden change in strain or stress is applied to the material and the resulting stress or strain, respectively, is measured. The resulting ratio of stress over strain is termed the modulus, G, if the strain is modified by a fixed rate, then the ratio of stress over strain rate is termed viscosity, η. For many viscoelastic materials the viscosity and modulus are strongly time dependent. To characterize rheological properties for these materials, dynamic measurements are required.

For dynamic measurements, an oscillatory strain or stress is imposed on the material and the resulting stress or strain is measured. The oscillatory nature of the measurement now results in two quantities, an amplitude and phase angle relative to the imposed perturbation. The result is a complex modulus which describes the ratio of the stress over the strain. The complex modulus, $G^* = G' + iG''$, has a real part which is termed the storage modulus, G', and an imaginary component, G", which is termed the loss modulus. The storage modulus represents the elasticity of the material, the in-phase component of the stress and the loss modulus represents the viscous dissipation of the material, the 90 degree out-of-phase component of the stress (i.e. the material response to the strain rate). The complex modulus is also parameterized by the frequency of the oscillation which explicitly introduces the time dependence of the material. The complex modulus parameterized by frequency is directly related to the relaxation spectrum and explicitly defines the elastic and viscous contributions of the material for oscillatory deformations.

Dynamic viscoelastic measurements can be made in a number of geometries. The sample can be deformed in extension, compression or shear. The dynamic measurements described in the work by Janmey and colleagues on single component cytoskeletal networks were performed in a shear geometry(64).

Oscillatory shear measurements of viscoelastic materials are made by placing the samples between two parallel plates separated by a known distance. One of the parallel plates is deformed by a small amplitude torsional deformation and the resistance to the deformation is characterized by free or forced oscillations. For free oscillatory measurements, one plate of the sample is held fixed while the other is momentarily displaced through a small angular deformation. Subsequent measurements of the free rotational trajectory of the deformed plate can be used to calculate the rheological parameters of the sample. For viscoelastic materials the angular position after the deformation takes the form of a damped oscillation. Intuitively, the oscillatory motion is due to the elasticity of the material and the damping is due to viscous losses in the sample. The combination of the frequency of oscillation and rate of damping can be related to the storage and loss moduli(27, 63, 139). Free oscillatory measurements are conducted using a torsion pendulum(63), a simple instrument which has been used for a variety of biological materials such

as fibrin clots (62), cytoskeletal networks(64, 85) and cell suspensions(24).

Forced oscillatory measurements apply a fixed sinusoidal stress or strain to one plate of the sample and measure the induced strain or stress, respectively, in the other plate. The stress and strain waveforms can be used directly to calculate the storage and loss moduli of the sample. Forced oscillatory measurements are primarily conducted using commercial rheometers and have been used for a variety of biological materials including cytoskeletal networks such as f-actin(65-67, 103) and IF gels(64, 85). Forced oscillatory instruments can measure moduli over a large range of deformation frequencies. Frequency dependent measurements are important understanding the molecular mechanisms of relaxation and elasticity(59, 77, 91, 102).

In addition to oscillatory measurements in which complex shear moduli are measured over a range of time scales, a number of other time dependent rheological measurements are useful in characterizing material properties. In a stress relaxation experiment a step strain is applied to a material and the resulting stress is measured over time. The initial imposition of strain results in relaxation of short time scale modes and a subsequent terminal behaviour, i.e. at long times, which represents the longest relaxation times, or elastic-like parameters, in the network. This is a useful test to determine the presence of crosslinking in polymer networks, since the presence of crosslinking eliminates polymers being unable to slide past each other and thereby diminishes the contribution of long time scale dissipative modes. The creep experiment is the dual of the stress relaxation in that a step stress, rather than a strain, is imposed on the material. The step stress elicits an instantaneous elastic response from the network which then flows. As a result, the creep experiment tends to measure viscous parameters at long experiment times. The creep experiment is useful in determining when a network has become more viscous either by a loss of crosslinking or by shortening of the polymers.

Another important rheological measurement is the dependence of viscoelastic properties on extent of deformation. Viscoelastic responses are usually measured in the linear regime of the material (< 5% strain). When the strain is increased the linear response is no longer preserved and new material properties can emerge. In particular, materials can stiffen rapidly with increasing strain, a property termed strain hardening. Many biomaterials such as cytoskeletal networks and extracellular matrices exhibit strain hardening. Strain hardening is not predicted to occur in synthetic flexible networks(27, 28), indicating a unique microscopic mechanism of elasticity at work in biomaterials which has yet to be understood.

Previous work has characterized the viscoelastic properties of pure cytoskeletal networks(64-67, 85). A comparison of the viscoelastic properties of each of the cytoskeletal network in a strain sweep experiment is given in figure 1-2. At small strains (the horizontal axis) f-actin networks have the largest elastic modulus (vertical axis) when compared to the other cytoskeletal elements

at equal weight fraction. As the extent of deformation is increased (horizontal axis), the f-actin network increases in its elastic modulus, exhibiting strain hardening, which persists until ~20% strain at which point the elastic modulus decreases unrecoverably indicating an irreversible change in network structure. Microtubule networks have a small storage modulus at small strains and exhibit no strain hardening at increasing strain. An IF network, as represented by vimentin in figure 1-2, has a small elastic modulus at small strains, but has a large regime of strain hardening, increasing its elastic modulus by over 100 times at large strains (> 50%).

The distinct viscoelastic properties of each cytoskeletal element can be used as a versatile structural element in the cell. Within the cell all three filament systems are interpenetrated and interconnected by proteins described in subsequent chapters. The connections between filament systems is expected to yield a material with mechanical properties unlike those of the single component networks. Understanding the response of the whole cell to mechanical deformation will require an in-depth study of these composite materials.

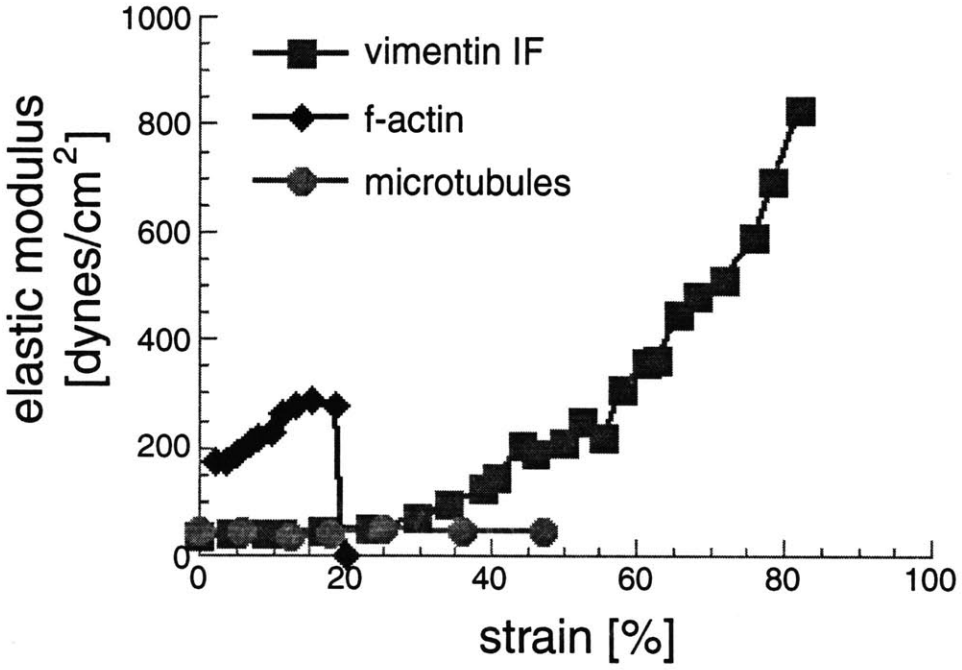

Figure 1-2 : **Rheological properties of cytoskeletal networks.** Networks (2 mg/ml) of actin filaments (diamonds), MTs (circles) and vimentin IFs (squares) show distinct mechanical properties in a strain sweep experiment. The increase in elastic modulus at increasing strains exhibited by f-actin and vimentin is called strain hardening.

1.1.2 Intracellular transport

Due to the large size of biological cells diffusion is too slow a process to distribute molecules from their site of synthesis to where they are required. To expedite the transport of molecules within the cell the cytoskeleton and its associated motor molecules provides an intracellular transport system. As described above, MTs and f-actin are polar filaments, having biochemically distinct ends and motor proteins which can exploit this polarity to carry out unidirectional motion along the filament contour. In the case of MTs, there are dyneins (minus-end directed) and kinesins (predominantly plus-end directed) motors which are responsible for transport of vesicles, organelles and other molecular cargoes around the cell. The radial array of MTs present in non-neuronal interphase cells acts a transport highway for these motors and their cargoes. In the case of dividing cells, MT motors play an essential role in assembling the MT spindle apparatus and in segregating the chromosomes to each of the daughter cells. Neuronal cells have a specialized transport system which runs the entire length of the axon (centimeters in length in some organisms) and mediates the transport of membrane bound and cytoskeletal elements along the axon between the cell body to the synaptic terminal.

Myosins, the f-actin associated motor protein, play an essential role in force generation in muscle contraction whereas non-muscle myosins are important in cell motility, cell division and transport. In particular, a number of myosins are important in vesicular and organelle transport(78, 100). Although there are few polarized actin structures identified within non-muscle cells, f-actin plays an essential role for transport at the cortex of cells for secretion and in the axonal cortical shell in axonal transport. Unlike MTs which are nucleated with their minus ends at the MTOC, the regulation of f-actin polarity to support this transport function is only poorly understood.

There exists evidence that some vesicular and organelle cargoes have both MT and f-actin motors bound to their surface and that these cargoes utilize both filament systems for transport(100). This type of motile behaviour requires 'crossover' points where a cargo can switch from one filament system to another. For this purpose proteins mediating the interactions between f-actin and MTs must exist. A number of candidate proteins are discussed below and one such protein, MAP2c, is specifically examined in chapter three.

1.1.3 Intracellular organization

To understand mechanics and transport functions of the cytoskeleton, the filamentous nature of the cytoskeleton is of primary importance. The cytoskeleton, however, also presents a tremendous surface area onto which molecules can bind and biochemical reactions can occur. Binding to the surface of the cytoskeleton enables molecules to be localized to a specific

distribution in the presence of thermal energy driving diffusion. In addition, the binding of a molecule to the cytoskeleton can also regulate biochemical reactions either by sequestering it away from a soluble enzyme or perhaps bring it closer to a cytoskeletal associated enzyme. The possible colocalization of an enzyme and its substrate to the cytoskeleton would change the dimensionality of the interaction, enhancing the rate and affinity over three-dimensional solution experiments.

In most cells f-actin is present at the cortex of the cell consistent with its mechanical function. Its unique distribution also allows it to locally sequester molecules within a small volume of the cell. For example, some have proposed that actin through its association with elongation factor 1-alpha (ef-1α) helps to maintain messenger RNA at particular regions of the cell(2, 115).

MTs have also been implicated in the sequestration of molecules to the cytoskeleton. One particularly well studied example is that of NF-κB. This transcription factor is specifically sequestered to MTs to prevent its nuclear function. However, under certain activating conditions NF-κB complexed to the MT through other molecules, can be released from the MT and migrate to the nucleus to carry out its transcription activity(121).

IFs have also been shown to bind a variety of molecules within the cytoplasm and thus participates in the 'molecular' organization of the cytoplasm. The large number of molecules that have been shown to bind to the cytoskeletal filaments is best understood by their polyelectrolyte properties, that is their high negative surface charge density makes them a docking site for many positively charged molecules. The polyelectrolyte properties of cytoskeletal filaments have been extensively studies by Tang and Janmey(142, 143) and illustrate the role the cytoskeleton can play as a structure for transient or permanent docking through electrostatic mechanisms.

Another organizational principle of the cytoskeleton is its role in spatial layout of the cytoplasm. Organelles such as the endoplasmic reticulum, golgi apparatus and mitochondria have been shown to be localized in the cell by MTs. IFs are thought to play a role in maintaining nuclear position(124) and morphology(96). In dividing cells, the MT and f-actin cytoskeleton play important roles in aligning and segregating chromosomes and in cleavage of the cytoplasm. These large length scale organizational principles (compared to the size of soluble molecules) could only be carried out by the integrated cytoskeleton resulting from the length and mechanical continuity of the constituent filaments.

1.2 Cytoskeletal associated proteins - controlling filament length, dynamics and network topology

In addition to the cytoskeletal filaments themselves there are a host of proteins which modulate

filament and network properties. Accessory proteins can modulate the length and polymerization state of cytoskeletal filament by either severing filaments (e.g. gelsolin for f-actin(162), katanin for MTs(99)) or sequestering monomeric units to change the polymer/monomer balance (e.g. thymosins/profilin for f-actin, stathmin for MTs). The polymerization state of IFs is regulated by phosphorylation which is most dramatic during mitosis(12, 57). Cytoskeletal binding proteins can also modulate the filament stiffness (e.g. MAPs for MTs(22)), dynamics (e.g. ADF/cofilin for f-actin)(9) and connectivity (filamin for f-actin)(39). By modulating the individual properties and topology of cytoskeletal filaments, the cell can change its mechanical properties, pathways for transport and change the organization of molecules and organelles (e.g. by releasing them upon depolymerization).

1.3 Cytoskeletal motor proteins

Motor proteins can, in principle, play a number of roles in the cytoskeleton. Although considered primarily in transport processes, motors can play a role in localizing molecules within the cell and generating a contracted network which may have unique mechanical properties.

Myosin motor proteins which translocate along f-actin are responsible for contraction in both muscle and non-muscle cells. Other isoforms of myosins are also involved in intracellular transport(78). The intracellular transport role of myosins is poorly defined since, unlike MTs there is no well-described polarized arrangement of actin filaments in most cells. Myosins are also present in the actin-rich cortical rim of cells and may be an important element in defining the mechanical properties of cells.

MT motor proteins have been well studied for their role in transport. Both dynein and kinesin family members have been shown to be essential in the transport of molecules and organelles. Dynein motor proteins were originally discovered in flagella and cilia and are the motor activity responsible for flagellar and ciliary beating. Dyneins are also present in the cytoplasm and form the primary retrograde transport element in cells, taking material from the endoplasmic reticulum to the golgi in many cells. In neurons, dynein is the primary motor responsible for the transport of materials from the synaptic end of the axon to the cell body. Cytoplasmic dyneins are linked to their cargo through the dynactin complex which also acts as a regulatory complex(34). In addition, dynein and dynactin play an essential role in assembling the mitotic spindle.

Kinesins form a large family of proteins, many of which have been sequenced but whose functions have yet to be identified. Kinesins are related through conserved MT binding and motor domains. These domains appear in the N-terminus, C-terminus or middle of kinesin related proteins. It is hypothesized that N-terminal kinesins, those proteins with the conserved domains

in N-terminus, move to the plus end of MTs, whereas the C-terminal kinesins move to the minus ends(130). The proteins with the domain within the molecule have not been fully characterized. Kinesins often play a dual function with respect to dyneins in that they form the anterograde transport system taking materials from the golgi to ER or from the cell body to synapse. The role of minus-end directed kinesins is not yet defined. Kinesins are also essential in chromosome alignment and segregation in mitosis.

1.4 Interfilament interactions in the cytoskeleton

The role of the individual filament systems of the cytoskeleton account for a large number of phenomena within the cell, as described above. Interactions between the cytoskeletal filament systems have been recently explored to identify their intracellular functions. This investigation demonstrates three distinct physical mechanisms by which cytoskeletal filaments can interact. The effects of such interactions are tested in vitro and the potential intracellular roles are discussed.

The polymeric nature of the cytoskeleton requires a different viewpoint of interaction mechanisms. Traditional solution biochemistry investigates the reaction between two point-like particles which diffuse through the solution and can interact during collisions in the solvent. When the molecules start to become elongated, as with polymers of the cytoskeleton, the number of collisions begins to increase due to the increased length and writhing motions of the polymers. As the concentration of polymer begins to increase the dominant interaction is steric. That is, the motion of one polymer is restricted by the presence of the other polymers since they cannot occupy the same space or pass through each other. These steric interactions make polymeric solutions fundamentally different than solutions of small molecules. Within the cell, the cytoskeleton is a polymeric meshwork where steric interactions must play a role. In addition, these steric interactions can be augmented by proteins which mediate binding interactions between the filaments or motor proteins which provide both binding and force between the filament systems. Taken together the potential for interactions is large and the resulting effects within the cell, varied.

1.4.1 Steric interactions - fundamental polymer physics

Two seminal ideas in theory of polymer networks are the tube model proposed by Edwards(23) and reptation proposed by de Gennes(17). The tube model describes the restricted motion of a single polymer in a polymer network. A polymer in the network cannot move arbitrarily in space due to the steric constraints of the neighbouring polymers. The model proposed by Edwards consolidates the steric constraints of many filaments into a single constraint which takes the form

of a cylindrical tube. The polymer is confined in lateral mobility to dimensions on order of the tube diameter. The tube confinement, however, is relaxed at the ends of the tube where de Gennes proposed that the polymer could diffuse along the longitudinal axis of the tube. This one-dimensional diffusive motion is termed reptation and has been verified in a number of biopolymer networks including DNA(113), f-actin(71) and MTs(11).

Work by Käs(71) and Perkins(113) used fluorescently derivatized biopolymers to visualize single polymers within a network. By monitoring single polymers using video fluorescence microscopy, the thermal fluctuations and the centre of mass motion of a single polymer can be visualized. The transverse fluctuations of the polymer within the network define the diameter of the confining tube as described by Edwards. The longitudinal motion of the polymer can be used to derive a one-dimensional diffusion constant. As predicted by de Gennes(17) and Doi and Edwards(20) the longitudinal diffusion constant ($D_{||}$) scales with inverse length for f-actin(72). Fundamental measurements of tube diameters and reptation times are essential for polymer theorists who have proposed models for macroscopic viscoelastic properties of cytoskeletal networks(59, 77, 91, 102, 126).

By using the tube model and reptation, a set of qualitative relationships between polymer state and the effect on the mechanical response can be derived. The length of polymers within the network must be long enough to ensure the existence of steric constraints for each polymer. If the polymers become too short, the single filaments will have access to rotational and transverse degrees of freedom which can be used to dissipate energy, that is the material will tend to flow since the filaments are not constrained to the tube. A cellular example of 'fluidizing' a network is the action of filament severing proteins such as gelsolin. Gelsolin severs f-actin in a calcium dependent manner resulting in short filaments. Bulk rheological measurements of gelsolin acting on an f-actin network results in viscous flow of the network under deformation rather than the elastic response seen with unsevered filaments(67).

The role of steric interactions in polymer physics is well documented for its contribution to mechanical properties. However, the role for simple steric interactions in the context of intracellular transport or spatial organization is less clear and still speculative.

1.4.2 Passive binding interactions

Steric interactions demonstrate a physical mechanism due to the cytoskeletal polymers alone. Within the cell there also exist a variety of cytoskeletal binding proteins. Some of these have the ability to crosslink the filaments together, such as filamin family members which crosslink f-actin(39). The crosslinking of f-actin results in a network with an increased elastic modulus(66)

and resistance to solvent flow(61), both important properties in maintaining the shape of a cell. There also exists evidence for proteins that link different filaments to each other(7, 8, 16, 31, 38, 48, 81). These interactions link filaments with different bulk mechanical properties to potentially produce a novel material with unique mechanical properties.

These passive connections can also act as transfer points for motor bound cargoes in intracellular transport. Cargoes being carried along MTs can be transferred to f-actin at junctions where MTs are crosslinked to f-actin(80, 100, 119). Such junction points may be important in a number of cell types where vesicular traffic fuses with the plasma membrane in areas where MTs are not detected. In many of these cells, however, f-actin is present near the cortex of these cells and there is a short overlap between the distribution of MTs and f-actin implicating a role for MT-f-actin crosslinking proteins. Although somewhat speculative, these connection points can also act as points for biochemical reactions between molecules localized to different cytoskeletal elements.

1.4.3 Active force-generating binding interactions

Motor molecules in biological systems represent a novel polymer crosslinker not present in synthetic systems. In addition to providing links between the filaments, motors have the added effect of inducing sliding and generating a pre-stressed condition within the network. From the mechanical point of view, this type of interaction would be predicted to increase the stiffness of a network, even if it were already crosslinked. The origin of this increase in stiffness has not been studied directly but in an analogous system - platelets in fibrin networks - the increase in network elasticity results from straightening of the polymer chains by the contractile activity of the platelet(132).

The role of motor activity between filaments can be an important mechanism in transporting filamentous polymers around the cell to be localized far from the site of synthesis. An important example of such a mechanism is the transport of cytoskeletal polymers along the axons of neuronal cells. Motor activity can also be used to localize filaments of the cytoskeleton to particular area of the cell through active mechanisms.

1.5 Interfilament interactions in the cytoskeleton

Presented above are two schemes by which interfilament interactions in the cytoskeleton can be classified. Classification can proceed by function, i.e. how does this interaction contribute to cellular function, and three broad areas were described : mechanics, transport and organization. Interfilament interactions can also be classified by the nature of the interactions which aids in

experimental design. Three broad interaction mechanisms were outlined : steric, passive binding and active binding. Some speculation as to the cellular role (i.e. mechanical, transport and organizational) of each type of interaction mechanism was described.

Having laid out a scheme in which to classify and understand the role of interfilament interactions, this study has investigated a number of such interactions. As the following chapters will describe, each example demonstrates a variety of possible cellular functions which can be a focus for further study. Previous work has identified a number of proteins which have been characterized as interfilament crosslinkers and a number are outlined below and within each chapter. A list of putative interfilament crosslinking proteins is given in table 1-1. Passive versus active interactions are differentiated by plain and bolded text, respectively. The molecules which have been investigated within this study are further delineated by italics.

	Actin	**MTs**	**IFs**
Actin			
MTs	MAPs(40) (e.g. *MAP2c*(16)) MIP-90(38), CLIP-170(81), calponin(31)		
IFs	*direct*(10)(vimentin) BPAG1n(161)(NFs) filamin(7), calponin(90)(desmin)	plectin(140), tau(8), **kinesin**(42, 88, 116) (vimentin) MAP2(48), direct(50, 84), ***kinesin, dynein/dynactin*** (NFs)	

Table 1-1 : **Interfilament crosslinking proteins.** Passive binding interactions are shown in plain text and active interactions are shown in bold text. The interactions explored in this thesis are in italics.

1.5.1 F-actin - microtubule

There exist a variety of cellular contexts where f-actin and microtubules are colocalized, such as during cytokinesis, cell polarization and cell motility. However, the identification of interfilament

linking agents has been inconclusive. Falling ball viscometry studies by Griffith and Pollard(40, 41) in the late 1970's demonstrated that mixtures of f-actin and microtubule proteins, i.e. tubulin and microtubule-associated proteins (MAPs), had a significantly higher relative viscosity when compared to mixtures of f-actin and polymerized tubulin. This implicated an interfilament interaction mediated by a MAP. The specific MAP, however, was not identified in these studies.

Work by Cunningham et al(16) demonstrated the potent f-actin gelation properties of MAP2c, a juvenile splice isoform of MAP2 exclusively expressed in neurons. The activity of a microtubule associated protein (MAP) in gelating f-actin provides evidence for an in vivo MT-f-actin link. In fact, Cunningham et al showed that the microinjection of MAP2c into non-neural cells which lacked an endogenous f-actin crosslinking protein, ABP-280/filamin-1, rescued the blebbing phenotype(15) normally present in these cells. In addition to rescuing the blebbing phenotype the microinjected cells also formed a variety of MT structures near the cell cortex further implicating MAP2c as a putative MT-f-actin crosslinking protein. Within neural cells MAP2c localizes to MTs in growing neurites and continues into the actin-rich regions of the neuronal growth cone. Colocalization of MAP2c at the MT-rich neurite-actin-rich growth cone junction is further evidence of its function as a MT-f-actin crosslinking protein.

Using an assay based on polymer diffusion described in chapter two, the interaction between MTs and f-actin was investigated both in the presence and absence of MAP2c. As described in chapter three, the steric interaction between a MT embedded within a f-actin network exhibited a novel dependence on MT length not predicted by polymer theory. Further studies with crosslinking indicated that in vitro crosslinking, even in the presence of MAP2c, produced heterogeneous networks showing polymer diffusion data which suggested a role for crosslinking in MT diffusion.

1.5.2 F-actin - intermediate filament

Interactions between intermediate filament family members and f-actin have been explored by a number of investigators (7, 10, 54, 60, 85, 145, 161). Brown and Binder identified filamin, an actin crosslinking protein, as a desmin IF associated protein(7). However, no further evidence of such an interaction have been reported. Yang and co-workers identified BPAG1n, a neuronal isoform of the bullous pemphigoid antigen, as an essential crosslinker between NFs and f-actin. Mice deficient in BPAG1n have gross, rapid sensory neuronal degeneration. The mechanism for this degeneration has not been identified.

Vimentin IFs have also been implicated in binding f-actin through a number of intercellular studies(10, 145). As described in chapter four a direct interaction between a c-terminal peptide

from vimentin, previously used by Cary et al(10), and f-actin was examined. The results indicated that the c-terminus of vimentin binds f-actin in a saturable manner. In addition, the c-terminal vimentin peptide can bundle actin filaments, further demonstrating the interaction between f-actin and vimentin.

1.5.3 Microtubule - intermediate filament

A number of investigations have identified two proteins that link microtubules to vimentin intermediate filaments. Work by Svitkina et al(140) identified plectin as a interfilament crosslinking protein between MTs and vimentin. Given previous work identifying plectin as a partner for f-actin and integrins, it can serve to mediate a wide variety of cytoskeletal binding interactions(156). Another MT-vimentin crosslinking protein that has been recently identified is kinesin. Work in the late 1980's by Gyoeva and Gelfand (42) showed that the injection of anti-kinesin antibodies resulted in the collapse of the vimentin network. Further investigations by the Gundersen lab (76, 88) have shown that kinesin and a post-translation detyrosination of MTs is essential for MTs to localize vimentin within the cell. Prahlad and co-workers showed the translocation of vimentin along MTs in a cellular context and identified kinesin as the motor responsible(116). The isolation of a specific kinesin isoform which is responsible for interaction with the vimentin intermediate filament network is likely to follow.

MTs are also thought to interact with neuronal intermediate filaments, or neurofilaments (NFs), within the neuron. In situ colocalization and in vitro biochemistry have shown that MAPs play a role in the interaction between neurofilaments and MTs(44, 48, 50, 86, 87).

Chapter five examines a MT-motor mediated interaction between MTs and NFs. Unlike vimentin, the interaction is mediated by both kinesin and dynein, giving rise to a bidirectional translocation of NFs along MTs.

Chapter six summarizes the findings from the filament interactions presented and discusses possible intracellular functions.

Chapter 2

Analysis of fluorescent filaments

2.1 Introduction

In investigating interfilament interactions in the cytoskeleton, the large size of biopolymers, when compared to synthetic polymers, permits their direct visualization. The length and extended conformation of biopolymers such as f-actin, IFs, MTs, or DNA allows visualization and manipulation of single macromolecules in solution. Such studies have been useful for verifying classical and modern theories of polymer physics(36, 72, 113, 118). In particular, the visualization of single biopolymers has enabled quantitative measures of filament stiffness, diffusion constants in isotropic and nematic networks, and electrophoretic constants.

To investigate biopolymer interactions a direct visualization of interfilament binding would be a useful technique for both. Polymer diffusion within a network, or reptation, has been visualized in both f-actin(71) and DNA networks(113). The addition of crosslinks in such a network should result in a change in the reptative motions of the visualized filament. Thus a reptation based system could be used to detect novel f-actin or DNA crosslinking agents.

The f-actin reptation system developed by Käs et al(71, 72) was modified, as described below, to visualize the motion of one type of polymer, microtubules, within a network of a different polymer species, f-actin. The visualization system and image analysis which were developed are described in this chapter. Its application to MT reptation in f-actin networks is examined in chapter 3.

2.2 Materials

Purified tubulin was either prepared from bovine brain microtubules(95, 150) or a kind gift of Dr. Christoph Schmidt (University of Michigan, Ann Arbor, Michigan). Tubulin was stored at -80 C in PEM-80 buffer consisting of 80 mM PIPES (piperazine-N-N'-bisethane sulfonic acid), 1 mM EGTA (ethylene glycol-bis[ß-aminoethyl ether]-N,N,N',N'-tetraacetic acid), 1 mM $MgSO_4$, 1 mM guanosine triphosphate (GTP) at a pH of 6.8. Tubulin was labelled with an Oregon Green 488 succinimidyl ester (Molecular Probes, Eugene, Oregon) or a rhodamine B N-hydroxy succinimidyl ester according to published protocols(55). Tubules were polymerized by increasing the temperature of monomeric solution to 37 C for 30 minutes in the presence of 1 mM GTP. The polymerized tubules were stabilized by the addition of taxol to 10 µM (paclitaxel, Calbiochem, La Jolla, CA).

Actin was purified from rabbit skeletal muscle according to the method of Spudich and Watt(135) with slight modifications. G-actin was stored at -80 C in G-Buffer consisting of 2 mM Tris (Tris hydroxymethyl aminomethane), 0.2 mM $CaCl_2$, 0.5 mM adenosine triphosphate (ATP), 0.2 mM DTT (dithiothreitol) at a pH of 8.0. G-actin was polymerized by the addition of KCl to 150 mM and $MgCl_2$ to 2 mM. f-actin was stabilized and fluorescently labelled through the addition of equimolar TRITC (tetramethylrhodamine isothiocyanate) phalloidin (Sigma Chemicals, St. Louis, MO).

2.3 Visualization of single filaments

Fluorescently labeled biopolymers were visualized on a Nikon Diaphot 300 inverted microscope equipped with epifluorescence optics and a Nikon PlanApo 60x (NA 1.40) or PlanFluor 100x (NA 1.30) objective. Biopolymer motion was captured to a DAGE-MTI silicon intensified target (SIT) camera (DAGE-MTI, Michigan, IL) through a 2X or 4X optics coupler, and digitized to a Power Macintosh (Apple computer, Cupertino, CA) through a Scion AG-5 video capture board (Scion Corporation, Frederick, MD). Motion was simultaneously recorded to VHS videotape. Although the native diameter of an actin filament is 7 nm or microtubule is 25 nm, below the resolution of light microscopy, the fluorescent images (figures 2-1 and 2-2) are a result of the interference between the adjacent fluorophores(114).

Biopolymer motion was monitored over two time sequences : 1000 frames at 10 frame/sec, and 300 frames at 0.5 frames/sec. Biopolymers which diffused out of the focal plane were not used in the analysis. Samples in which the biopolymers began to experience photodamage were discarded.

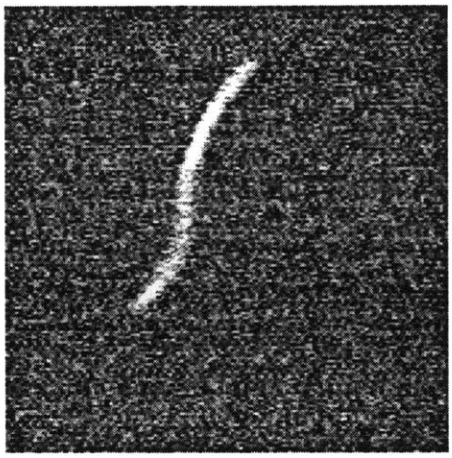

Figure 2-1 : **Fluorescent actin filament in dilute solution.**
Single video frame of a 20 μm actin filament in dilute solution far from any surfaces.

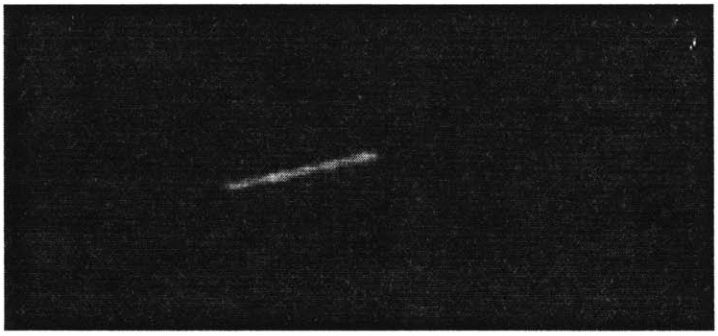

Figure 2-2 : **Fluorescent microtubule in an unlabeled f-actin network.**
Single video frame of a 7 μm MT embedded in an unlabeled 0.5 mg/ml f-actin network.

2.4 Extraction of single filament contours

For each digitized frame, the fluorescent filament image was traced using an automated algorithm described below, and the coordinates saved to a file. The algorithm design was based on the interference effects of the fluorophore on the filament and the point spread function of the microscope optics and camera.

The intensity profile of a fluorescent filament is well-approximated by an Airy function(114). The point spread function of the microscope optics and camera can be assumed to be gaussian. The convolution of these functions represents the optical transfer function that gives rise to the fluorescent image. A simulated filament is shown in figure 2-3 along with the cross-sectional intensity profile (panel A) and end intensity profile (panel B). The contour of the fluorescent filament is extracted from an image by locally determining the intensity profile and matching it to the convolved model.

The algorithm begins by locally interpolating a two-dimensional slice of the intensity profile and finds the best fit to a quadratic function. A quadratic function is used to compute the local intensity profile because its computation is simpler and faster than a gaussian fit and grossly approximates the local profile near the intensity extremum. The quadratic function is computed over a number of oblique cross-sections of the filament. The steepest quadratic, with an acceptable correlation coefficient, is chosen to be the cross-section of the filament. In this way the algorithm determines both the local orientation of the filament and the local intensity extremum which is the approximate location of the filament in space. The algorithm proceeds by advancing along the calculated direction of the filament and recalculating the local quadratic functions. Through this iterative scheme the body (non-end) points of the filament contour can be determined.

The endpoints are determined through a similar algorithm but quadratic fits are performed along the contour of the filament rather than in cross-section. Figure 2-3B has an example of a simulated filament end demonstrating the gaussian characteristic of the filament end intensity profile. By visual inspection the algorithm does an excellent job on both the body and ends of the filaments as demonstrated in figure 2-3C where the simulated filament and the trace are presented.

Analysing real fluorescent filaments can be difficult due to the presence of noise, both electronic and fluorescent. Before being traced each video frame undergoes a pre-processing step using a log-gaussian filter with spatial frequency optimized for the width of the fluorescent filament signal to enhance the filament intensity with respect to background noise. Figure 2-4A demonstrates a typical unprocessed filament intensity profile from an observed fluorescent filament. The general features are the same but the noise can make the local profile difficult to fit. This problem is overcome by using more points in the fit. This does result in poorer quadratic fits, as seen by the correlation coefficient. However, the fits are sufficient for determining the local orientation and

filament position. If the noise level is too large the correlation coefficient of the fit falls below a user-defined threshold and the algorithm exits. At this point the algorithm requires user input, via image processing or reorientation, to proceed with tracing.

Real filaments ends present a more diverse array of problems which are exemplified by the contour in figure 2-4B. This filament profile actually exhibits two end-type profiles near the same filament end. These issues were overcome by a number of ad hoc schemes. To accommodate the end profiles the algorithm was modified to include a general set of rules in which a region around the last filament endpoint (either the previous video frame or a user defined point) is defined to be a end searching area. The algorithm searches within this area for many filament end intensity profiles and an end is chosen from the many ends based on its shape and location in the region. This differs from the case of the simulated filament where the algorithm could stop when one end was found. Figure 2-4C demonstrates the fidelity of the algorithm by tracing the observed fluorescent MT with a variety of intensity inhomogeneities.

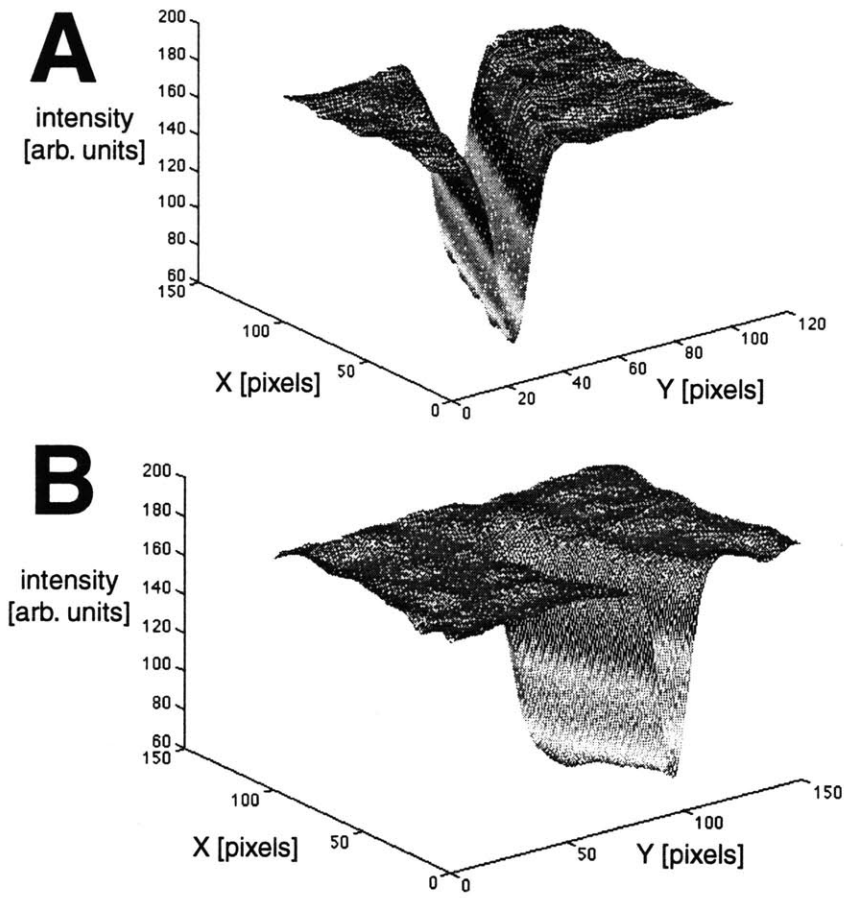

Figure 2-3 : **Tracing a simulated fluorescent filament.**
A, An intensity profile taken from a simulated filament contour. **B**, An intensity profile taken from a simulated filament end. **C**, Simulated filament and contour trace performed by the automated algorithm. Body and end intensity profiles were extracted from the simulated filament as illustrated.

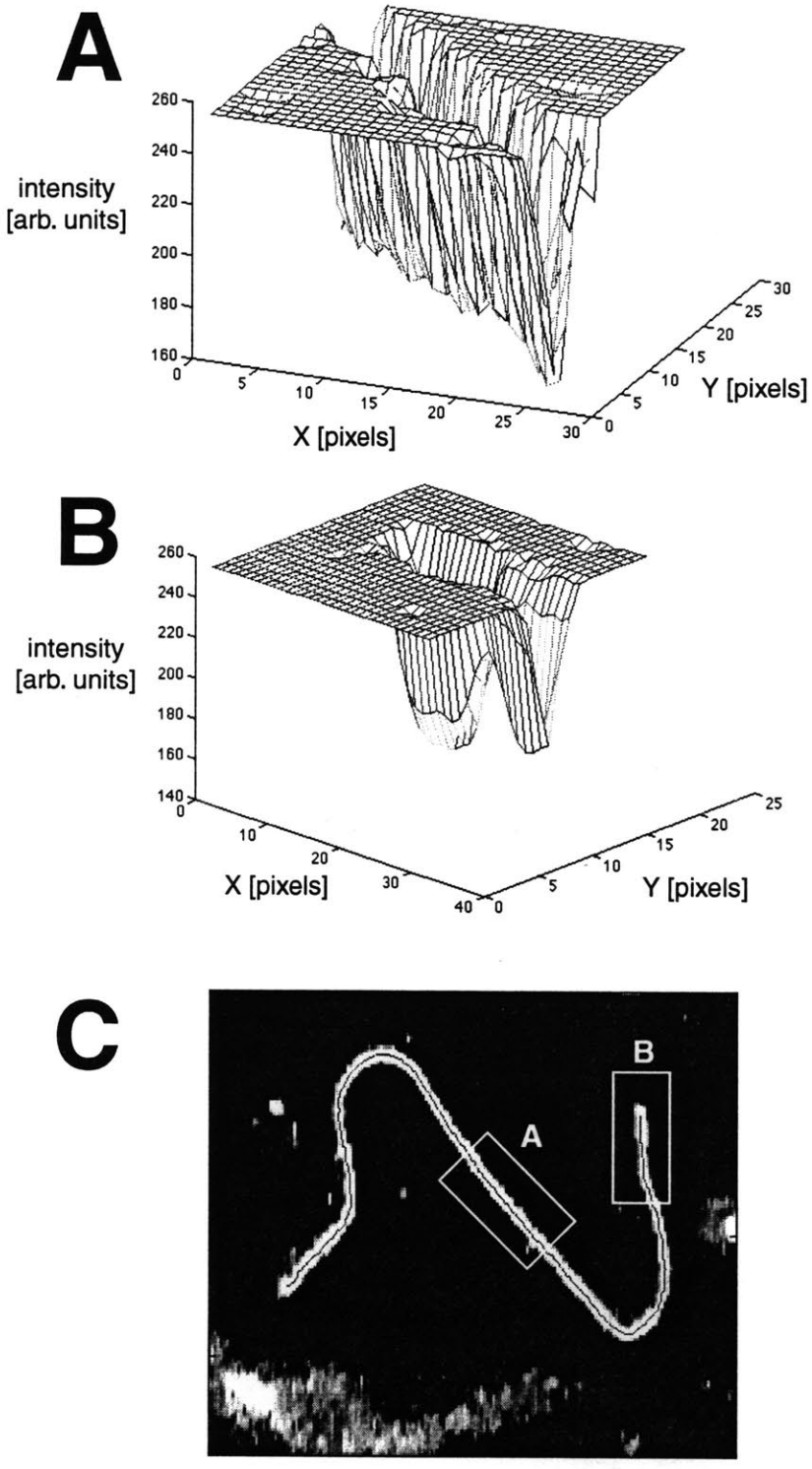

Figure 2-4 : **Tracing a real fluorescent filament.**
A, An intensity profile taken from a real filament contour. **B**, An intensity profile taken from a real filament end. **C**, Sample real filament (fluorescent MT) and contour trace performed by the automated algorithm with described modifications for end conditions. Body and end intensity profiles were extracted from the video frame image as illustrated.

2.5 Analysis of single filament motions

For filaments in free solution (figure 2-1) the filament contours can be fed directly into a number of analysis methods to determine centre of mass diffusion and filament stiffness(36, 72, 158).

For the purposes of reptative motions within a network (figure 2-2), the focus of this investigation, the coordinates of the end of the skeletonized filament were projected onto a one dimensional coordinate system parallel to the filament axis. The one-dimensional mean squared displacement ($\langle x^2(t)\rangle$) of the filament end was calculated from the projected coordinate data and a longitudinal diffusion constant ($D_{||}$) was calculated for filaments which exhibited diffusive motion ($\langle x^2(t)\rangle \sim t$) at long times (figure 2-5).

The longitudinal diffusion constant ($D_{||}$) was obtained over a number of interval times (Δt) using the formula :

$$D_{||}(\Delta t) = \frac{1}{2\Delta t} \cdot \frac{1}{(N-1)} \sum_{i=2}^{N} \{x(i\Delta t) - x((i-1)\Delta t)\}^2$$

where Δt is the time interval, N is the number of points in the measurement (i.e. $N\Delta t$ is the total measurement time) and x(t) is the position of the end of the filament in the one dimensional coordinate system. For long time intervals (Δt), $D_{||}$ was independent of the interval chosen. The long time interval $D_{||}$ is chosen as the longitudinal diffusion constant. For the MT data presented in chapter 3, the time interval to calculate the longitudinal diffusion constant was eight seconds. Filaments for which $D_{||}$ for each end differed by greater than 10% were discarded. Typical $D_{||}$ and $\langle x^2(t)\rangle$ measurements required time sequences of at least 100 seconds in duration and at least 100 frames (i.e. N>100) to detect diffusive motion and ensure satisfactory statistics.

The next chapter describes the reptation of MTs within f-actin networks measured with the above algorithm. The use of a reptation-based assay in detecting interfilament interactions is discussed.

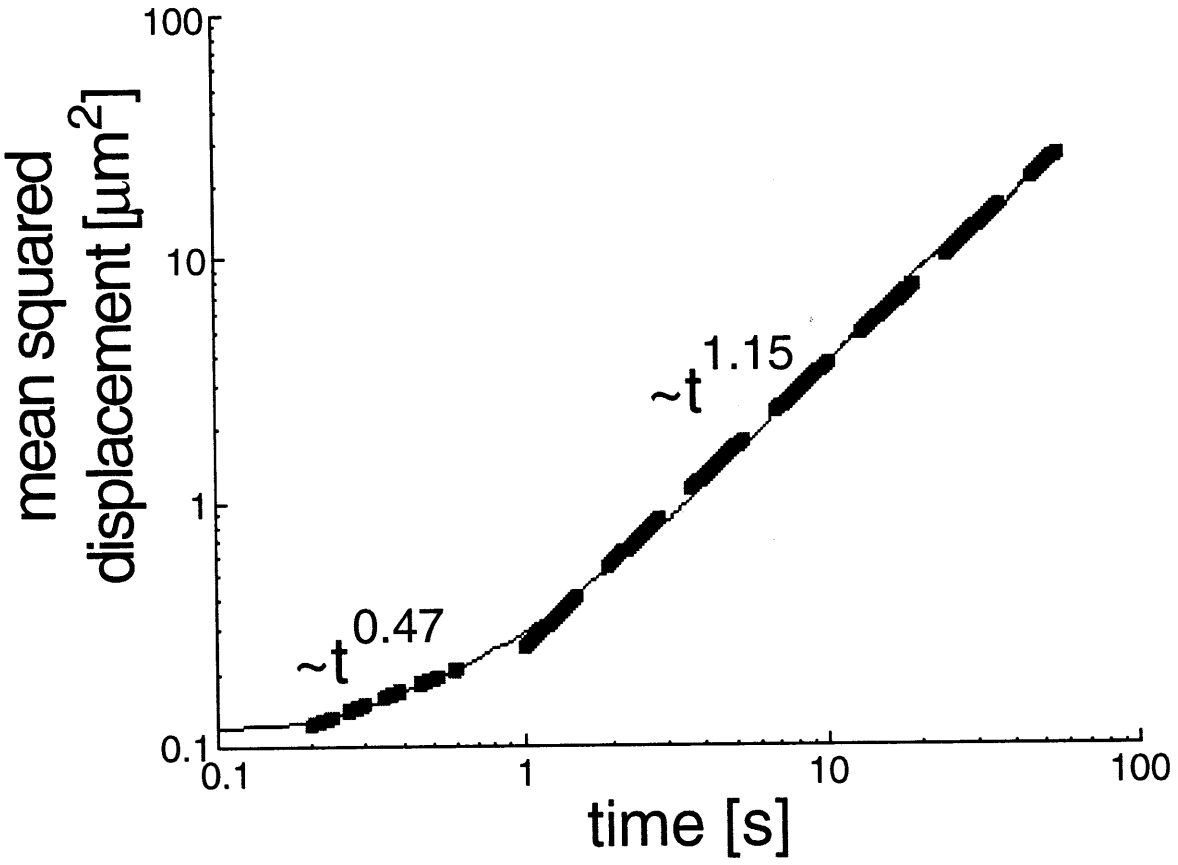

Figure 2-5 : **Mean squared displacement of a reptating MT.**
The mean squared displacement of a reptating MT within an f-actin network exhibits a linear relationship with time, as expected for a diffusive process. MTs which did not exhibit this relationship were not used in the reptation analysis.

Chapter 3

Microtubule reptation in an f-actin network

3.1 Polymer physics - tube model and reptation

The tube model, originally proposed by Edwards(23), describes the restricted motion of a filament in an entangled network. The test filament cannot move arbitrarily in space due to the steric constraints of the neighbouring filaments. The model proposed by Edwards consolidates the steric constraints of many filaments into a single constraint which takes the form of a cylindrical tube. The filament is confined in lateral mobility to distances on order of the tube diameter. At the ends of the tube de Gennes(17) proposed that the filament could diffuse along the longitudinal axis of the tube. This one-dimensional diffusive motion is termed reptation and has been verified in a number of biopolymer networks including DNA(113), f-actin(71) and MTs(11). As predicted theoretically(17, 20) the longitudinal diffusion constant of the filament within the tube ($D_{||}$) scales with the inverse of the length of the filament(71).

The work described by de Gennes and Edwards considered networks in which the filaments were entangled or chemically crosslinked. These two networks represent the extremes of reptative motion. The entangled network allows the filaments to slide past each other, whereas in the chemically crosslinked network the filaments are fixed in place relative to each other. Many molecular interactions in biological systems have the unique property of having transient interactions(127). The effect of such interactions on reptative motion have not been measured. If the effect of the transient interaction could be measured, such a scheme could be the basis for an assay to detect interfilament interactions.

In this chapter the interactions between MTs and f-actin are explored using a reptation based assay, partially described in the previous chapter. MT diffusion is measured in f-actin networks which are entangled, permanently crosslinked and crosslinked with a putative MT-f-actin crosslinking protein, MAP2c.

MAP2c is a developmentally regulated splice isoform of MAP2, a microtubule associated protein. In addition to its ability to bind MTs, MAP2c has also been shown to crosslink f-actin in vitro(16). As a result, MAP2c is an excellent candidate for MT-f-actin crosslinking.

The results described in this chapter demonstrate that MT diffusion in entangled f-actin networks does not follow an inverse length relationship, as predicted by theory, but rather a sigmoidal one. The origin of the sigmoidal relationship is unclear but due only to steric interactions, thereby underscoring the importance of steric constraints and their possible role in intracellular interactions.

In addition, MT diffusion in crosslinked, either transient or permanent, results in data that generally follows the sigmoidal relationship but is variable making a strict interpretation difficult. Although no direct evidence is given, one possible origin of such scattered data is that the crosslinked network is heterogeneous in its filament density giving rise to some tightly crosslinked areas and other less densely crosslinked areas.

3.2 Materials and methods

3.2.1 Sample Preparation

Tubulin, tubulin derivatives and g-actin were prepared as described in chapter 2. Fluorescent tubulin polymers (Rh-MTs) were prepared by mixing rhodamine-tubulin and unconjugated tubulin (10 mg/ml) in a molar ratio of 1:2 at 0 C. The mixture was then diluted 1:1 with PEM-80 with 1 mM GTP and incubated at 37 C for 1 hour. The polymerized tubulin was then diluted twenty times into prewarmed PEM-80 with 1 mM GTP and 10 μM taxol. The MT solution was allowed to sit in the dark at room temperature overnight before being used. When fluorescent biotinylated tubulin polymers (BRh-MT) were made, a ratio of 1:1:1 for rhodamine: biotinylated:unconjugated tubulin was used.

Actin (1 mg/ml, 1:10 ratio of biotinylated:unconjugated actin) was polymerized using PEM-80 with 0.5 mM ATP and 12 μM phalloidin and allowed to incubate at room temperature for 1 hour.

Rh-MTs were diluted 1:500 into PEM-80 with 1 mM GTP, 0.5 mM ATP, 12 μM phalloidin and an antibleaching solution (2 mg/ml glucose, 360 U/ml catalase, 0.1 vol % ß-mercaptoethanol, 8 U/ml glucose oxidase)(73). The f-actin solution was mixed with an equal volume of diluted Rh-MTs. Mixing was done slowly using a large diameter micropipette tip with diameter cut to 5 mm to minimize filament breakage. The mixing procedure was carried out in a 2.0 mL microcentrifuge tube.

The network was crosslinked through the addition of streptavidin to the diluted Rh-MT (or BRh-MT) solution at a molar ratio of 1:2 streptavidin:biotinylated actin and mixed as described above.

A small volume of the Rh-MT/f-actin mixture was gently placed (using a large diameter micropipette tip) in a chamber between coverslip and slide and sealed with vacuum grease. The sample was allowed to equilibrate for 45 minutes before observing filament motions. Observations were carried out under fluorescent optics as described in chapter two.

Due to the large persistence length of MTs, the filaments visualized had a straight conformation. The straightness of the MT also indicated that the filament was in equilibrium, with respect to bending, with the f-actin network.

3.2.2 Preparation of MAP2c

MAP2c was prepared by Dr. Lisa A. Flanagan by SF-9 expression and further purification by ion exchange FPLC. The ability of MAP2c to gelate f-actin was determined by rheology of f-actin-MAP2c mixtures (16). MAP2c also bound tubulin polymer as determined by sedimentation (Lisa A. Flanagan, personal communication).

3.2.3 Other materials

Streptavidin and biotinylated actin were purchased from Cytoskeleton (Boulder, CO) and taxol was purchased from Calbiochem (paclitaxel, La Jolla, CA). All other reagents were purchased from Sigma (St. Louis, MO).

3.3 Results

3.3.1 Microtubule diffusion in entangled f-actin networks

Microtubule diffusion in 0.5 mg/ml f-actin networks was visualized as described above. Figure 3-1 shows a series of digitized frames of a fluorescent microtubule within a dense unlabelled f-actin network. The fluorescent filament in each frame was traced as described in chapter 2 and the longitudinal diffusion coefficient constant calculated. The graphs in this chapter have the values for both ends of the filament plotted, resulting in two error bars per point.

Figure 3-2 shows the relationship between $D_{||}$ for microtubules in an entangled f-actin network and the inverse length (L^{-1}) of the microtubules. A linear fit as predicted by Doi and Edwards(20) fits the data poorly. The data is best fit by a sigmoidal function. The transition in length of the sigmoid is approximately $(15\ \mu m)^{-1}$. The sigmoid in figure 3-2 is presented as a guide ($y = c + a/(1+e^{-(x-b)})$) and does not correspond to a specific model. The origin of the sigmoidal relationship is unclear and a theoretical model is presented in the discussion at the end of this chapter.

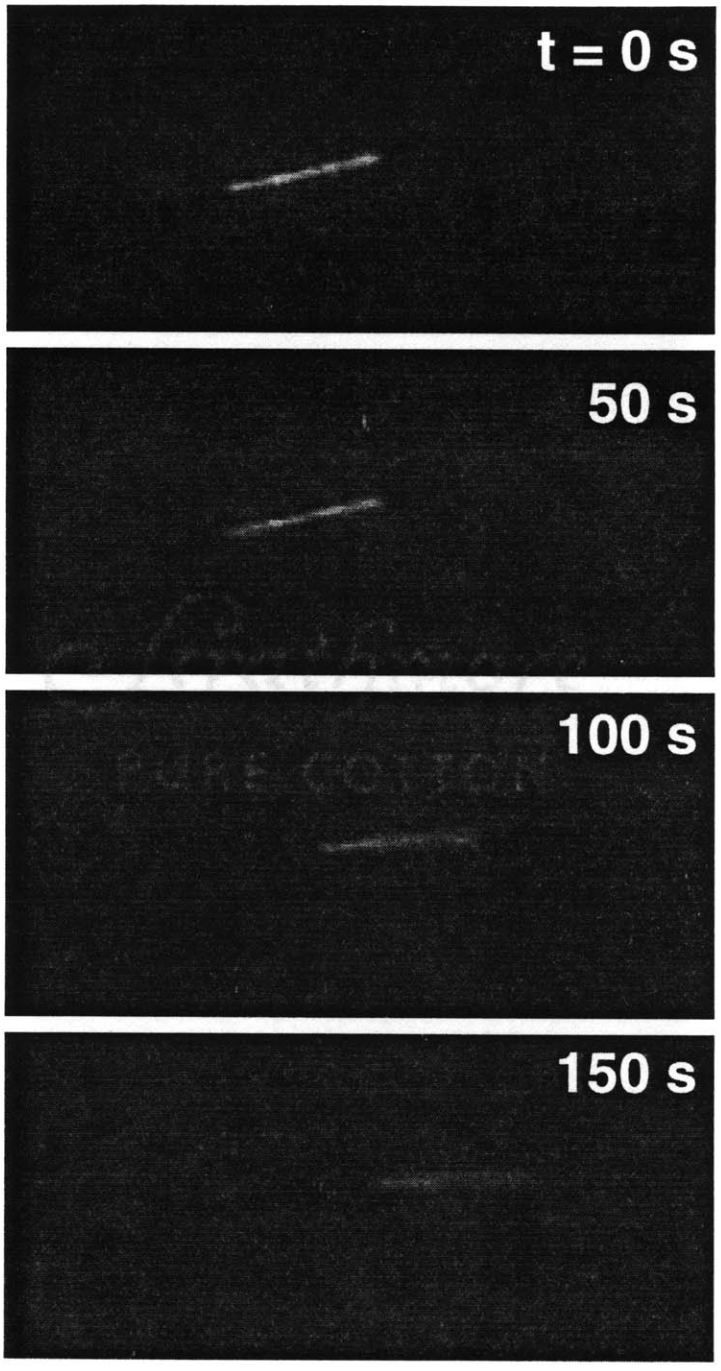

Figure 3-1 : **Microtubule reptation in an f-actin network.** Video sequence of a 7 μm fluorescent MT embedded in a 0.5 mg/ml f-actin network.

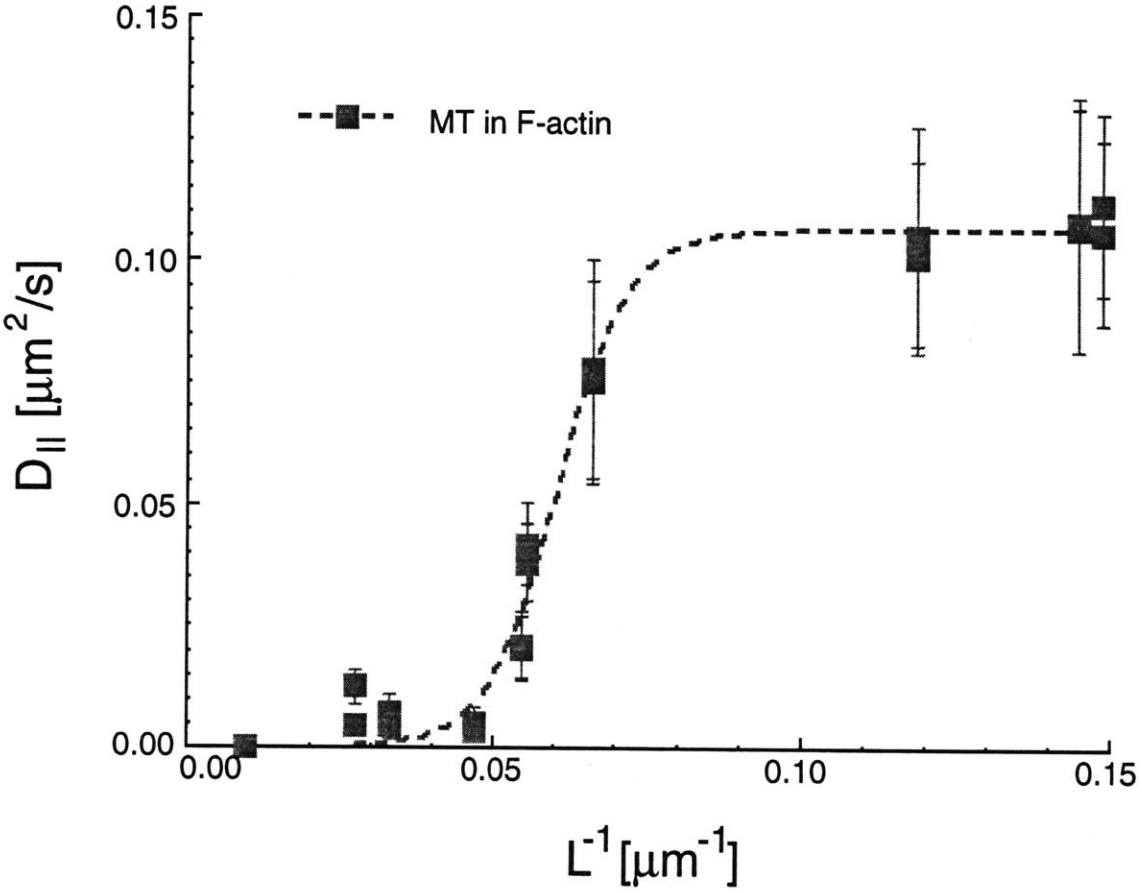

Figure 3-2 : **Microtubule diffusion in an entangled f-actin network.** The longitudinal diffusion constant for a variety of MT lengths was measured in a 0.5 mg/ml f-actin network. The fit shown is a sigmoidal function as a visual aid and is not based on a model.

3.3.2 Microtubule diffusion in crosslinked f-actin networks

Figure 3-3 shows the longitudinal diffusion constant ($D_{||}$) of MTs in a crosslinked f-actin network. The links between actin filaments are formed by streptavidin bridging biotinylated actin that has been copolymerized at a ratio of 1:10 with unconjugated actin. The data are much more scattered than the entangled case but do exhibit a transition region that has been shifted to smaller MTs when compared to the entangled case (shown for comparison). The large scatter in the data is probably a result of network heterogeneity induced by crosslinking.

Figure 3-4 shows the longitudinal diffusion constant ($D_{||}$) of biotinylated MTs in a network of f-actin (10% biotinylated) after addition of streptavidin at a ratio of 1 streptavidin : 2 biotin. Since both MT and f-actin subunits bind with the streptavidin crosslinker, the biotinylated microtubules are crosslinked into the surrounding f-actin network and are immobile. As a result the microtubules have much smaller values of $D_{||}$ over all lengths when compared to unbiotinylated microtubules (Figures 3-2 and 3-3). Any remaining MT motions represent the collective motions of the entire network, and as expected the inverse length dependence of the longitudinal diffusion constant breaks down.

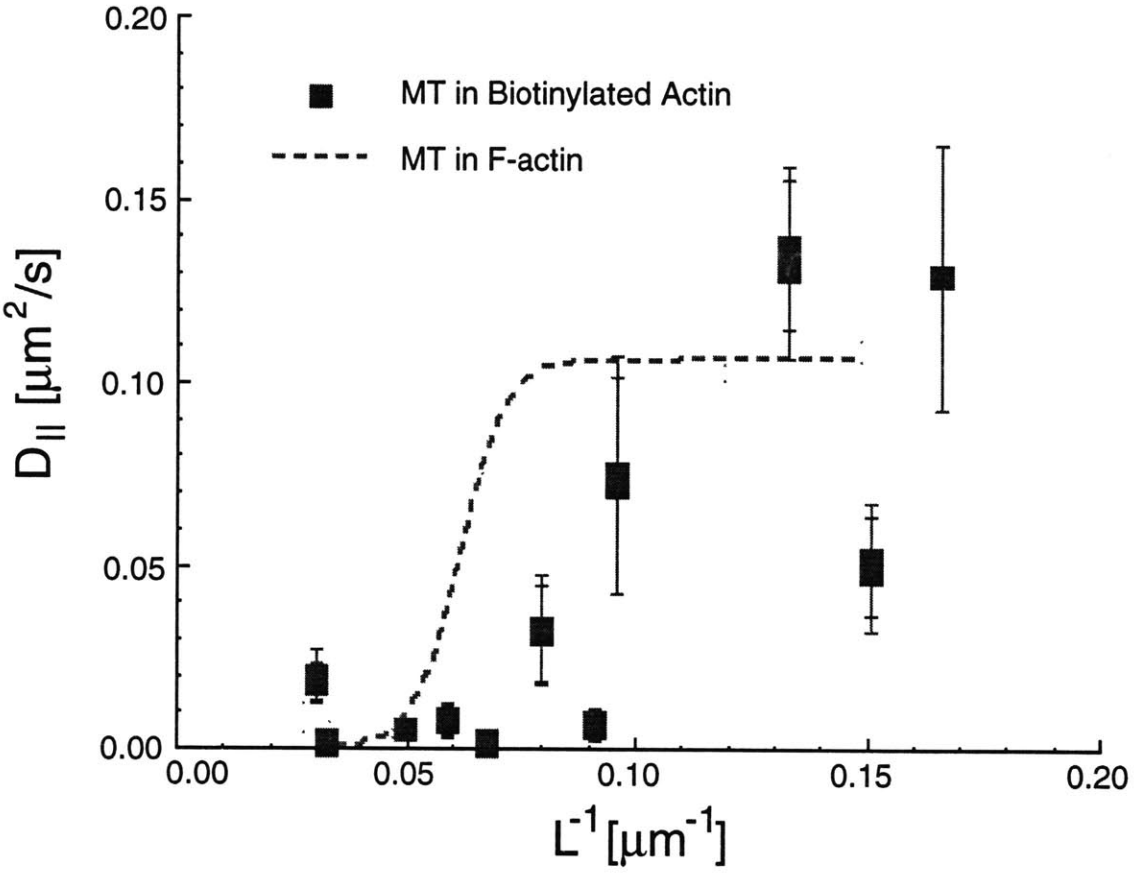

Figure 3-3 : **Microtubule diffusion in a crosslinked f-actin network.** The longitudinal diffusion constant for a variety of MT lengths measured in a 0.5 mg/ml crosslinked f-actin network. The fit shown is the sigmoidal fit for an entangled network for comparison.

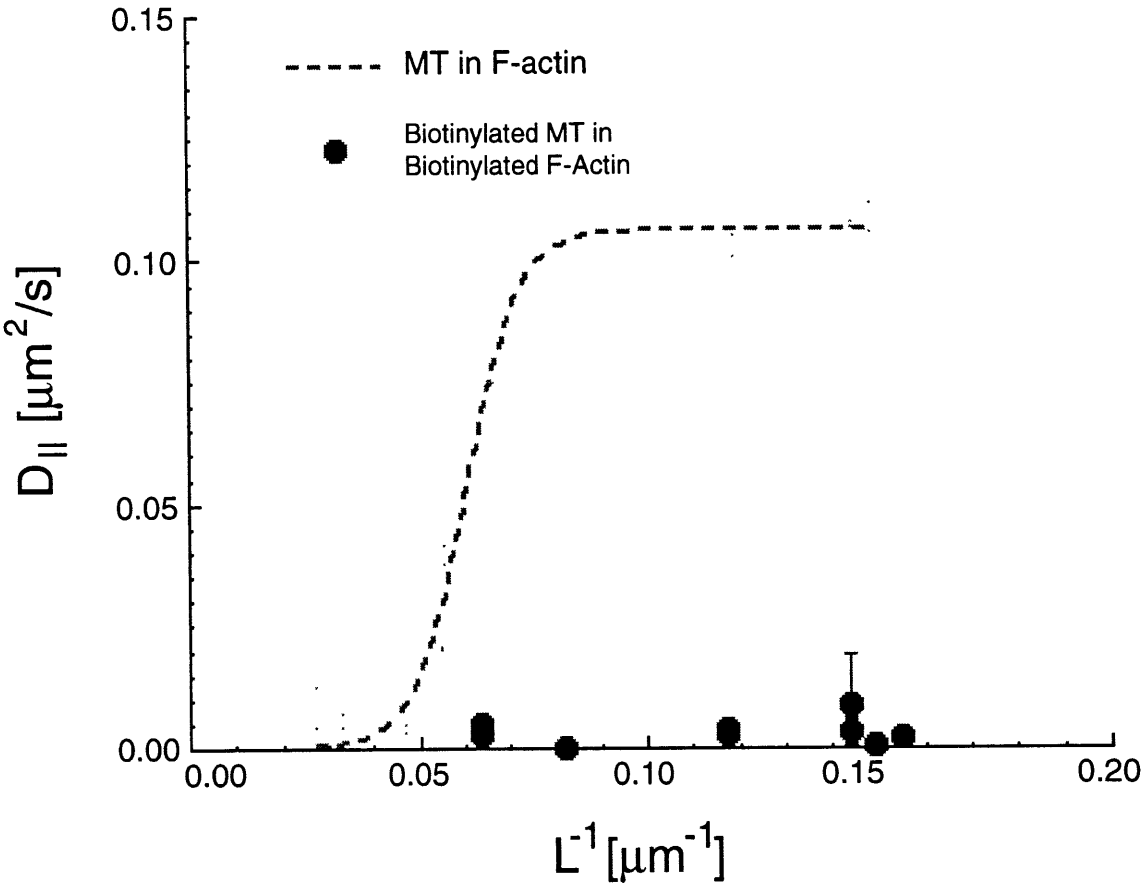

Figure 3-4 : **Microtubules diffusion in a crosslinked MT-f-actin network.** The longitudinal diffusion constant for a variety of MT lengths measured in a 0.5 mg/ml crosslinked MT-f-actin network. The fit shown is the sigmoidal fit for an entangled network for comparison.

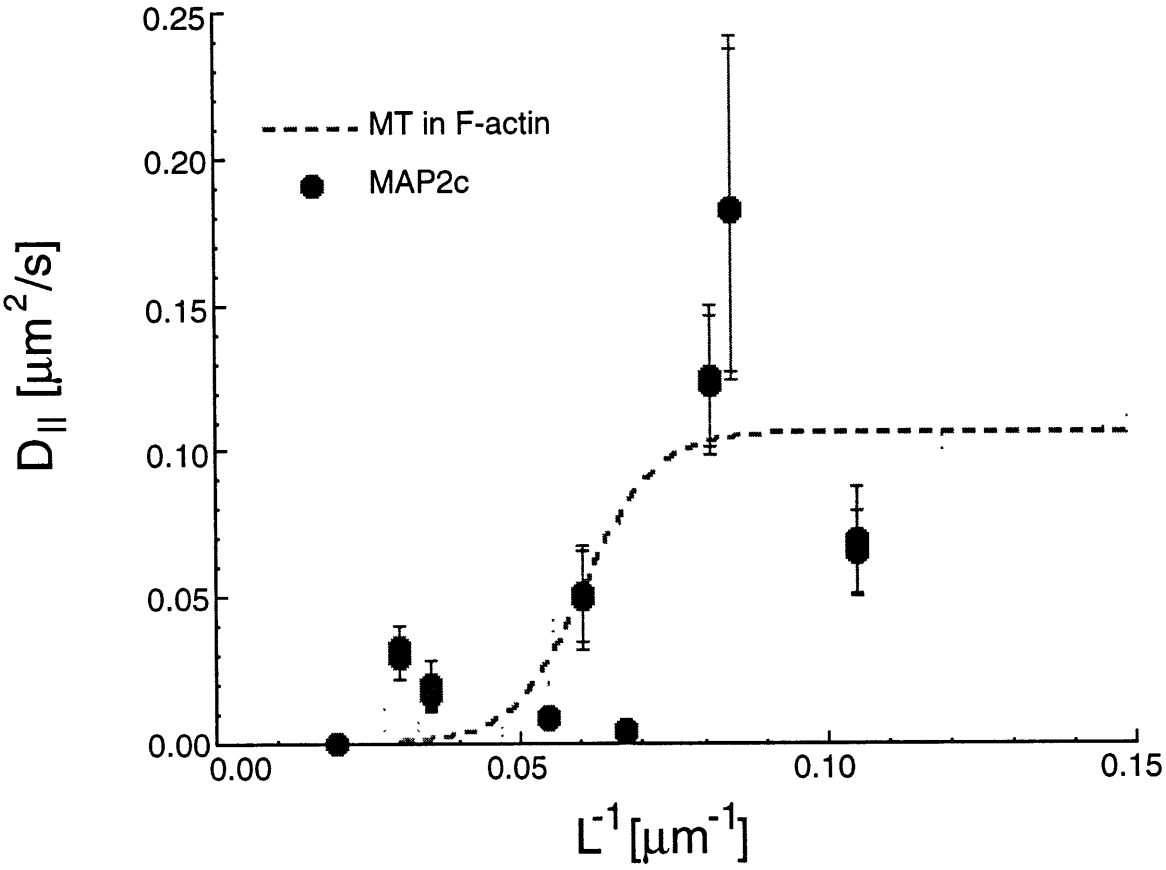

Figure 3-5 : **Microtubule diffusion in an MAP2c-crosslinked f-actin network.** The longitudinal diffusion constant for a variety of MT lengths measured in a 0.5 mg/ml f-actin network in the presence of 1:100 MAP2c:actin molar ratio. The fit shown is the sigmoidal fit for an entangled network for comparison.

3.3.3 Microtubule diffusion in map2c-f-actin networks

Figure 3-5 shows MT diffusion within an f-actin network crosslinked by MAP2c. As with the biotinylated f-actin network, the MT diffusion is highly scattered. However, in this case the scattering is high enough to preclude an interpretation.

3.3.4 Further characterization of MT diffusion within entangled f-actin networks

To investigate the origin of the sigmoidal relationship observed in figure 3-2, the tube diameter was measured for a large number of filaments to detect any change that may take place over the lengths examined (figure 3-6). The tube diameter was measured over a short time scale (~ 2 seconds) to ensure that the MT was confined to its original tube. Measurement of the tube diameter revealed no change over the MT lengths measured, as predicted theoretically(20, 131) and observed in f-actin networks(72). The mean tube diameter was 326 +/- 147 nm. Scaling arguments proposed by Semenov indicate that the tube diameter scales with the -1/5 power of the persistence length (a measure of filament stiffness) and the 3/5 power of the network concentration ($a \sim l_p^{-\frac{1}{5}} \rho^{-\frac{3}{5}}$, where a is the tube diameter, l_p the persistence length and ρ, the concentration)(131). Work by Käs et al(72) reported the tube diameter of an actin filament within a 0.5 mg/ml actin network as 800 nm. Using a persistence length of 15 μm for f-actin and 1 mm for MT(36) the scaled tube diameter for a MT, using the Semenov result, is 340 nm - in good agreement with the measured value.

A possible explanation for the sigmoidal relationship is that short filaments may gain access to rotational degrees of freedom. The short time scale rotational motion of the MTs was measured in analogy with the longitudinal diffusion replacing the position of the filament with its orientation, θ. The short time scale motion reflects the rotation of the filament within the virtual tube, not the rotation of the filament as it reptates around the network. The rotational diffusion constant, D_θ, is shown in figure 3-6. The rotational diffusion constant exhibits a power law relationship with the MT length with an exponent of approximately -1.7. Theoretical derivations of rod motion within a network predict that this short time scale motion should follow that of a rod in free solution which goes with the -3 power of the length(20), this discrepancy is not well understood. More importantly, this data does not exhibit a sharp transition in rotational freedom which might indicate the sudden onset of new degrees of freedom.

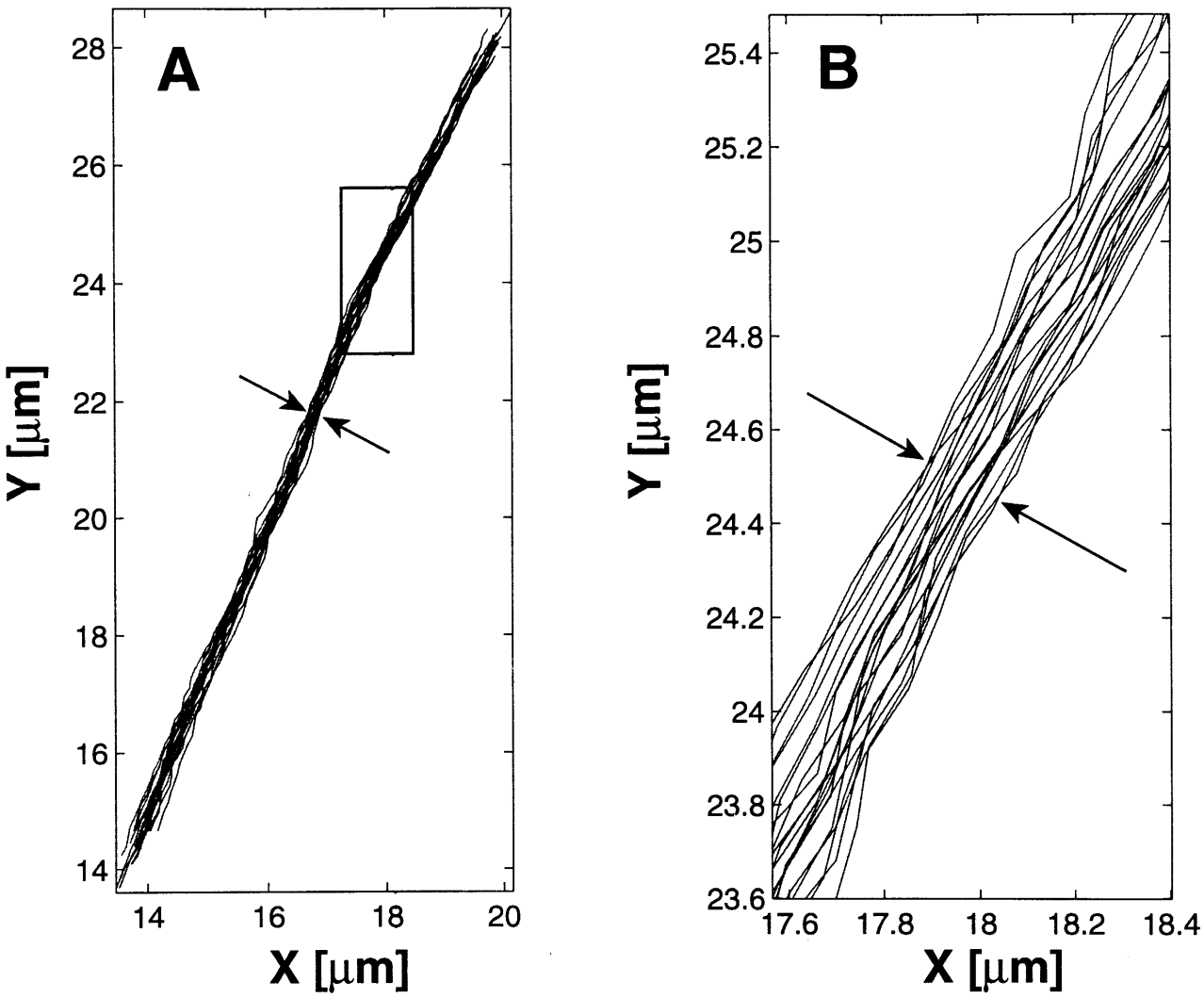

Figure 3-6 : **Determination of the tube diameter.**
Consecutive traces of a reptating MT were superimposed and the transverse fluctuations measured directly to determine the tube diameter. The time scale used for this measurement is four times smaller than that used for computing the longitudinal diffusion constant thereby ensuring that the filament is still confined to its original virtual tube. **A**, Traces for the entire contour length. **B**, An enlargement of the rectangle in **A**.

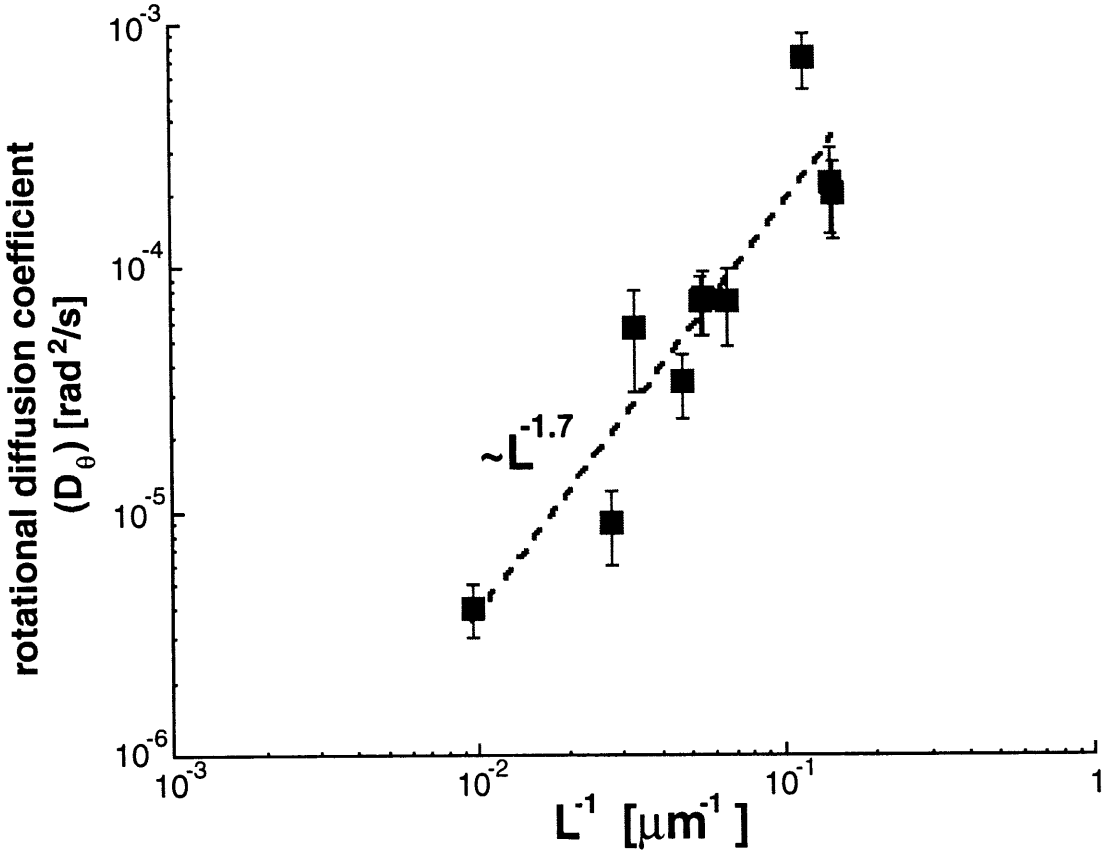

Figure 3-7 : **Rotational diffusion of MTs in an entangled f-actin network.**

3.4 Discussion

Biopolymers have been used to understand fundamental theories in polymer physics. Their large size permits their direct visualization and manipulation. Studies to verify theories of reptation have been previously carried out in homogeneous mixtures of polymers(11, 71, 113). This investigation examined the diffusion of MTs in f-actin networks to understand reptation in a mixed polymer system. In addition, the reptation measurement is expected to be sensitive to crosslinking agents, both permanent and transient, and can in principle be used as an assay to detect interfilament interactions.

3.4.1 Comparison of microtubule and f-actin diffusion in f-actin networks

Previous work by Käs et al(72) has characterized the longitudinal diffusion constant of f-actin filaments in an uncrosslinked f-actin network. Figure 3-8 shows the data of Käs et al and the MT diffusion data in an entangled f-actin network (figure 3-2). Despite their smaller diameter, suggesting less hydrodynamic drag, actin filaments diffuse slower than the MTs within the uncrosslinked f-actin network. In addition, the longitudinal diffusion constant of the MTs does not follow an inverse length dependence as it seems to for f-actin.

The sigmoidal dependence of MT diffusion in f-actin is a novel dependence for a reptating filament. The dependence can be intuitively understood at the extrema, i.e. at long and short lengths. At long lengths, the MTs become entangled to such an extent that the MT diffusion is too slow to be measured in this system. At short length scales (but still greater than 1 μm), the MTs have a diffusion constant which seems to be independent of their length. This could be a result of the discrete nature of the network, that is the tube is actually formed from discrete filaments separated by a spacing on the order of ~100 nm in a 0.5 mg/ml f-actin network. This spacing, the mesh size, represents the lower limit for hydrodynamic interactions, thereby screening the effect of length for short filaments. One candidate for the origin of the transition length scale is the deflection length(109). The deflection length, λ, is the length between polymer tube collisions. It is defined as $\lambda=(a^2 l_p)^{(1/3)}$, where a is the tube diameter and l_p is the persistence length, a measure of the filament stiffness. The deflection length is a natural length scale on which pure translational motion transitions to a combination of translation and rotation. In this system the deflection length is 5 μm, only a factor of three from the transition length scale. Although, the deflection length may be related to the transition in diffusion, as seen in figure 3-2, the rotation in this system exhibits no sharp transition (figure 3-7) . Thus there is no sudden onset of rotational motion which enhances diffusion. Further studies with different concentrations of f-actin (i.e. mesh size) are necessary to

understand the origin of this novel diffusive behaviour.

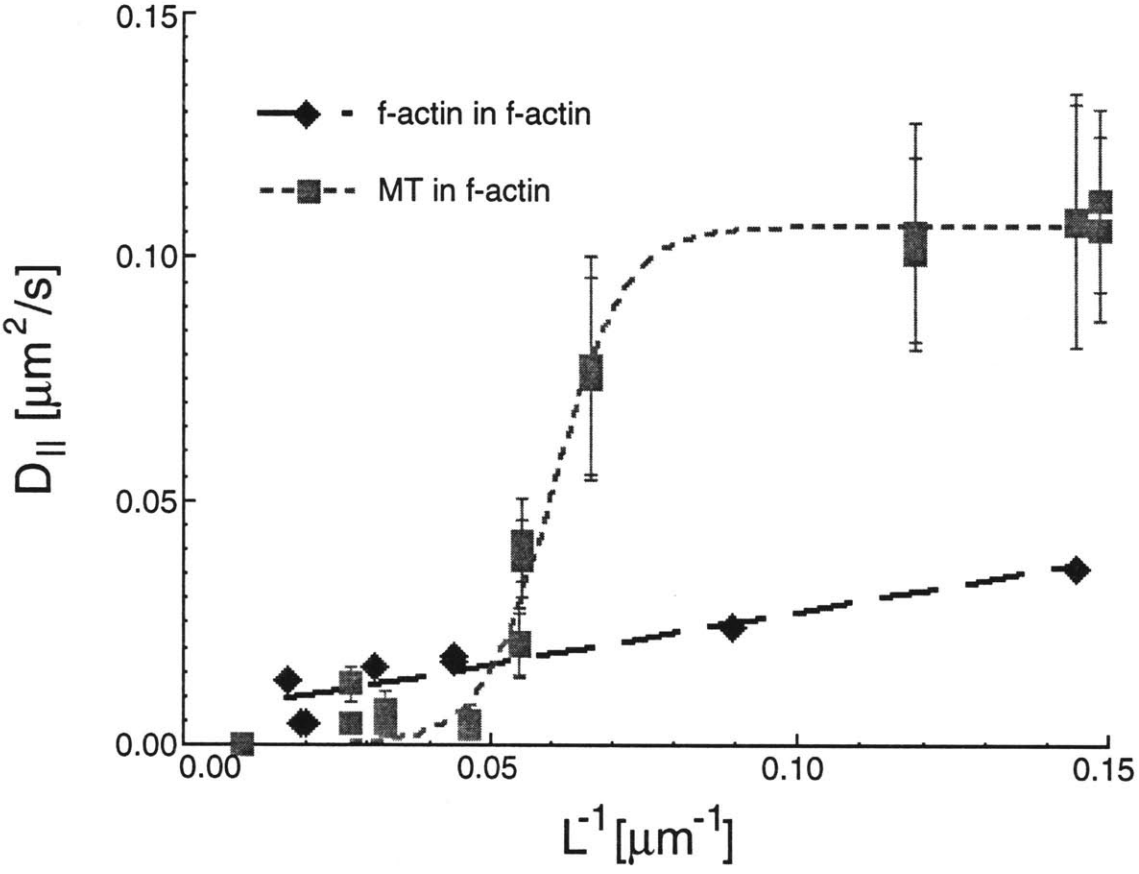

Figure 3-8 : **Microtubule versus f-actin diffusion in f-actin networks.** The diffusion constant of a MT and an actin filament in an f-actin network.

3.4.2 MT diffusion in uncrosslinked versus crosslinked networks

The crosslinking of the f-actin network produced a large variability in the measured longitudinal diffusion constant of the MTs. One speculation is that the crosslinking by MAP2c or biotin-streptavidin produces a heterogeneous network with a widely varying mesh size throughout the network. Thus the MTs observed can experience different mesh sizes locally giving rise to different longitudinal diffusion constants. A direct method to check this hypothesis would be to study the ultrastructure of the network by quick-freeze deep-etch electron microscopy techniques. Based on such work one could devise other sample preparation methods which reduces the level of network heterogeneity.

3.4.3 Reptation based assays for the detection of interfilament interactions

This investigation is the first attempt to use a reptation based assay to detect interfilament interactions. In principle, the effect of transient interactions should result in changes in the longitudinal diffusion constant. The scattered data obtained from observations of MTs in biotin/streptavidin and MAP2c crosslinked networks indicates that the reptation assay, as it is currently designed, cannot be used to detect interfilament interactions. Future studies in which other filament mixing or polymerization schemes are used to reduce network heterogeneity will be useful in evaluating reptation as an assay for detection of interfilament interactions.

3.4.4 Intracellular role for microtubule-f-actin interactions

The anomalous diffusion of a MT in f-actin underscores the possible role of steric constraints in the cytoskeleton. In the absence of actin-binding proteins or MT-associated proteins, the longitudinal diffusion of a MT was perturbed by the presence of the f-actin network. Thus steric constraints represent a fundamental interaction between cytoskeletal filaments which can give rise to a novel mechanism of cytoskeletal organization. In the context of the cellular environment, the steric constraints imposed by the f-actin network against the motion of the MT could explain the infrequent appearance of MTs in the f-actin meshwork both at the cortex and leading edge of cells(153).

Building upon steric interactions, the next two chapters explore the role of binding interactions, both passive and active, in the cytoskeleton.

Chapter 4

Interactions between vimentin and f-actin

4.1 Introduction

Vimentin is an intermediate filament protein preferentially expressed in tissue of mesenchymal origin. The role of vimentin has proven enigmatic(25). Mice homozygous for a null mutation in vimentin display no dramatic defects(14). More detailed observation, however, indicates that these animals have defects in the flow induced dilation of mesenteric arteries(45), increased lethality after reduction of renal mass(144) and defects in cerebellar neuronal organization(13). In isolated cell culture, changes in lipid metabolism(125) and nuclear morphology(124) have also been correlated to the presence or absence of a vimentin network.

In vitro studies indicate that vimentin's n-terminal "head" domain is essential for assembly into 10 nm filaments(47). The role of its c-terminal tail domain, in contrast, has been much more controversial. Rogers et al(120) examined the effects of removing various regions of vimentin's c-terminal tail domain in vivo. In contrast to reports by others(3, 94), they found no dramatic effects on the ability of the truncated polypeptides to assemble into 10 nm filaments in vitro, and subtle effects on the spatial organization of intracellular vimentin filament networks. The c-terminus of intermediate filaments is the least conserved part of the protein family members and may be important for specialized functions in the specific differentiated tissue.

Cary et al(10) examined the behavior of vimentin's tail (c-terminus) in vivo and found it colocalized with actin containing structures. Tint et al(145) described a morphological change in the vimentin network concomitant with the ATP-dependent contraction of the f-actin network. That IFs can interact directly with f-actin filaments is also supported by the observation that f-actin changes the rheological properties of neurofilament networks(85) and that f-actin is disrupted by polymerizing vimentin(133).

To directly study the interaction between f-actin and vimentin, the in vitro binding of a c-terminal vimentin peptide(10) to f-actin was investigated. The studies described in this chapter confirm that the vimentin polypeptide can bind directly to f-actin but has no significant effect on actin polymerization kinetics. The mechanical role of a vimentin-f-actin interactions is discussed.

4.2 Materials and methods

4.2.1 Expression and purification of myc-tagged vimentin construct

Myc epitope tagged vimentin tail peptide was provided by Prof. Michael Klymkowsky (University of Colorado, Boulder, CO). When compared to the original mycVimentin Tail polypeptide from Cary et al(10), this polypeptide has the sequence Asn-Cys-Arg-Gly inserted between the myc epitope and the vimentin tail sequence (figure 4-1) and has a calculated molecular weight of 7394 daltons. The polypeptide was purified from bacteria using the same protocol as described previously for the mycVimTail polypeptide(10). For use in actin experiments the peptide was dialysed against G buffer (2 mM Tris, 0.2 mM $CaCl_2$, 0.5 mM DTT, 0.2 mM ATP, pH 8.0).

4.2.2 Pyrene-iodoacetamide-actin assembly

Actin was prepared according to published methods(135) with slight modifications. Modification of actin with pyrene-iodoacetamide (Molecular Probes, Eugene, Oregon) was carried out by standard methods(75). Fluorescence measurements of pyrene-labelled actin were made using a Perkin-Elmer LS-5B luminescence spectrometer (Norwalk, CT), with 365 nm excitation wavelength and emission detection at 386 nm. A minimum sample volume of 300 µl was required, using a glass test tube of 8 mm diameter. Various concentrations of vimentin C-terminal tail peptide were mixed with 3 µM g-actin (in G buffer) 30 s before addition of 2 mM $MgCl_2$ and 150 mM KCl to initiate actin polymerization.

4.2.3 Dynamic light scattering (DLS)

The same samples used for pyrene-actin polymerization assays were measured by DLS approximately 12 hours after polymerization was initiated and the sample had reached a steady state fluorescence. DLS was performed with a Brookhaven Instruments (Holtsville, NY) device consisting of a 10 mW He-Ne laser, a BI-160 goniometer, a photomultiplier connected to a BI-2030AT correlator, using a 4 domain multiple sample time method to extend the range of times in the autocorrelation functions. The total scattering intensity and the intensity autocorrelation function were measured at 23 C and a 90 degree scattering angle.

4.2.4 Sedimentation assay

G-actin was diluted to 12 µM in G buffer containing various concentrations of the vimentin tail peptide. Actin polymerization was initiated by the addition of $MgCl_2$ and KCl to 2 mM and 150

mM, respectively. The samples were allowed to polymerize for 30 minutes at 23C and then centrifuged (TL100, Beckmann Instruments, Columbia, MD) at 100 000 g for 60 minutes at 25C. This centrifugal field sediments actin filaments which are longer than tens of subunits in length. The supernatants were removed and prepared for SDS-PAGE analysis. SDS-PAGE sample buffer was added directly to pellets and allowed to incubate for 10 minutes at 50 C before the pellets were homogenized by pipetting and vortexing. SDS-PAGE analysis was carried out by standard methods(79). Actin content in supernatant and peptide content in pellets were analysed by coomassie blue densitometry using NIH Image (Bethesda, MD).

4.2.5 Electron microscopy

G-actin in G buffer was polymerized at 1.2 μM as described above in the absence and presence of 12.5 μM vimentin peptide. Glow discharged formvar-coated copper mesh grids were inverted on a drop of sample and subsequently washed in buffer A with 2 mM $MgCl_2$ and 150 mM KCl and then stained with 2% uranyl acetate. Grids were observed in a JEOL-1200EX electron microscope at 100 kV.

4.2.6 Rheological measurements

Rheological measurements were done in the laboratory of Søren Hvidt (Roskilde University, Copenhagen, Denmark) using a Rheometrics RFS rheometer (Piscataway, NJ) with a cone and plate geometry. Measurements of the shear storage modulus (G') were made at 23C at a frequency of 50 rad/s over a range of strains from 1% to 50%. Unpolymerized vimentin (a kind gift of Prof. Peter Traub, Max-Planck Institute for Cell Biology, Heidelberg, Germany) was prepared at 6 mg/ml in 10 mM Tris-acetate, 0.2 mM DTT, pH 7.6 and in some cases mixed with G-actin and gelsolin. Polymerization of both actin and vimentin was initiated by addition of 2 mM $MgCl_2$ and 150 mM KCl in G buffer. Measurements of the strain-dependent shear moduli were started 2 hours after polymerization was initiated. Gelsolin was purified according to Yin et al(162).

4.3 Results

Previously Cary et al presented evidence that a myc-epitope tagged vimentin tail polypeptide colocalizes with actin-rich structures in cultured cells(10). Given that vimentin polypeptides typically form parallel dimers, a dimeric form of the vimentin tail domain was constructed by

introducing a single cysteine residue between the N-terminal myc-epitope and the vimentin tail domain (figure 4-1). As in the case of the original mycVimTail polypeptide, the myc-cys-VimTail polypeptide could be purified to homogeneity from bacteria. Under reducing conditions, the purified vimentin tail peptide migrated by SDS-PAGE as a single band with an apparent molecular weight of ~15 kDa; the oxidized form migrated with an apparent molecular weight of 25 kDa (figure 4-2). Under the mild reducing conditions used in the experiments some fraction of the vimentin tail peptide was dimerized.

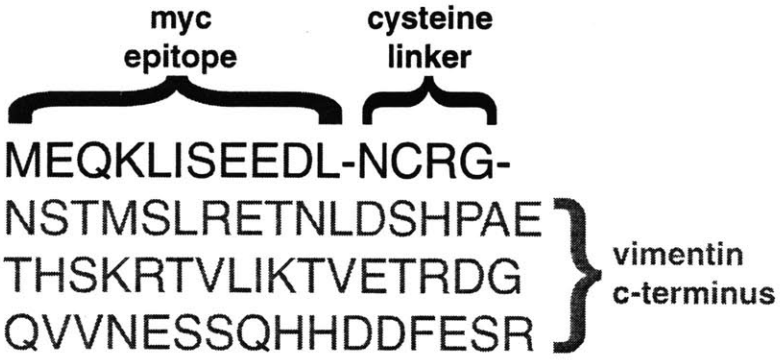

Figure 4-1: **Sequence of the myc-cys-vimentin tail peptide.**

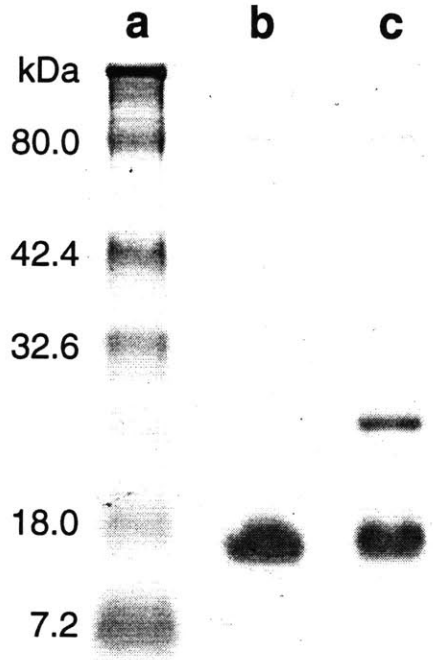

Figure 4-2: **SDS-PAGE analysis of myc-cys-VimTail.**
The myc-cys-VimTail polypeptide was analysed by SDS-PAGE following reduction (lane **b**) or in the absence of reducing agents (lane **c**). Molecular weight standards are shown in lane **a**.

4.3.1 Vimentin tail peptide does not affect actin polymerization

Pyrene assembly experiments were conducted in the presence of varying concentrations of the vimentin tail peptide. The principle of this assay is the finding that monomeric actin labeled at cys-374 with pyrene-iodoacetamide undergoes a 25x increase in fluorescence intensity when the actin subunits are incorporated into filaments(75). Therefore, changes in fluorescence are a quantitative measure of the kinetics and extent of actin polymerization.

The kinetics of actin polymerization with and without the vimentin tail polypeptide demonstrated no significant change in actin polymerization kinetics indicating that the peptide did not directly affect the polymerization of actin filaments (Sarah Michaud and Paul Janmey, personal communication).

4.3.2 Vimentin tail increases scattering from f-actin solutions

Dynamic light scattering (DLS) of actin filament-vimentin peptide mixtures were performed under reducing conditions to investigate the possible binding of the peptide to actin filaments. For long polymers arranged in an interpenetrating meshwork with mesh size (interfilament distance) much less than the filament length, measurements of DLS are dominated by bending motions of the filaments(68, 129). Ligands that bind the side of the actin filament and alter filament stiffness or induce the filaments to form bundles retard the rate of autocorrelation decay. The rate of intensity autocorrelation function decay can then be used to detect filament bundle formation independent of the measure of total scattering intensity which also increases with increasing bundle diameter. Preliminary measurements indicated that the myc-cys-vimentin-tail peptide tended to aggregate in the absence of f-actin thereby increasing the scattering intensity. The value for scattering from the peptide alone was subtracted from the total scattering of actin-peptide mixtures to qualitatively correct for the different scattering particles. Figure 4-3A shows that the total scattering intensity from a network of f-actin increased with increasing concentration of the vimentin peptide, strongly suggesting the formation of actin filament bundles since the extent of polymerization is nearly complete for actin alone and the mass contributed by the vimentin peptide is too small to account for the large change in scattering intensity. In addition to the increased total scattering, the intensity autocorrelation functions shown in figure 4-3B decayed more slowly at higher concentrations of vimentin peptide which along with the increase in scattering intensity support the interpretation that thicker filaments, or bundles, have formed.

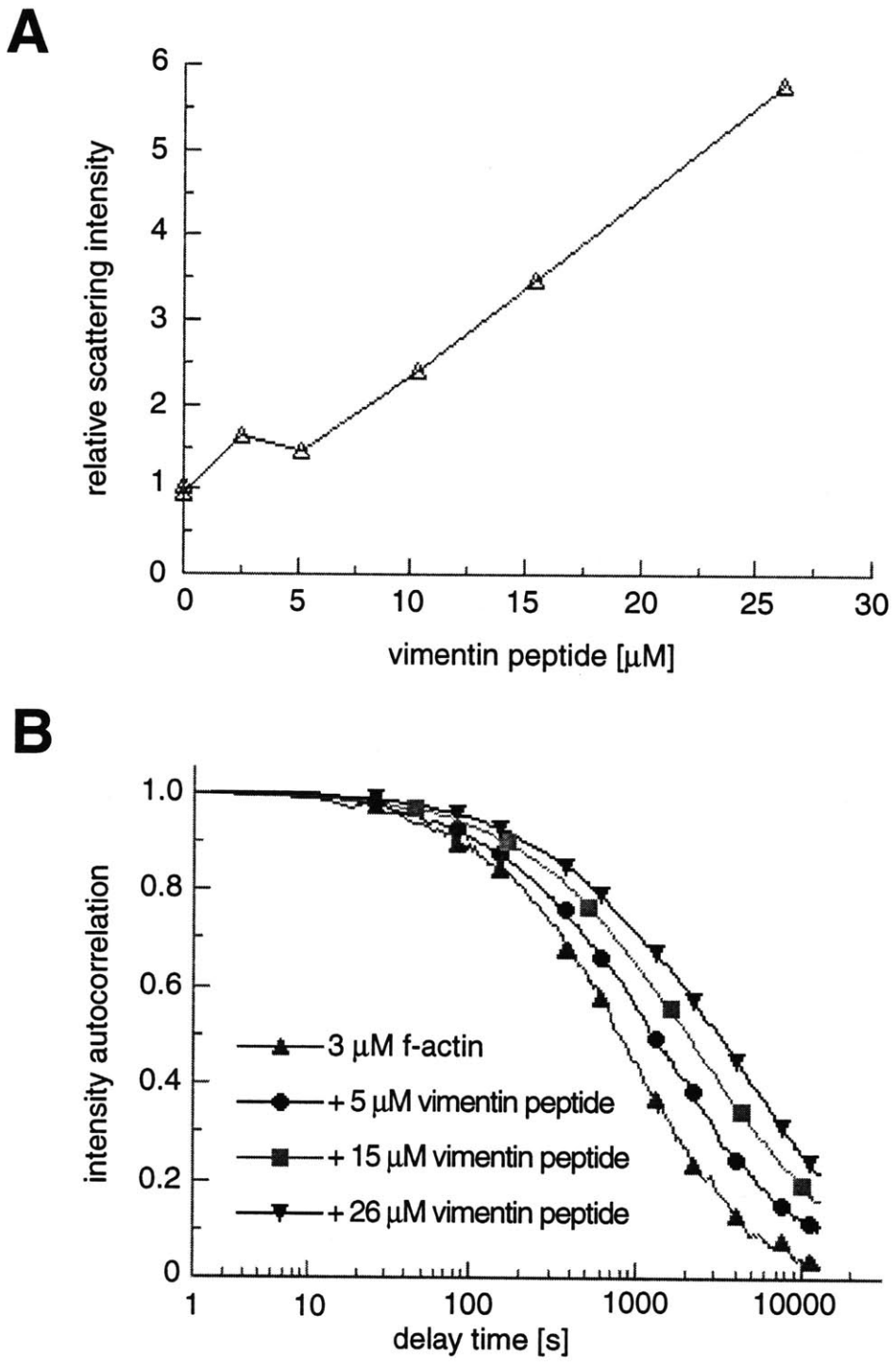

Figure 4-3 : **Effect of vimentin peptide on dynamic light scattering from f-actin.** **A**, Total scattering intensity for 3 μM f-actin with various concentrations of vimentin peptide. **B**, Scattering intensity autocorrelation functions for the same conditions as in **A**. Reaction conditions are given in materials and methods.

4.3.3 Vimentin tail cosediments with f-actin

F-actin was sedimented in the presence of various concentrations of vimentin tail polypeptide. Supernatants and pellets were analysed by SDS-PAGE (figures 4-4 and 4-5). Vimentin tail polypeptide in the pelleted f-actin was further analysed by densitometry. No detectable vimentin tail pelleted in the absence of f-actin, indicating that the sedimented vimentin tail was bound to f-actin. Figure 4-6 shows the densitometric signal from the sedimented vimentin tail as a function of the total vimentin tail concentration. The vimentin tail signal in the pellet increases to a plateau for increasing vimentin tail indicating saturable binding to f-actin.

4.3.4 Increasing vimentin tail decreases supernatant actin

Analysis of actin content of sedimentation supernatants indicated a decrease in coomassie signal as vimentin tail concentration was increased (figure 4-7). The decrease in supernatant actin is consistent with vimentin tail, or possibly vimentin tail dimers, bundling actin filaments. This would allow small actin oligomers which would not usually sediment to form large, sedimentable complexes with other actin filaments.

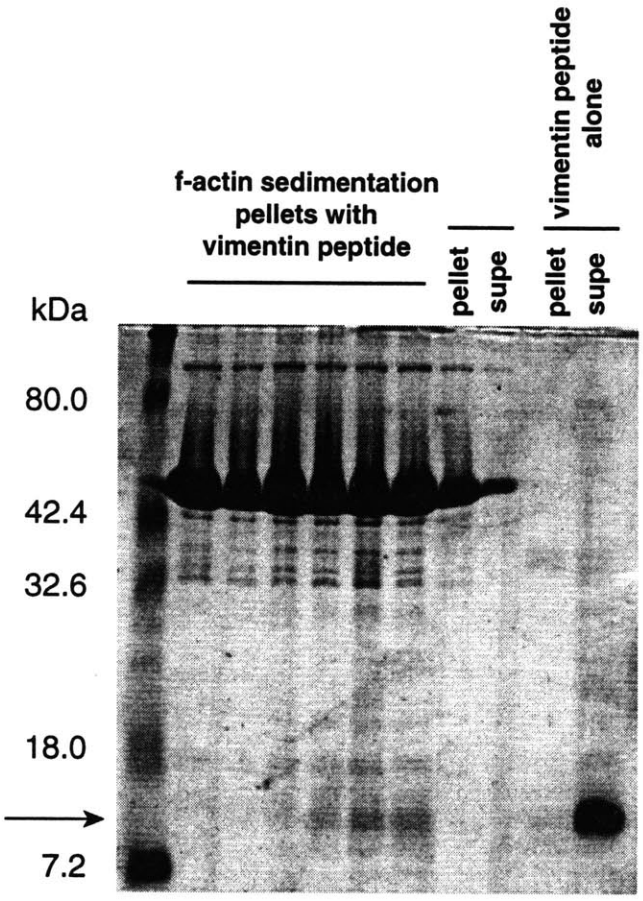

Figure 4-4 : **SDS-PAGE analysis of f-actin co-sedimentation pellets.** Electrophoretic analysis of pellets of 12 μM f-actin centrifuged with (from left to right) 0.6 μM, 1.3 μM, 3.1 μM, 6.3 μM, 9.4 μM and 12.6 μM vimentin peptide. Centrifugation of 12 μM f-actin alone and 12.6 μM vimentin peptide alone is also shown. The vimentin peptide in pellets is highlighted by the arrow.

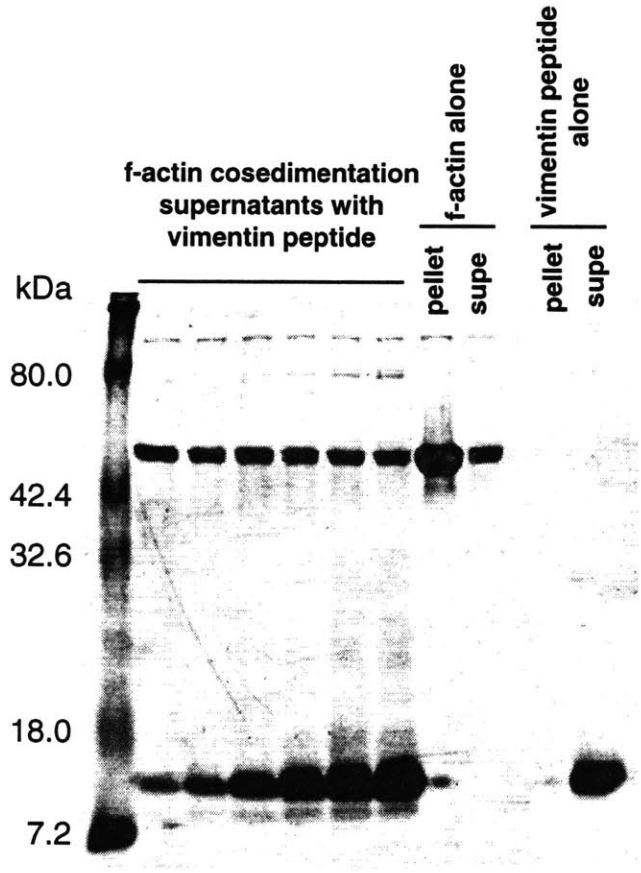

Figure 4-5 : **SDS-PAGE analysis of f-actin co-sedimentation supernatants.** Electrophoretic analysis of supernatants of 12 μM f-actin centrifuged with (from left to right) 0.6 μM, 1.3 μM, 3.1 μM, 6.3 μM, 9.4 μM and 12.6 μM vimentin peptide Centrifugation of 12 μM f-actin alone and 12.6 μM vimentin peptide alone is also shown.

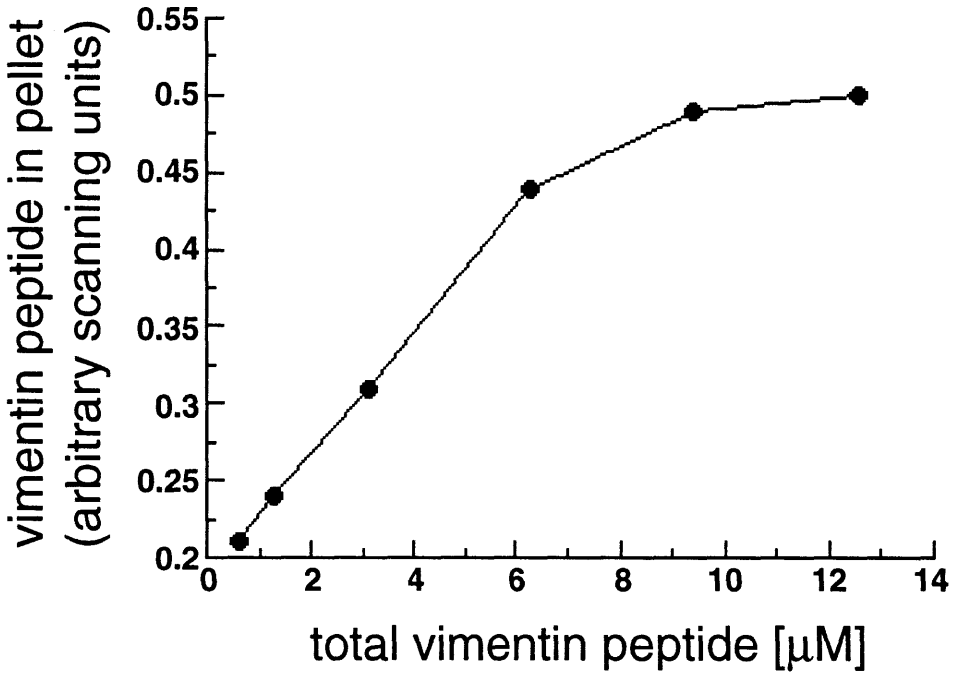

Figure 4-6 : **Vimentin peptide content in co-sedimentation pellets.** Myc-cys-VimTail peptide content in sedimentation pellets is shown in arbitrary densitometric units for a range of total vimentin peptide concentrations.

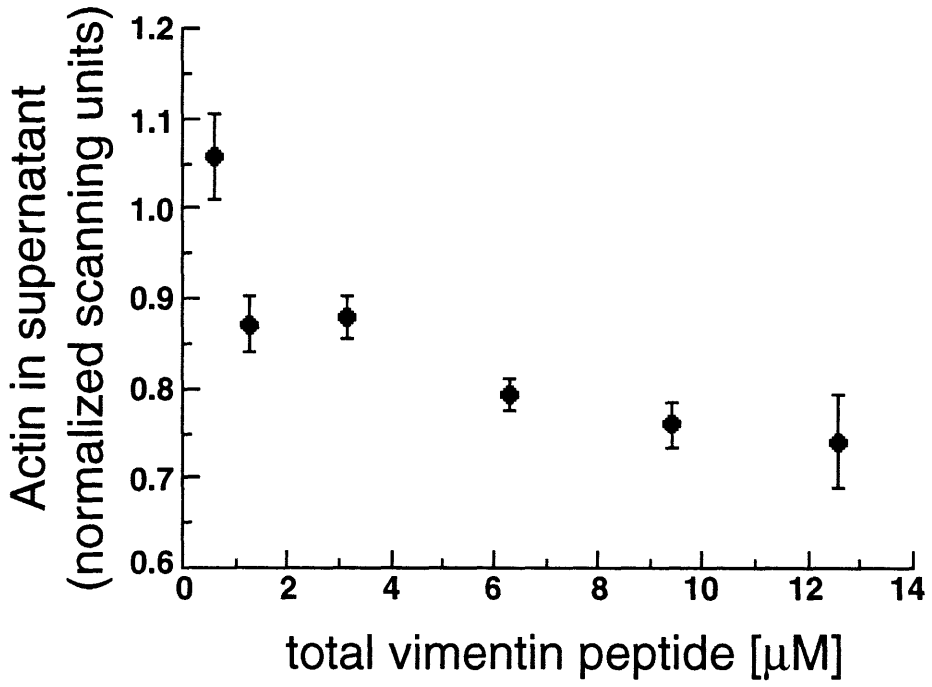

Figure 4-7 : **Actin content of co-sedimentation supernatants.**
Actin content in sedimentation assay supernatants is shown in arbitrary units normalized to a control supernatant (no vimentin peptide) for a range of vimentin peptide concentrations (mean +/- standard error).

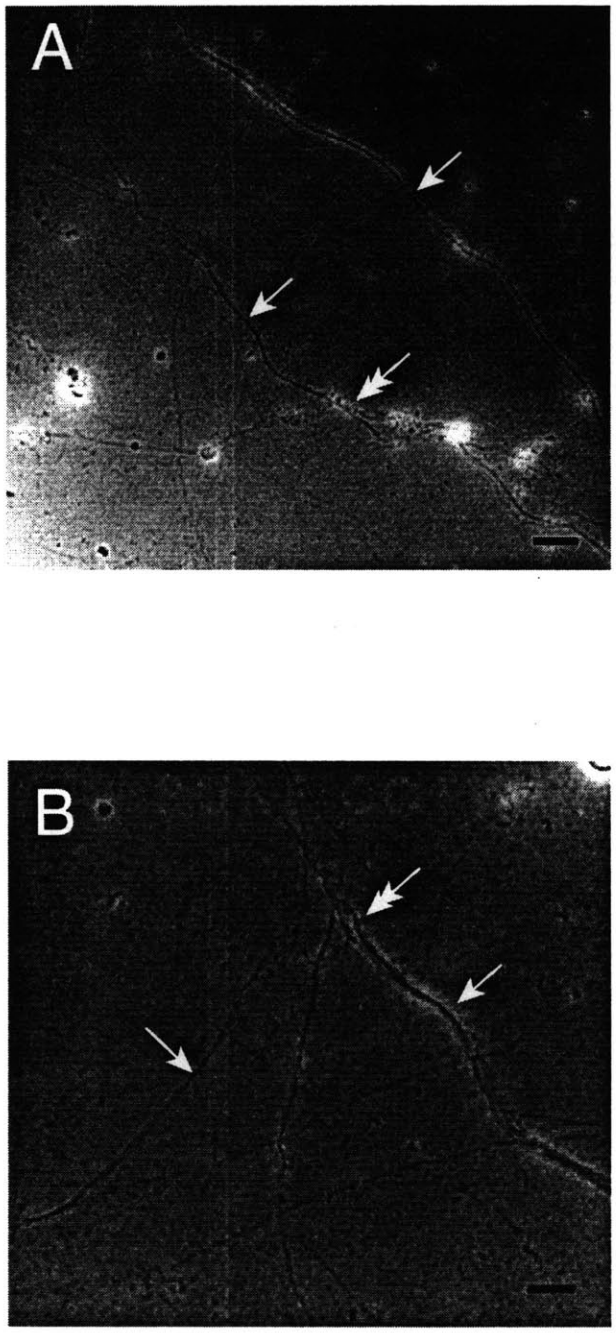

Figure 4-8 : **Electron micrograph of f-actin-vimentin peptide mixture.** Representative fields from uranyl acetate stained f-actin-vimentin peptide mixture. Arrows indicate bundled actin filaments and double arrowheads indicate unraveling bundles. Scale bar in **A** is 200 nm, in **B** is 100 nm.

4.3.5 Vimentin tail bundles actin filaments

The effect of the vimentin tail polypeptide on f-actin was examined by electron microscopy to determine any possible ultrastructural changes. Figure 4-8 demonstrates the presence of bundles when vimentin tail is mixed with actin filaments. In the absence of vimentin tail, bundles are not present and only single actin filaments are observed.

4.4 Discussion

Previous studies have described a possible direct interaction of vimentin with f-actin (10, 133, 145). Following the in vivo work of Cary et al, a C-terminal vimentin peptide was investigated for its role in the vimentin-f-actin interaction. The tail domain of vimentin is thought to play a role in the localization of vimentin filaments(120) and has been implicated in filament assembly(3, 47, 94). Using a variety of biochemical techniques, it was determined that the vimentin tail peptide bound and bundled actin filaments. The direct binding of a the tail domain of vimentin to f-actin illustrates the role for direct, passive binding between filaments of the cytoskeleton.

4.4.1 Binding and bundling ability of the vimentin peptide for f-actin

The purified tail domain of vimentin bound to actin filaments as observed by cosedimentation experiments. Not only did the vimentin tail pellet with the f-actin, but it also decreased the amount of non-sedimented actin. Such a finding could be a result of two mechanisms. The vimentin tail could increase total polymer mass by affecting the polymerization of actin directly by shifting the equilibrium to a higher polymer to monomer ratio. The vimentin tail could also bundle the actin filaments resulting in complexes which includes small actin oligomers which would not have previously spun down.

Using a pyrene based assembly assay, the effect of the vimentin tail on actin polymerization was insignificant indicating no effect actin polymerization. To test the possible bundling ability of the peptide, DLS and EM observations were carried out. The light scattering demonstrated an increase in scattering intensity with increasing vimentin peptide consistent with binding of the peptide to f-actin. In addition the DLS results showed a decrease in the rate of decay in the intensity autocorrelation function with increasing vimentin peptide. The decrease in decay rate is consistent with the formation of bundles of filaments which are stiffer and flex more slowly than single filaments. Electron microscopy of vimentin tail-f-actin mixtures directly demonstrated the ability of the vimentin tail to form f-actin bundles (figure 4-8). The DLS and EM evidence indicate

that the vimentin tail is capable of bundling actin filaments.

An important difference between the peptide used by Cary et al and this investigation is the existence of a single cysteine residue in this study. This single cysteine can be used to crosslink the peptide into a dimeric form. The experiments described here were carried out under mild reducing conditions where some fraction of the peptide is dimeric (figure 4-1 lane C). The dimeric form of the peptide is the most likely explanation for the bundling ability of the vimentin tail, much like other actin-binding proteins such as alpha-actinin. Another possible bundling mechanism could be a counterion condensation mechanism as described by Tang and Janmey(143). However, the counterion induced bundling uses polyvalent cations or cationic proteins to promote an effective decrease in the surface charge of the actin filament allowing them to aggregate. The vimentin peptide used has a net negative charge (figure 4-1) and thus the counterion mechanisms are unlikely to play a primary role in the bundling of actin filaments. Further studies with a vimentin tail peptide without the cysteine residue or blockage of the cysteine with agents such as N-ethylmaleimide(NEM) can aid in dissecting the role of the peptide dimer in actin bundling. In addition, the specificity of the interaction could be tested by using a scrambled peptide to confirm that the binding is due a particular sequence.

4.4.2 Possible roles for vimentin-f-actin interactions

The direct binding of the vimentin c-terminus to f-actin may underlie a novel example of a passive binding interaction between different filaments in the cytoskeleton. There are many proteins that mediate passive binding between cytoskeletal filaments both within a filament system (e.g. filamin for f-actin, MAPs for MTs) and across filaments systems as documented in table 1-1. The role of a full-length vimentin-f-actin interaction in a mechanical context has been previously studied by Janmey and colleagues(69). Figure 4-9 illustrates the shear elastic modulus of f-actin-vimentin mixtures. Panel A describes the effect of long actin filaments, modulated by gelsolin(67), in vimentin-f-actin network mechanics. Panel B represents a similar experiment but carried out with short actin filaments. In both long and short filaments, the mechanical response is very different from each of the networks alone or from a simple linear superposition of the responses. An f-actin-vimentin composite within the cell is one possible implication of the c-terminus-f-actin interaction.

The f-actin-vimentin composite has not been studied at the ultrastructural level but two geometries of interaction are possible. The vimentin filament may act to bundle the actin filaments forming large diameter filaments throughout the network (figure 4-10A). Alternatively, the f-actin and vimentin may form an isotropic crosslinked network (figure 4-10B) or both interactions could co-exist. In either case, the observed macroscopic properties of the resulting network indicate

mechanical effect of a direct vimentin-f-actin interaction.

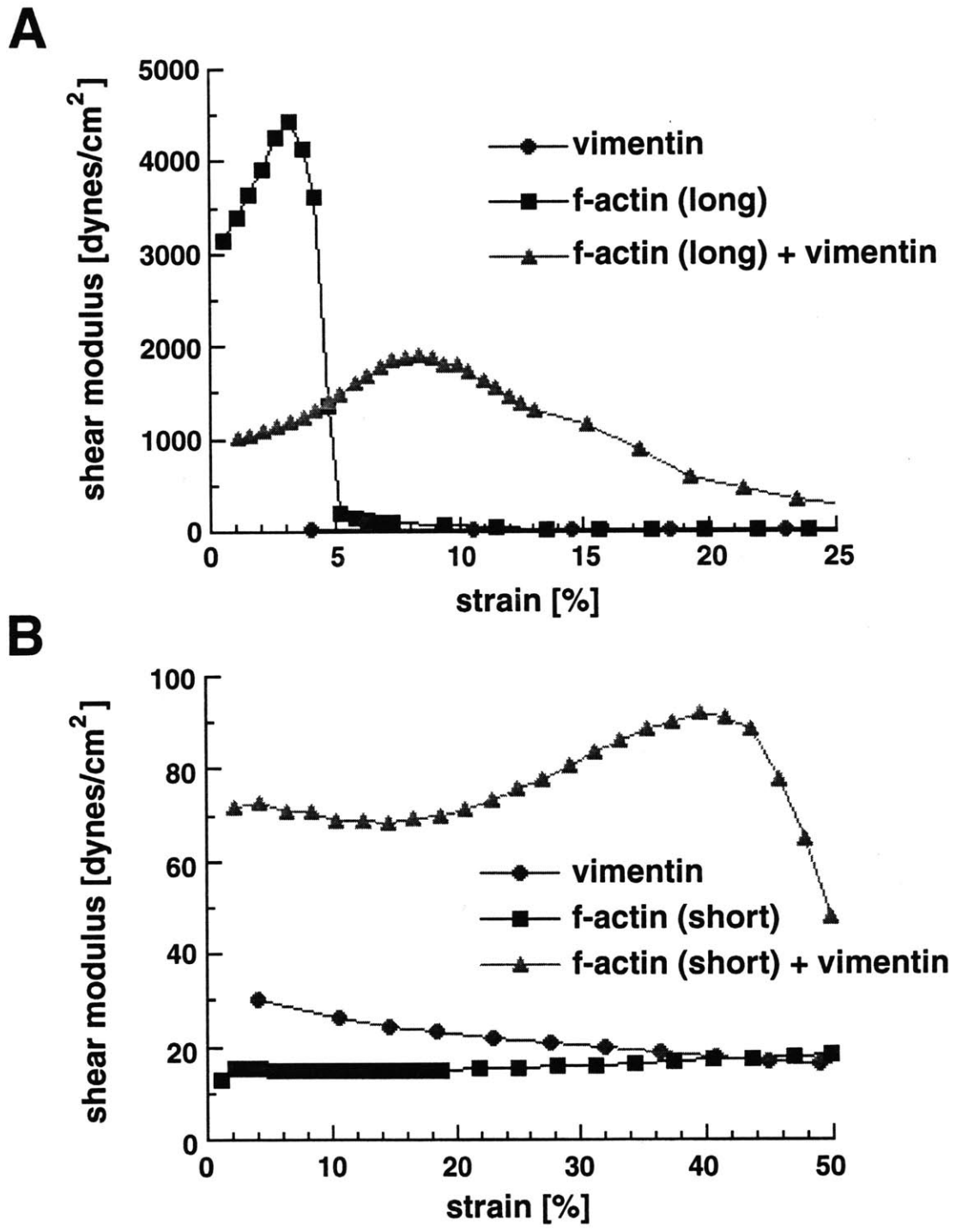

Figure 4-9 : **Effect of full length vimentin on the mechanical properties of f-actin networks.** **A**. 2 mg/ml vimentin (circles) was measured alone or polymerized together with 2.3 mg/ml actin and gelsolin at a 8000:1 actin:gelsolin molar ratio (triangles). The shear moduli for 2.3 mg/ml actin polymerized without vimentin is given by the squares. **B**. Similar conditions as for **A** but with 1.2 mg/ml actin and an actin:gelsolin ratio of 300:1.

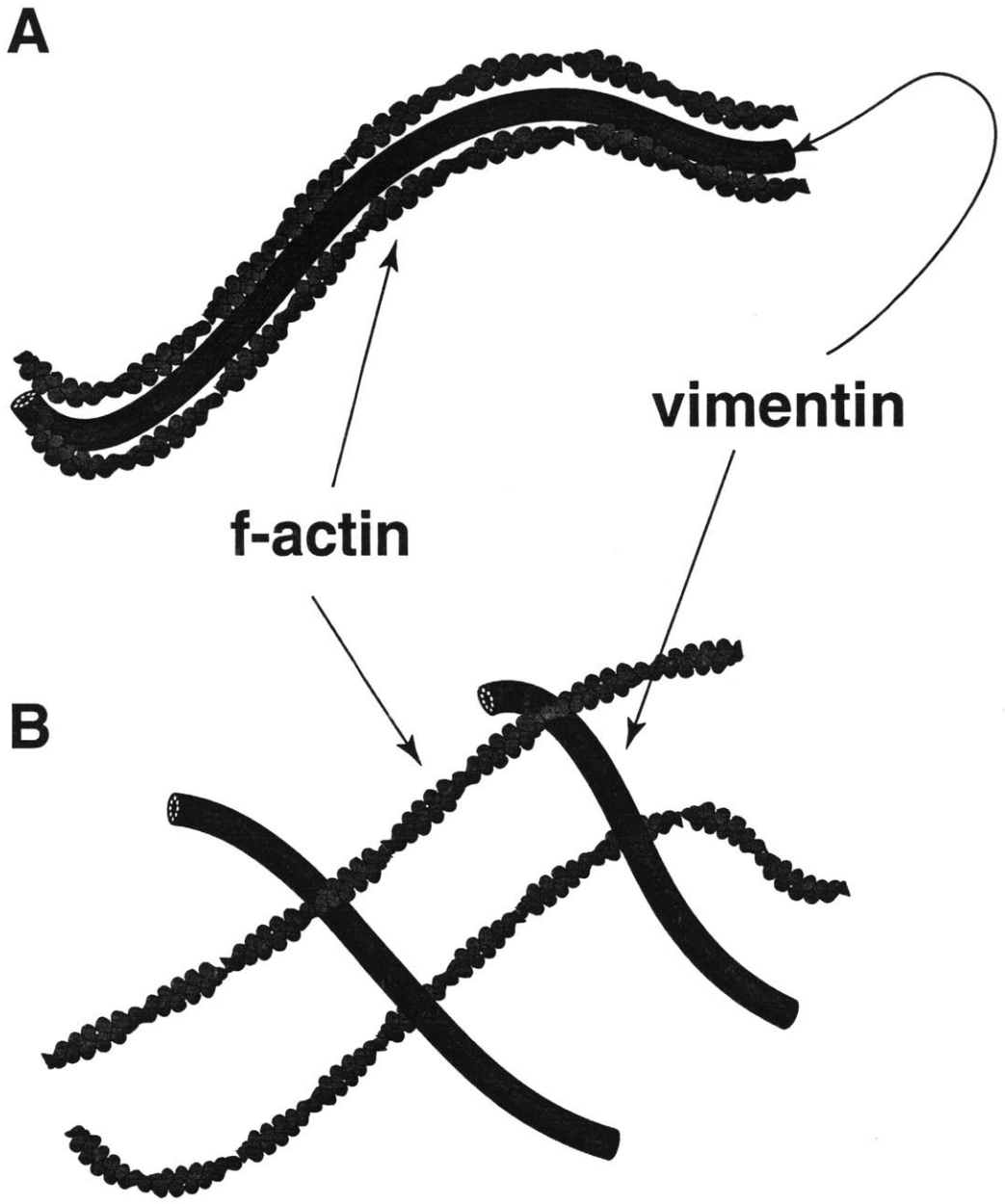

Figure 4-10 : **Model of full length vimentin-f-actin binding.**
The peptide binding studies implicate two geometries of f-actin-vimentin interaction. **A**, Full length vimentin may bundle f-actin and form large composite fibres or **B**, full length vimentin and f-actin may interact infrequently and form an isotropic network.

The possible full length vimentin-f-actin interaction is an example for a passive interaction between cytoskeletal filaments and found in polymer networks generally. The next chapter outlines a novel interaction between neuronal IFs and MTs which is mediated by force-generating MT motor proteins. This type of interaction is unique to biological systems and presents interesting material and transport issues for the cell.

Chapter 5

Neurofilament translocation along microtubules

5.1 Introduction

Intermediate filaments (IFs) are composed of cytoskeletal proteins that assemble into 10 nm filaments within the cytoplasm of most multicellular organisms(30). A diverse family of intermediate filament proteins are differentially expressed in specialized tissues. The putative role of IFs in vivo is to maintain cellular, and thereby tissue, integrity under mechanical stress(29, 32). IFs perform this function through unique mechanical properties(64, 85) and interactions with both f-actin(10, 133, 145, 161) and microtubules(48, 50, 84, 116, 140) to form an integrated filament network throughout the cytoplasm(53).

Neuronal cells are enriched in specialized IFs, neurofilaments (NFs), which are composed of three subunits, NF-L, M and H (low, medium and high) based on their electrophoretic mobility. The NF-H and M subunits bear sidearms that are thought to link NFs to each other and to other cellular structures, such as microtubules(50) and mitochondria(84). The transient or stable interactions of NFs with each other and with other cytoskeletal elements form a dynamic scaffold that is essential in maintaining axonal calibre(51).

This chapter demonstrates that MT-based molecular motors copurify with native neurofilaments and mediate their bidirectional translocation along MTs in vitro. Biochemical and immunological analyses indicate that dynein and dynactin are in part responsible for the minus end directed motion of NFs on MTs and suggest that a number of kinesin-related proteins make up the complement of the motility. In addition, dynein and at least one kinesin isoform (KIF3A) remain bound under a number of biochemical treatments of the NF preparation indicating that the motors are strongly bound to the NFs. These data suggest that a mechanism of saltatory bidirectional motion can be responsible for the slow net velocity observed for axonal NF transport.

5.2 Materials and methods

5.2.1 Purification and fluorescent labelling of native neurofilaments

Native neurofilaments were prepared from freshly obtained bovine (Arena and Sons, Hopkinton, MA) or rat spinal cords (INSERM Animal facility, Angers, France) according to Leterrier and Eyer(83) with modifications(85). Spinal cords were homogenized with an equal volume of RB

buffer (0.1 M MES (2-(N-morpholino) ethanesulfonic acid), 1 mM EGTA, 1 mM MgCl2, pH 6.8) with 100 µM PMSF (phenylmethylsulfonyl fluoride). The homogenate was centrifuged at 100 000 g for 60 minutes at 4 C and the supernatant was removed and mixed with a 50% volume of pure glycerol. This glycerol mixture was incubated at 4 C for at least three hours and then centrifuged at 100 000 g for 60 minutes at 4 C. The resulting supernatant is discarded and is designated 'supe' in subsequent figures. The pellet was homogenized with RB (10% of the original homogenization volume) including a protease inhibitor mixture (1 µM leupeptin, 1 µM pepstatin A, 0.05 mU/ml aprotinin, 100 µM chloroquine, 10 nM soybean trypsin inhibitor, 100 µg/ml TAME (Nα-p-tosyl-L-arginine methyl ester), 100 µM TLCK (Nα-p-tosyl-L-lysine chloromethyl ketone)). The homogenized pellet is the crude NF fraction and is designated 'crude' in subsequent figures. The crude NF fraction is loaded on a two step sucrose cushion (0.8 M and 1.5 M sucrose in RB) and subsequently centrifuged at 150 000 g for 10 hours at 4 C. The supernatant is collected by approximate sucrose content. The pellet is the NF fraction and is resuspended in RB with 0.8 M sucrose and protease inhibitors. NFs purified in this manner are highly phosphorylated.

NFs were fluorescently labelled by addition of rhodamine B N-hydroxy succinimidyl ester (a kind gift of Dr. Roland Vegners, Latvian Institute for Organic Synthesis, Riga, Latvia) to the crude NF homogenate, incubated for 30 minutes at 4 C and subsequently spun on a step sucrose cushion, as described above, to simultaneously purify NFs and eliminate unconjugated dye.

Fluorescent gel analysis was carried out on a BIO-RAD Fluor-S Multi-Imager (BIO-RAD, Hercules, CA). SDS-PAGE was carried out according to standard methods(79).

NFs were dephosphorylated by addition of 5 U/ml E.coli alkaline phosphatase (Sigma, St. Louis, MO) and incubated in dialysis against RB buffer (0.1 M MES (2-(N-morpholino) ethanesulfonic acid), 1 mM EGTA, 1 mM MgCl2, pH 6.8) at 4 C for 48 hours. Okadaic acid, a phosphatase inhibitor, (Sigma Chemicals, St. Louis, MO) incubated at 4 µM with NFs for 24 hours at 4 C, after which the NF solution was dialysed for 24 hours against RB buffer at 4 C.

Biochemical treatments of NFs were carried out by incubating the NFs with the appropriate treatment, either 1% Triton X-100 (non-ionic detergent), 1 M KCl, 0.6 M KI or RB buffer as a control treatment. After incubation at 4 C for 30 minutes, the NFs were sedimented through a 0.8 M sucrose cushion at 100 000 g for 60 minutes. The NF pellets were resuspended and dialysed against RB buffer for 24 hours before being prepared for SDS-PAGE, immunoblot and motility analysis.

5.2.2 Purification, labelling and assembly of microtubules

Purified tubulin was either prepared from bovine brain microtubules(95, 150) or a kind gift of Dr.

Christoph Schmidt (University of Michigan, Ann Arbor, Michigan). Tubulin was stored at -80 C in PEM-80 buffer (80 mM PIPES, 1 mM EGTA, 1 mM $MgSO_4$, pH 6.8). Tubulin was labelled with an Oregon Green 488 succinimidyl ester (Molecular Probes, Eugene, Oregon) or a rhodamine B N-hydroxy succinimidyl ester according to published protocols(55). Tubules were polymerized by increasing the temperature of monomeric solution to 37 C for 30 minutes in the presence of 1 mM guanosine triphosphate (GTP). The polymerized tubules were stabilized by the addition of taxol to 10 μM (paclitaxel, Calbiochem, La Jolla, CA). Polarity marked microtubules were prepared by nucleating an unlabelled/NEM-tubulin mix from brightly labelled tubule seeds(56).

5.2.3 ATPase assay

NF ATPase assays were performed as previously described(26). MT-stimulated activity was measured by the addition of 0.6 mg/ml taxol-stabilized tubulin polymer.

5.2.4 Motility assay

NF motility along MTs was carried out in flow chambers prepared from standard microscope slides adhered to a coverslip using double sided tape. The chamber was initially loaded with a dilute solution of polarity marked MTs in RBT buffer (0.1 M MES (2-(N-morpholino) ethanesulfonic acid), 1 mM EGTA, 1 mM $MgCl_2$, 10 μM taxol, pH 6.8). The MTs were allowed to adhere to the glass surface for 10 minutes. The chamber was then loaded with 10 μg/ml casein to block the remaining glass surface from nonspecific protein adsorption. The casein solution was flushed out after 10 minutes with 5 chamber volumes of RBT buffer. Fluorescently labelled bovine NFs were added to the chamber at 0.1-1 μg/ml. NFs were allowed to incubate with the MTs for at least 30 minutes. Excess NFs were removed by flushing the chamber with RBT buffer augmented with an oxygen scavenging anti-bleaching solution (2 mg/ml glucose, 0.1% ß-mercaptoethanol, 360 U/ml catalase, 8 U/ml glucose oxidase) (73). Biochemical and immunological effectors of motility were pre-incubated with the NFs before addition to the motility chamber. Vanadate experiments were carried out at pH 7.5 and without ß-mercaptoethanol to prevent vanadate oligomerization and reduction(111). These changes did not affect ATP dependent translocation. Antibody experiments were carried out at 1:100 dilutions unless otherwise indicated. All translocation assays were carried out at room temperature.

5.2.5 Motility analysis

Fluorescent filaments were visualized on a Nikon Diaphot 300 inverted microscope equipped with epifluorescence optics and a high numerical aperture objective. Motility was recorded by a SIT camera (DAGE-MTI 64L, Michigan, IL) and digitized to a computer. All video data were captured at 1 frame per second.

Bulk motility analysis (i.e. no polarity considerations) was carried out by viewing video sequences and determining the ratio of translocating NFs to the total number of MT-bound NFs. Motile NFs were determined qualitatively by visual inspection. For each condition tested at least 10 video sequences were inspected comprising at least 150 NFs.

Motile NF trajectories were measured by visual marking of NF centres using NIH-Image (NIH, Bethesda, MD). These trajectories were then projected onto the MT contour to yield a one dimensional trajectory. Point to point velocity analysis (at one second intervals) of the NF trajectories demonstrated a significant discretization artifact (figure 5-1). The resolution of the system was approximately 160 nm/pixel. The recurring peaks in the point to point velocity histogram correspond to the motion of one or two pixels over one second. Since the frames were acquired at one frame per second, these peaks are a result of human tracing error. To overcome these problems, the raw trajectory data was subjected to an algorithm which extracted persistent motions greater than three seconds in length. Briefly, the algorithm checks a rolling linear fit of the trajectory and those points which have a correlation coefficient (r^2) greater than 0.99 are treated as one motile event. A number of analyses were made on the processed trajectory data.

Net velocity analysis on processed trajectories was carried out by calculating the net displacement over the duration of each motile event. All the non-motile time is eliminated from the trajectories in this analysis and as a result the net velocities are much higher than would be expected from direct observation. The elimination of the non-motile time focusses the analysis on net displacements rather than possible increases in non-motile time which could also affect the net velocity.

The motility was also subjected to a transition probability analysis. Here the transitions between plus ended, zero and minus ended velocity states are expressed as probabilities. These probabilities are calculated as the fraction of transitions from state A which end up at state B. In this case the analysis of the processed trajectories included the non-motile time points. Using the transition data, a histogram of time spent in each state was also calculated for each movie. The time spent in each state was expressed as a percentage of the duration of the video sequence and averaged over all sequences in each condition.

Statistical significance was tested by ANOVA analysis using the STATISTICA software package (Statsoft, Tulsa, OK).

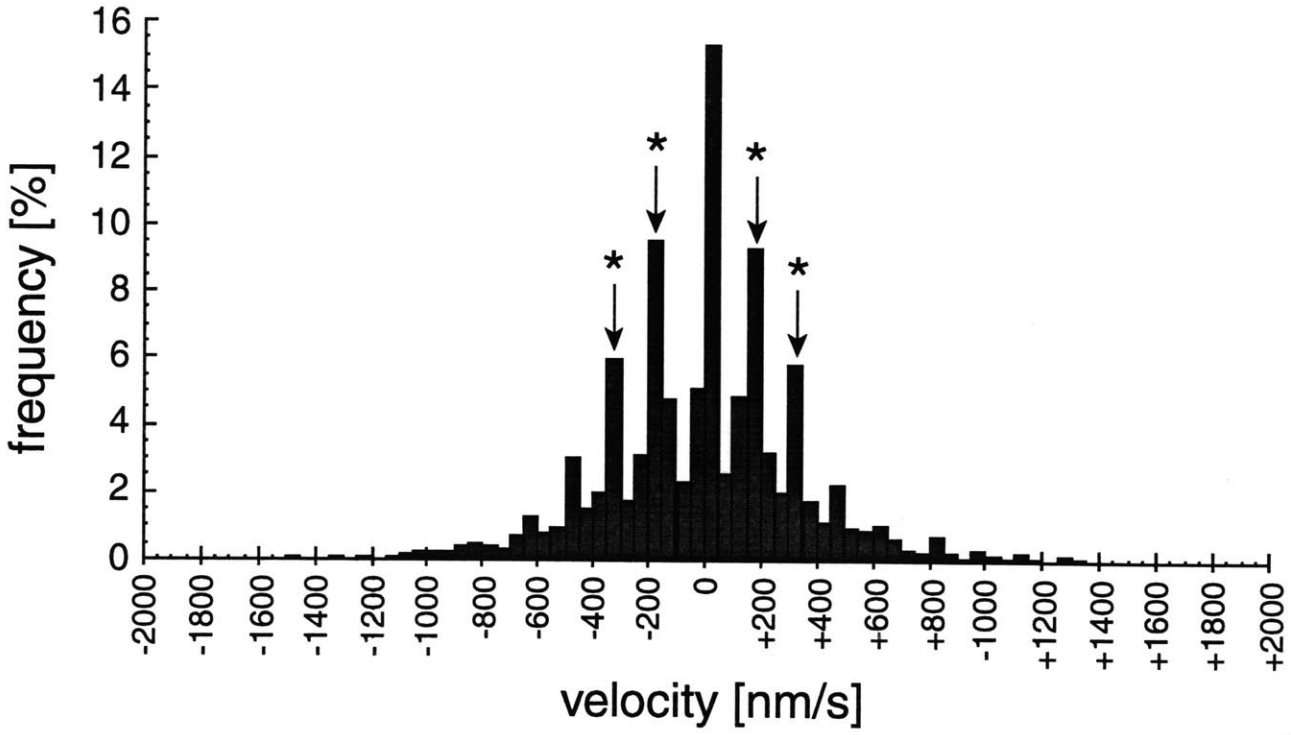

Figure 5-1 : **Velocity histogram of unprocessed trajectories illustrates a digitization artifact.** Calculation of NF velocities from unprocessed trajectories yields a histogram with a set of characteristic peaks (asterisks). These peaks correspond to a motion of one or two pixels in one video frame. The dominant nature of these peaks indicate that error in marking the trajectory has a significant effect on simple velocity calculations. An algorithm was applied to the trajectories to extract the persistent motions and remove short, quick motions which may be due to marking error. These processed trajectories were used in the motility analysis.

5.2.6 Antibodies

Commercial antibodies were obtained from Chemicon (Temecula, CA) for the detection of dynein intermediate chain (74.1) and anti-kinesin (H1). CapZ subunits (α subunit monoclonal 5B12 ; ß subunit monoclonal 3F2) were purchased from the Developmental Studies Hybridoma Bank (Iowa). Anti-kinesin II, K4.2 antibodies were purchased from BABCo (Berkeley, CA). Anti-neurofilament SMI-31 and SMI-32 were purchased from Sternberger Monoclonals (Lutherville, MD) and anti-GFAP was purchased from Sigma Immunochemicals (St. Louis, MO). Immunoglobulin isotype controls were purchased from Sigma Immunochemicals (St. Louis, MO). Dynactin antibodies (anti-p150^{glued}, anti-p50) were kindly provided by K.T. Vaughan and R. Vallee (University of Massachusetts Medical Centre, Worcester, MA), the anti-HIPYR kinesin peptide antibody was kindly provided by Arshad Desai and Timothy Mitchison (Harvard Medical School, Boston, MA), the conventional kinesin heavy chain antibody, SUK4, was kindly provided by Jonathan Scholey (University of California, Davis) and dynein heavy chain isoform 1b antibodies were kindly provided by J. Richard McIntosh (University of Colorado, Boulder). Anti-KIF3A antibodies were supplied in collaboration with Joe Marszalek and Lawrence Goldstein (University of California, San Diego). Adociasulphate-2 sponge toxin (AS-2) was supplied through a material transfer agreement by Lawrence Goldstein (University of California, San Diego). Immunoblotting was carried out according to standard methods(146).

5.2.7 Antibody disruption of dynein from NFs

NFs (0.04 mg/ml) were incubated with anti-dynein intermediate chain antibody (0.02 mg/ml), control antibody (IgG2b, 0.02 mg/ml, Sigma, St. Louis MO), or no antibody for 60 minutes at 4 C then pelleted at 100 000 g for 60 minutes on a step sucrose cushion in RB. Pellets were resuspended in SDS-PAGE sample buffer and subjected to SDS-PAGE and immunoblot analysis. The antibody signal was normalized to NF content in each lane to determine the amount of dynein intermediate chain that was displaced from the NFs.

5.2.8 Immunoelectron microscopy

Immuno-EM was performed by sequentially incubating glow-discharged, formvar-coated copper grids in the following solutions: RB, buffer A (RB + 2 M glycerol), NF diluted to 0.05 mg/ml in buffer A,10 min wash in buffer A, 10 min wash in buffer B (PBS + 1 M glycerol), 30 min in buffer B + 1% goat serum, 30 min in primary antibody diluted into buffer B + 1% goat serum, 3 x 10 min washes in buffer B + 0.1% goat serum, 30 min in secondary antibody (sheep anti-mouse coupled to 8 nm gold particles, kind gift of J.H. Hartwig) diluted into buffer B + 1% goat serum, 3 x 10 min washes

in buffer B + 0.1% goat serum, 1 x 5 min wash in buffer B, and 1 min in 2% uranyl acetate in deionized H_2O. Staining of MT-NF mixtures was carried out on glow-discharged, formvar-coated copper grids with 2% uranyl acetate. Grids were observed in a JEOL-1200EX electron microscope at 100 kV.

5.3 Results

5.3.1 Natively purified NFs have an associated a MT-stimulated ATPase activity

NFs were purified in their native polymerized state from bovine and rat spinal cords(83, 85). SDS-PAGE analysis of the purified NFs revealed greater than 95% neurofilament protein composed of the three subunits NF-H (200 kDa), NF-M (150 kDa) and NF-L (68 kDa) (figure 5-2A). A scan of a fluorescently labelled preparation (figure 5-2B) demonstrated primary incorporation of the fluorophore into the three NF subunits. A fourth band which appears in the fluorescence scan has been previously characterized as a mixture of glial fibrillary acidic protein and tubulin. Both contaminants vary widely in the levels with each preparation and do not qualitatively correlate to the motile characteristics described below. Electron microscopy of the NF preparation indicated the absence of MTs and membranous organelles (figure 5-3).

As previously described by Eyer et al(26), the NF preparation contains a significant ATPase activity. The ATPase activity was further characterized to demonstrate a modest (30-40% increase) stimulation by the addition of taxol-stabilized microtubules and sensitivity to micromolar vanadate and millimolar EDTA (figure 5-4) consistent with the presence of MT based molecular motors. Furthermore, inhibition at low vanadate concentrations (10 μM) is evidence for a dynein-like ATPase activity.

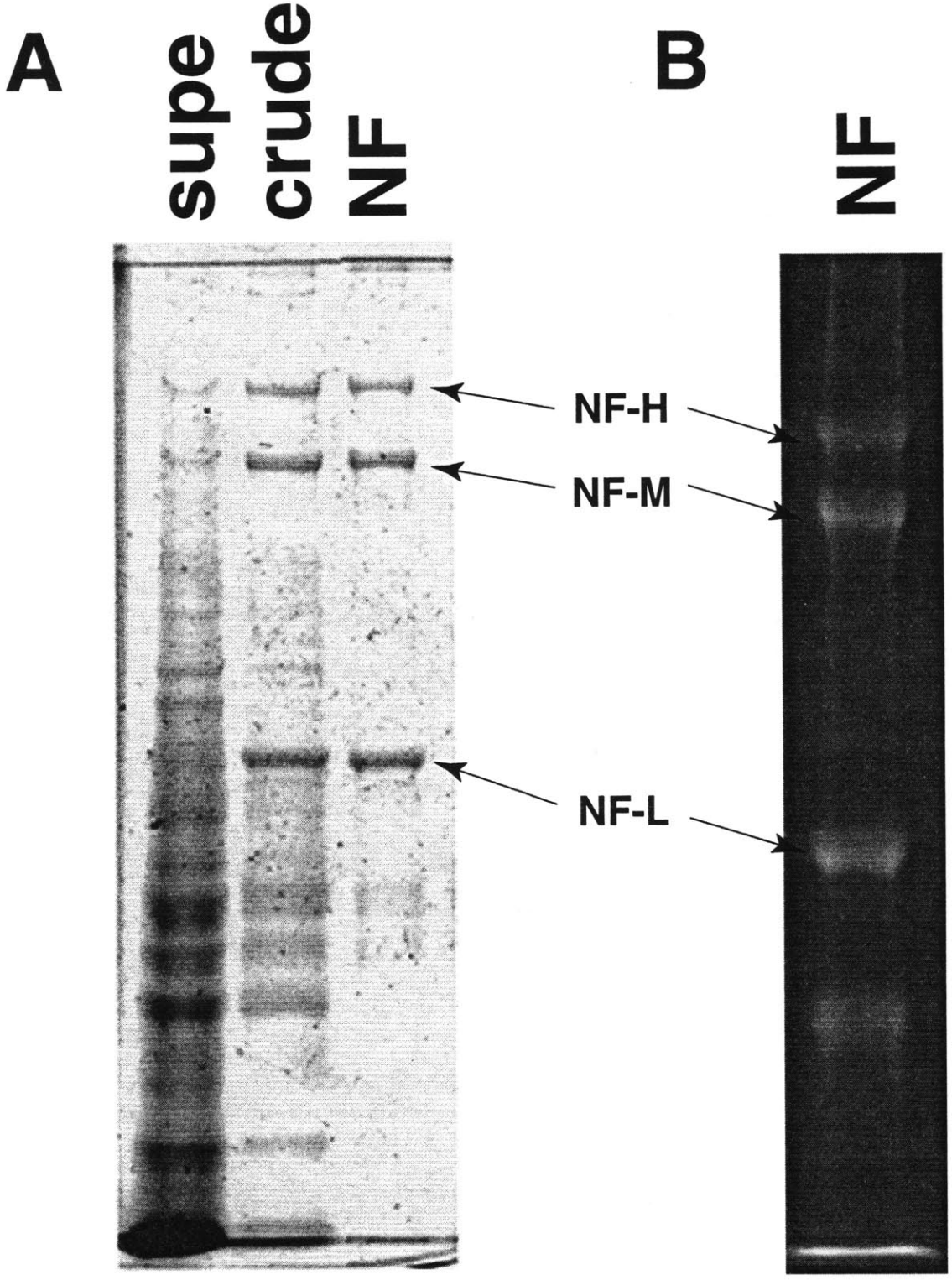

Figure 5-2 : **SDS-PAGE and fluorescence analysis of NF preparation.** **A**, SDS-PAGE analysis of a subset of the fractions from the NF purification shows the progressive enrichment of NF triplet protein in the preparation. Supe refers to the supernatant remaining after pelleting of crude NF, which were further purified over a 0.8 M sucrose cushion to give NF. **B**, Fluorescent scan of SDS-PAGE gel demonstrating incorporation of fluorescence into the three NF subunits.

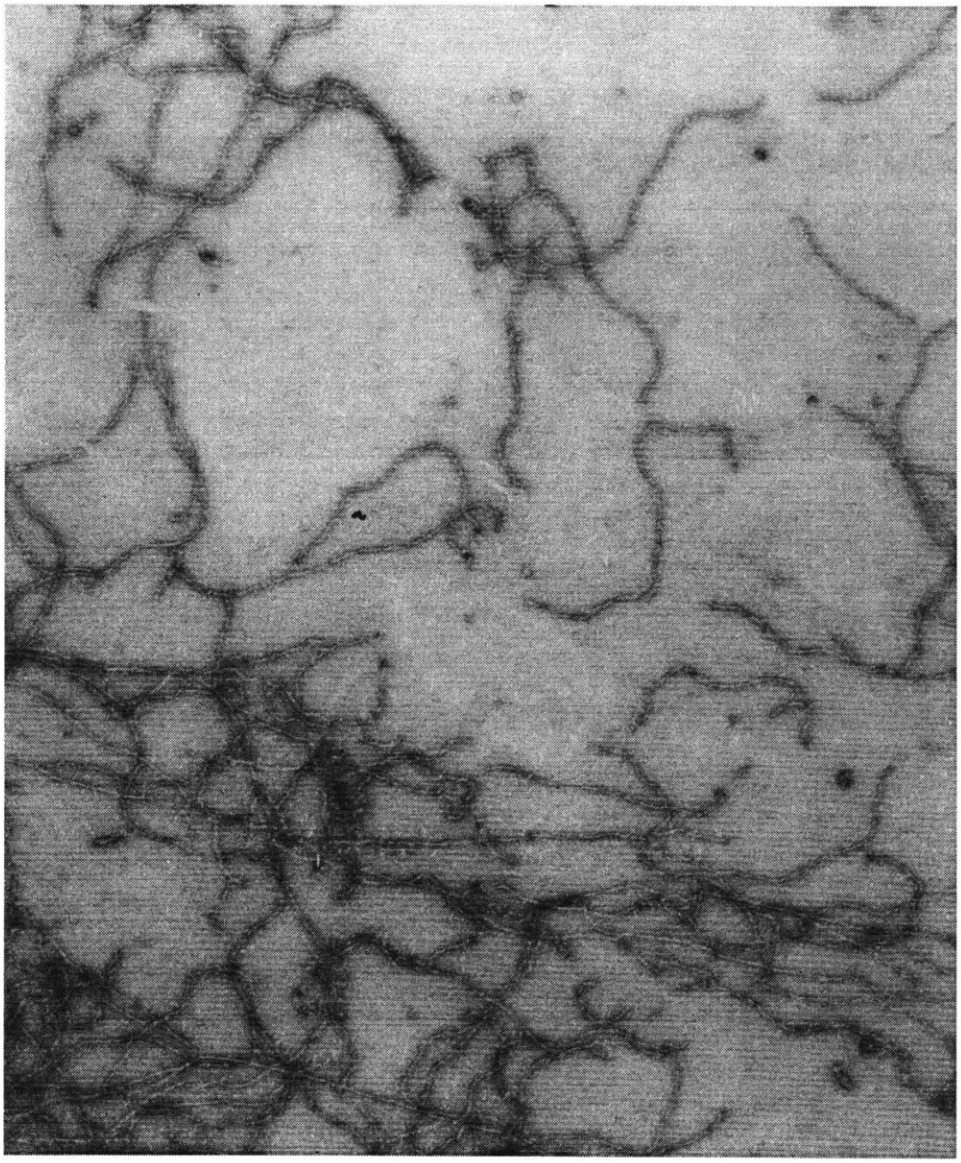

Figure 5-3 : **Electron micrograph of the NF preparation.**

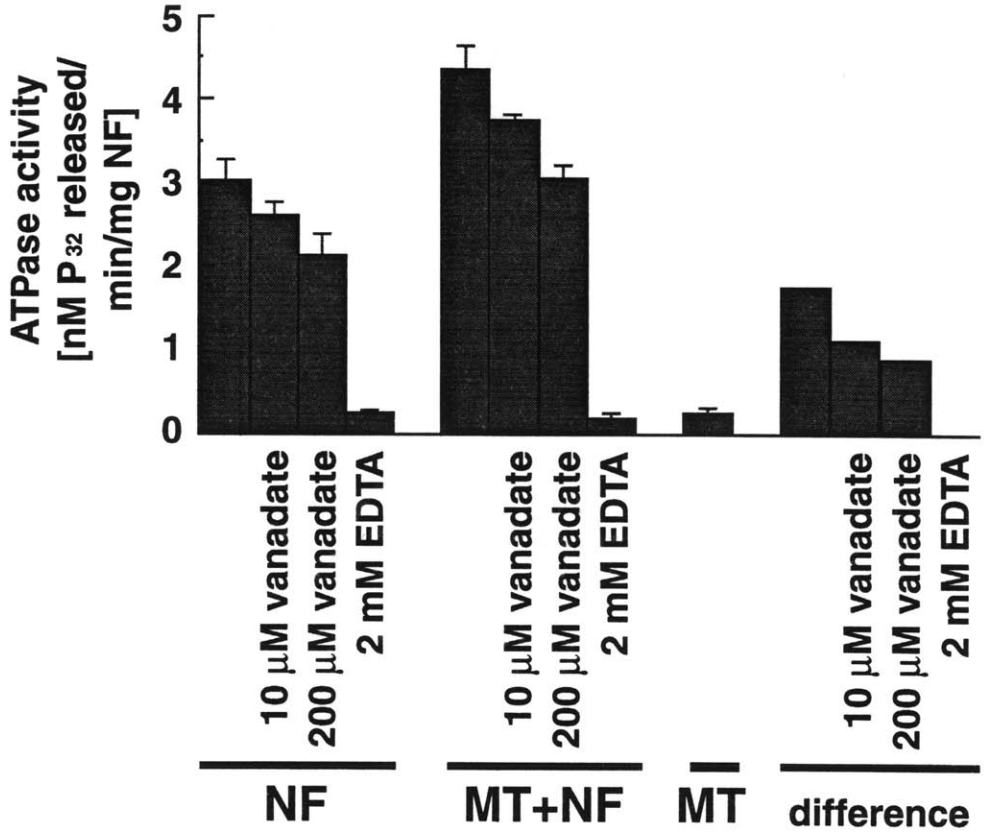

Figure 5-4 : **Microtubule stimulated ATPase activity of the neurofilament preparation.** The intrinsic ATPase activity of the NF preparation was stimulated by the addition of MTs. Furthermore, the activity was inhibited by micromolar vanadate and millimolar EDTA.

5.3.2 Native NFs translocate along MTs

To test the hypothesis that MT motors have copurified with NFs and that these motors can mediate NF transport, NFs were fluorescently labelled and their motion visualized on MTs fixed to a substrate. Due to their intrinsic flexibility, NFs appear as compact structures in solution and elongate into filaments when adsorbed to a glass surface(85). For motility assays, fluorescent, polarity marked taxol-stabilized MTs were adsorbed to the glass coverslip of a flow chamber and the remainder of the glass was blocked with casein. Rhodamine labelled NFs were introduced into the chamber at a low concentration to permit the visualization of single filaments. After incubation a large fraction of MT contours colocalized with compact NFs. Upon addition of ATP a substantial percentage of the MT-bound NFs (> 50 %) exhibited bidirectional motion along MTs. Figures 5-5A-C show representative video sequences of bidirectional NF translocation along MTs.

Figure 5-5A shows an example of a NF with one end bound to the glass and the other translocating bidirectionally along the MT contour. In this sequence the NF is extended from its compact conformation by the force provided by the MT motor. Figures 5-5B and 5-5C show examples of NFs moving along polarity-marked MTs. In Figure 5-5B the NF moves predominantly to the plus end of the MT while engaging in brief minus-ended excursions. Figure 5-5C shows a NF moving predominantly to the minus end of the MT while undergoing brief plus-ended excursions (the trajectories of NFs in figures 5-5B,C are shown in figure 5-7A). Figure 5-5D shows an electron micrograph prepared using the same conditions as the motility assay revealing an interaction between NFs and MTs. The motility was not due to contaminating vesicles since no spherical particles were revealed by labeling with a fluorescent lipid dye (3,3'-dioctadecyloxacarbicyanine perchlorate, 'DiO', Molecular Probes, Eugene, OR) or by electron microscopy.

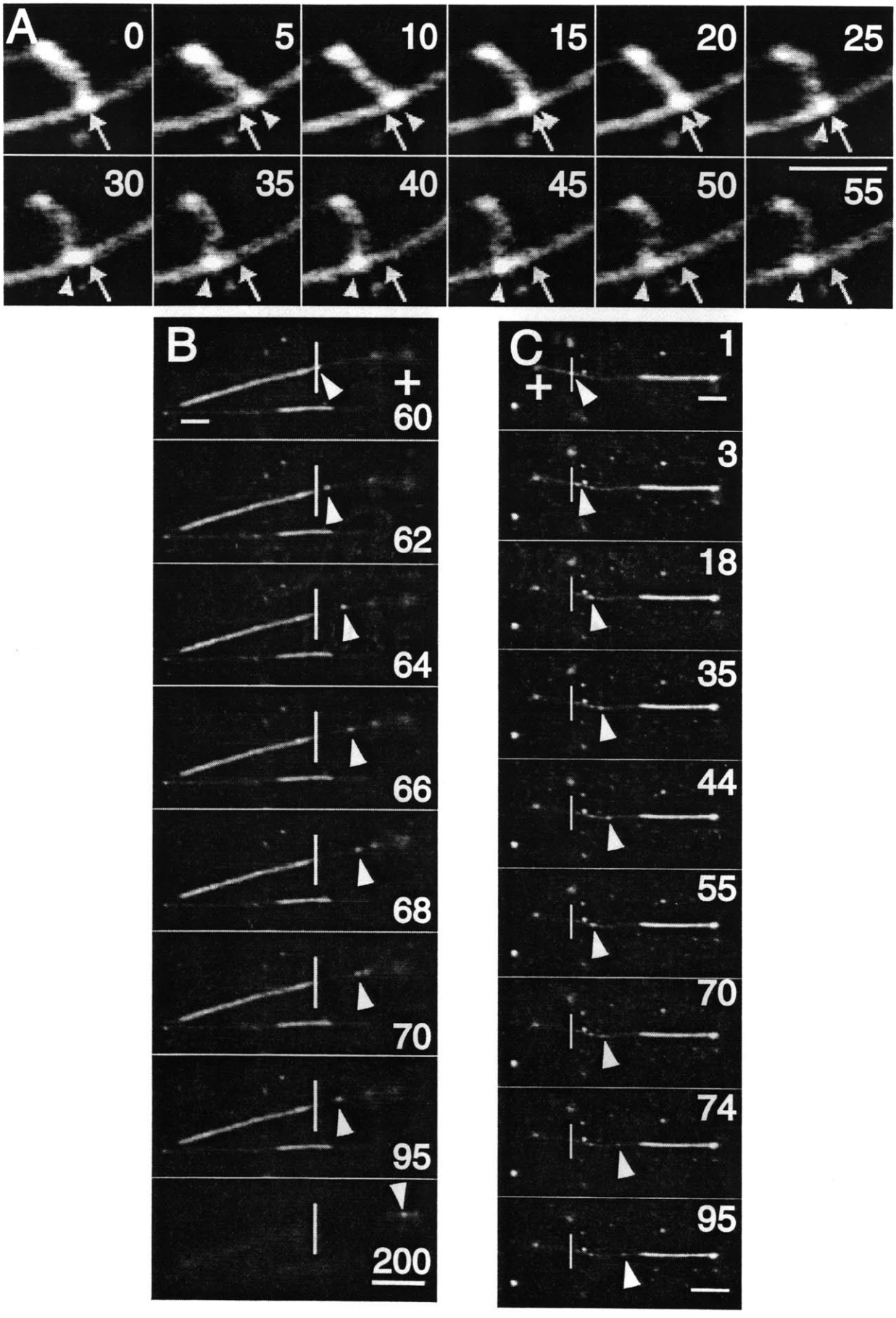
A
0
5
10
15
20
25
30
35
40
45
50
55
B
+
–
60
62
64
66
68
70
95
200
C
1
+
–
3
18
35
44
55
70
74
95
–

D

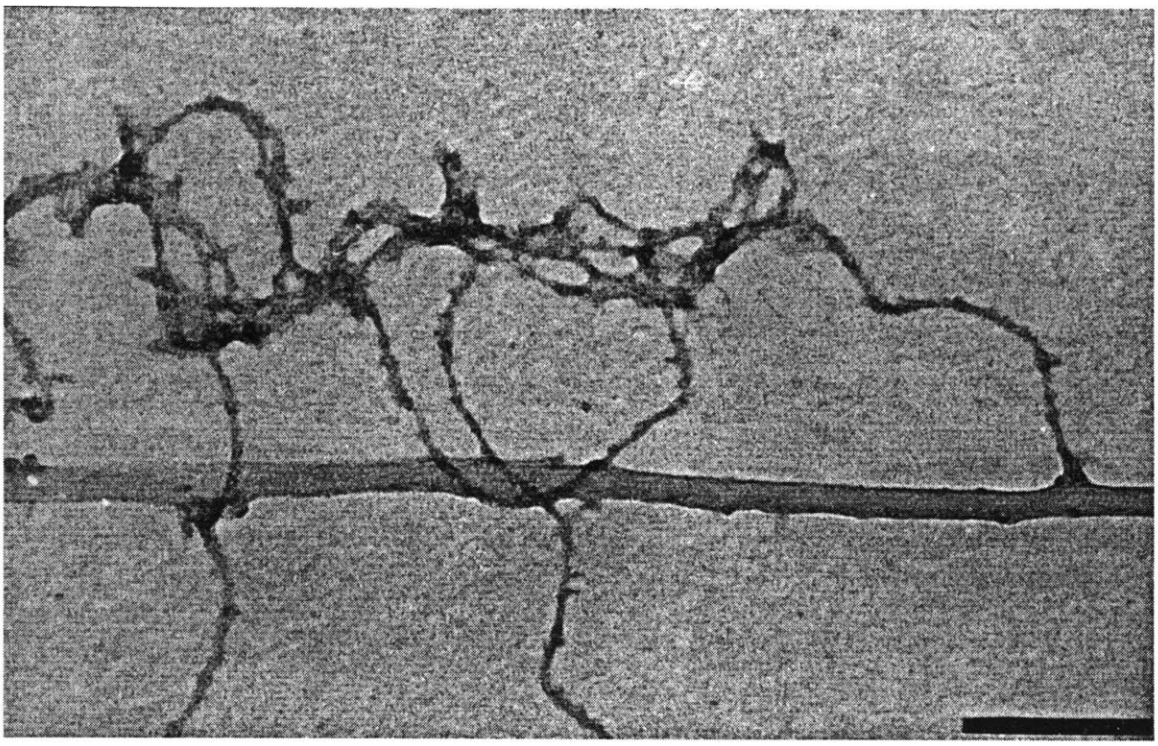

Figure 5-5 : **Bidirectional NF translocation along microtubules.**
A, A video sequence of a fluorescently labelled NF (arrowhead) with one end bound to glass and the other translocating bidirectionally along a fluorescently labelled MT. The arrow represents initial position of NF. **B**, A NF (arrow) translocating bidirectionally along a polarity-marked MT. The bar represents the initial position of the NF indicating a biased motion towards the plus end. **C**, A NF (arrow) translocating bidirectionally along a polarity-marked MT. The bar represents the initial position of the NF indicating a biased motion towards the minus end. All scale bars are 5 μm. NF motility was carried out in the presence of 100 μM Mg-ATP. The plus and minus ends of polarity-marked MTs are indicated, as are the timings of the video sequences (in seconds). **D**, An electron micrograph of NFs and MTs prepared in the same manner as the motility assay. Scale bar is 100 nm.

5.3.3 NF translocation is ATP-dependent and sensitive to agents that disrupt MT motors

To characterize the motor(s) involved in the translocation of NFs, the biochemical and immunological sensitivity of their motility was investigated (figure 5-6). Activity was measured as the percentage of MT-bound NFs that were motile. Baseline activity was measured in the presence of 100 μM Mg-ATP. Depletion of ATP by hexokinase and glucose, and chelation of Mg^{2+} by EDTA significantly decreased the observed motility, consistent with the presence of ATP-dependent mechanoenzymes (figure 5-6A). The addition of vanadate over a broad range of concentrations (5-200 μM) significantly decreased the motility in a dose responsive manner (figure 5-6A). A decrease of motility at low concentrations of vanadate (5-10 μM) is characteristic of a dynein ATPase. Addition of 1 mM EHNA or 2 mM NEM, both inhibitors of dynein ATPase activity(111, 149), decreased NF motility strongly suggesting a role for dynein (figure 5-6A).

Although NFs make up greater than 95 percent of the preparation and incorporate a significant portion of the fluorescent dye, NF antibodies were added to the motility assay to confirm that the NFs were indeed part of the motile complex and to observe their effect on NF translocation. Two NF antibodies which recognize complementary phosphorylated (SMI-31) and unphosphorylated (SMI-32) epitopes(137) disrupted motility to various degrees (figure 5-6B). SMI-31 which recognizes the phosphorylated NF epitope disrupted motility strongly, whereas the antibody to the unphosphorylated epitope, SMI-32, disrupted motility to a lesser degree. Addition of an anti-GFAP (glial acidic fibrillary protein) antibody did not disrupt motility. All three antibodies were obtained in murine ascites fluid. The absence of an effect with the GFAP antibody indicates the effect of the SMI-31 and SMI-32 antibodies is specific and not due to a factor in the murine ascites. To test the role of phosphorylation in the motility the NFs were subjected to treatment with alkaline phosphatase and okadaic acid. The alkaline phosphatase treatment decreased NF motility, primarily due to a large number of NFs bound. This is consistent with observations by Hisanaga and Hirokawa who demonstrated an increase in affinity between NFs and MTs upon dephosphorylation of NF-H(50). Okadaic acid produced no measured change in percentage of motile NF. One important qualitative finding is that the NF preparation used to obtain the okadaic acid measurements had a low total number of motile elements. The okadaic acid treatment, described in the materials and methods, significantly increased the total number of motile NFs although the percentage motile of total MT-bound NFs remained approximately the same.

The anti-dynein intermediate chain antibodies, 74.1(19) and 70.1(138) disrupted NF translocation along MTs (figure 5-6C) to a similar extent as EHNA (figure 5-6A). Antibody isotype controls showed similar NF motility to that of ATP alone (figure 5-6C), demonstrating a specific effect of the anti-dynein intermediate chain antibodies. Previous use of these antibodies has demonstrated an effect on dynein mediated motility ((43), Kevin Pfister, personal communication)

The addition of the adociasulphate-2 kinesin toxin(123) to the motility chamber dramatically decreased NF motility (figure 5-6D). Unlike the dynein antibodies little residual motility remained after kinesin toxin treatment. The concentration of AS-2 used to block motility was significantly higher than the reported 50 percent inhibitory concentration (IC_{50} ~ 5 μM)(123) making it possible that the AS-2 may also interact with another component of the preparation. The use of an antibody against the kinesin family member KIF3A did not affect motility, however, there is no reported effect of the antibody on KIF3A-mediate motility and such a negative result is difficult to interpret.

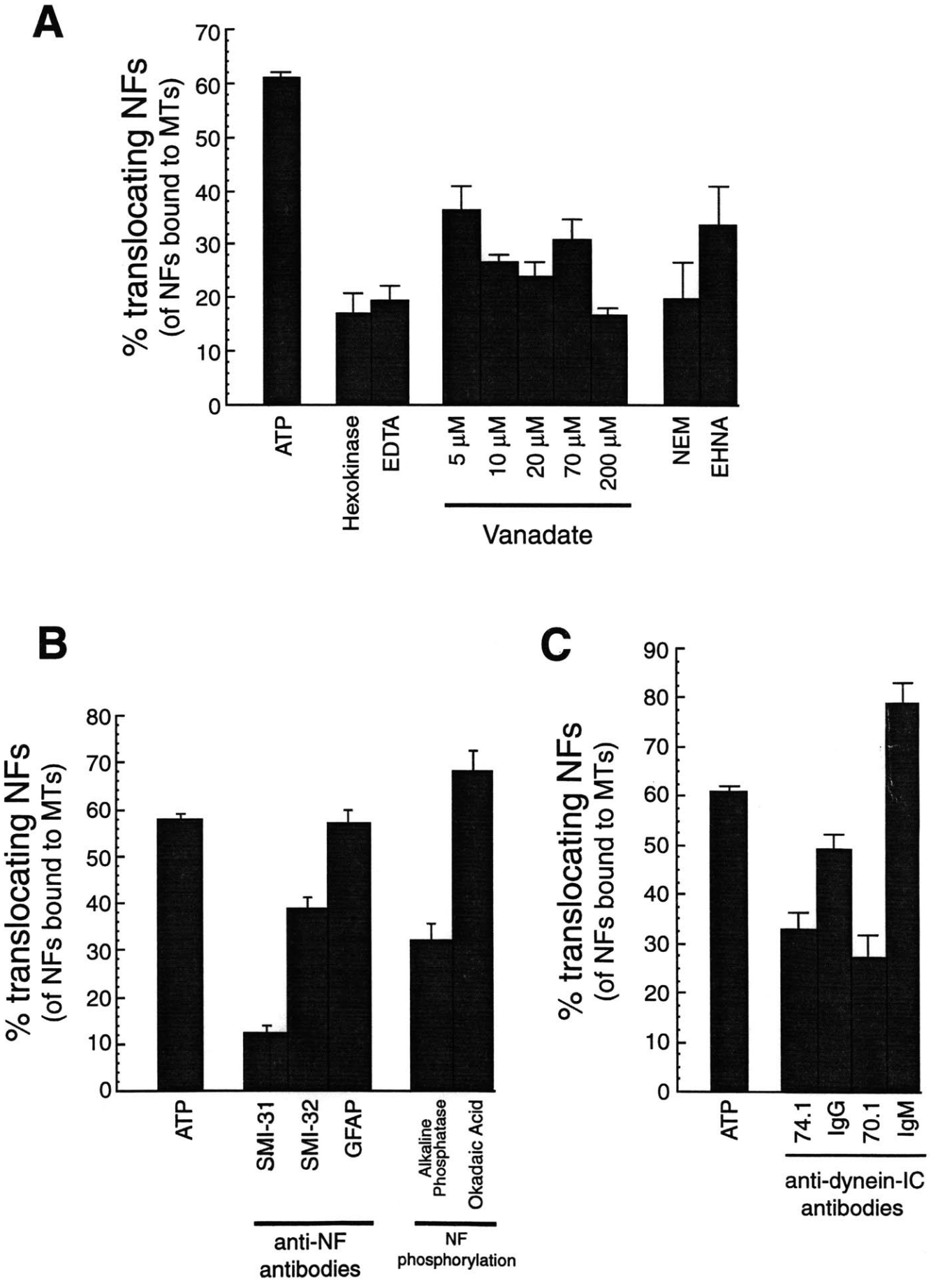
A
% translocating NFs
(of NFs bound to MTs)
0
10
20
30
40
50
60
70
ATP
Hexokinase
EDTA
5 µM
10 µM
20 µM
70 µM
200 µM
Vanadate
NEM
EHNA
B
% translocating NFs
(of NFs bound to MTs)
0
10
20
30
40
50
60
70
80
ATP
SMI-31
SMI-32
GFAP
anti-NF
antibodies
Alkaline
Phosphatase
Okadaic Acid
NF
phosphorylation
C
% translocating NFs
(of NFs bound to MTs)
0
10
20
30
40
50
60
70
80
90
ATP
74.1
IgG
70.1
IgM
anti-dynein-IC
antibodies

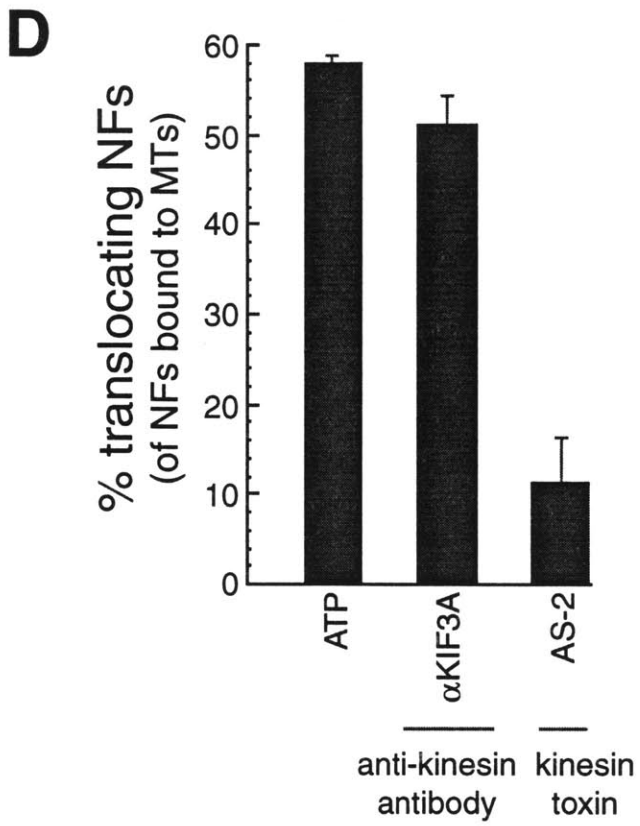

Figure 5-6 : **Analysis of neurofilament translocation.**
A, The percentage of NFs translocating (of the total bound to MTs) is shown for 100 μM Mg-ATP (baseline), ATP depletion by 2 U/ml hexokinase/5.5 mM glucose, and Mg2+ depletion by 2 mM EDTA. Vanadate sensitivity for 5 concentrations (5, 10, 20, 70, 200 μM) and the effect of 2 mM NEM and 1 mM EHNA are also shown. **B**, Motility after preincubation with NF antibodies recognizing phosphorylated (SMI-31) and unphosphorylated (SMI-32) NF epitopes and anti-GFAP (glial acidic fibrillary protein) antibodies. **C**, NF translocation after preincubation with two anti-dynein intermediate chain antibodies 74.1, 70.1 indicate disruption of motility. The corresponding Ig isotype controls are shown and also act as controls for panels **B** and **D**. **D**, NF translocation after preincubation with an anti-kinesin antibody, anti-KIF3A, and the kinesin toxin, AS-2 (650 μM). Bars indicate the average (+/- standard error) of at least 10 independent video sequences comprising at least 150 NFs measured per condition.

Figure 5-7A shows the measured trajectory of the NFs depicted in figures 5-5B and 5-5C, demonstrating bidirectional motility. The distances traversed by the NFs before changing direction or stopping (up to 4 μm) are consistent with persistent motor driven motion of the NF along the MT. Analysis of a large number of translocating NFs is summarized in the velocity histogram of figure 5-7B. The velocities were extracted from the raw trajectory data as described in the materials and methods section. The observed velocities in each direction were in the range of 100-250 nm/s which is consistent with MT motor speeds seen in MT gliding assays(117) and measurements of organelle motility(149, 157). Traditionally, a motor driven process can be characterized by a plot of the mean square displacement, however, the presence of bidirectional motion in this system precludes using this type of analysis. In this system the motor driven nature of the motility was investigated by disrupting a specific motor, dynein, and observing the residual motility. The bias in motility was analysed using four methods : total net displacement, velocity histograms, time spent in plus or minus ended motility and transition probabilities from motile to non-motile states. Each analysis was performed on the processed trajectory data as described in the material and methods section.

Motility analyses were performed in the presence of a number of dynein inhibitors, namely EHNA, vanadate(111) and the 74.1 dynein intermediate chain antibody (Kevin Pfister, personal communication). Under each of these conditions a number of parameters were measured to detect a bias in motility due to dynein inhibition.

Figure 5-8 shows the velocity histograms after treatment with dynein inhibitors. These histograms should be compared to figure 5-7B which has no dynein inhibitors added. Treatment with the dynein intermediate chain antibody (figure 5-8A), 200 μM vanadate (figure 5-8B) and 1 mM EHNA (figure 5-8C) significantly change the shape of the velocity profile observed.

To quantitate the direct effect of the dynein inhibitors, the net velocity was calculated for each of the conditions (figure 5-9A). Figure 5-9A shows the net velocity due only to motile events. The motility in the presence of ATP alone shows no significant bias to the plus or minus ends of MTs. The effect of the dynein intermediate chain antibody and 200 μM vanadate significantly increase bias of the motility to the plus end of the MT over that of ATP alone. EHNA causes an apparent bias to the plus end, however, the change is not statistically significant. The use of an antibody to disrupt and bias motility is strong evidence for a motor driven process responsible for the bidirectional motion and that dynein is responsible, in part for the minus end motility observed.

Figure 5-9B shows the analysis of time spent in each mode of motility. For the processed trajectories the dynein specific agents did not significantly change the time spent in plus or minus ended motility over ATP alone.

Figure 5-10 shows the transition probability diagrams for each of the conditions. In each diagram

the three motile states are diagrammed as circles. The connecting arcs represent the state transitions and the transition probabilities are indicated. The transition probabilities were not significantly changed by the presence of the dynein inhibitors. Thus figures 5-9 and 5-10 demonstrate no change in the temporal characteristics of the motility, i.e. the NFs spend the same amount of time in plus, minus and zero motility states and switch between these states at the same frequency. However, figures 5-7 and 5-8 show a significant change in the net motility observed. A number of hypotheses are presented in the discussion of this chapter to explain the changes in directional but not temporal characteristics of the NF translocation.

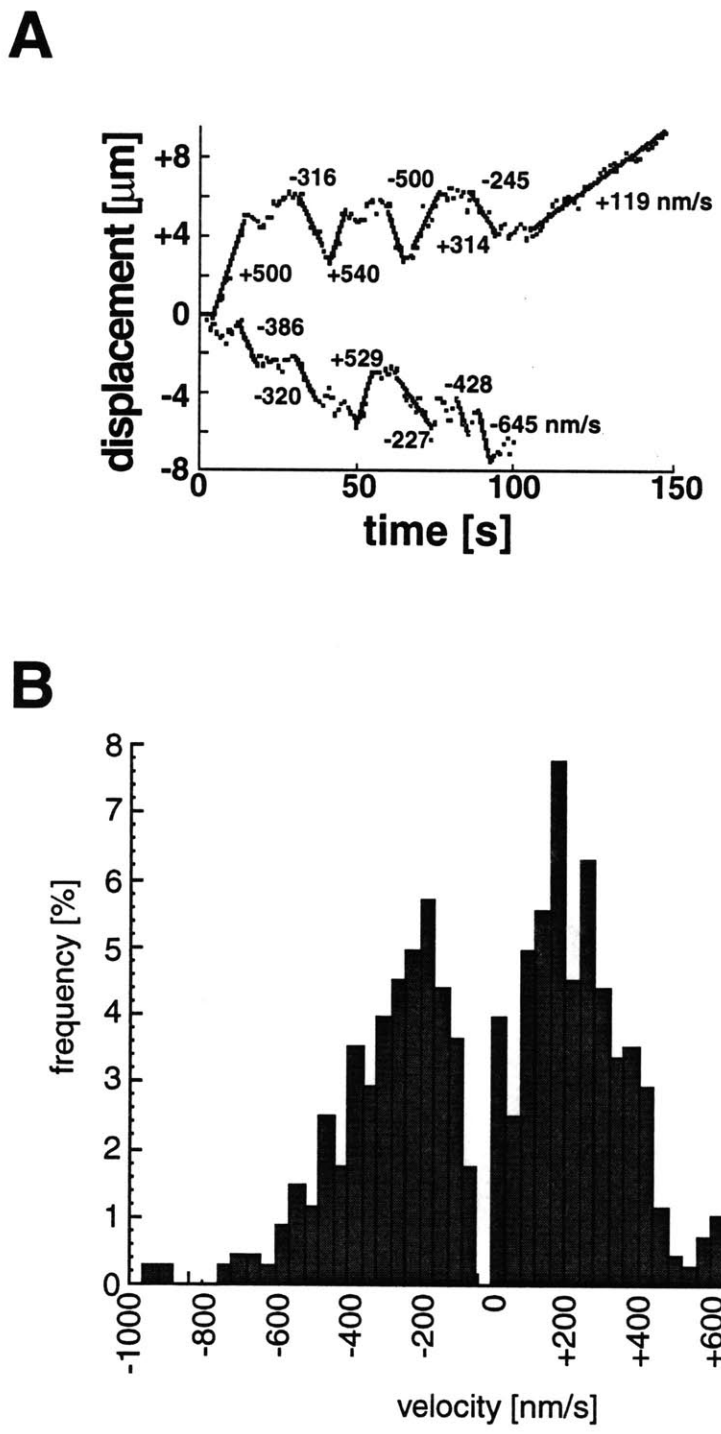

Figure 5-7 : **Directional analysis of neurofilament translocation.** **A**, The trajectories for the NFs in Figs. 5-4**B** and 5-4**C** demonstrate the bidirectional nature of the NF motility. Calculated velocities are shown for various segments of the trajectories. **B**, Distribution of velocities of transported NFs in the presence of 100 μM Mg-ATP (680 motile events from 90 different NFs).

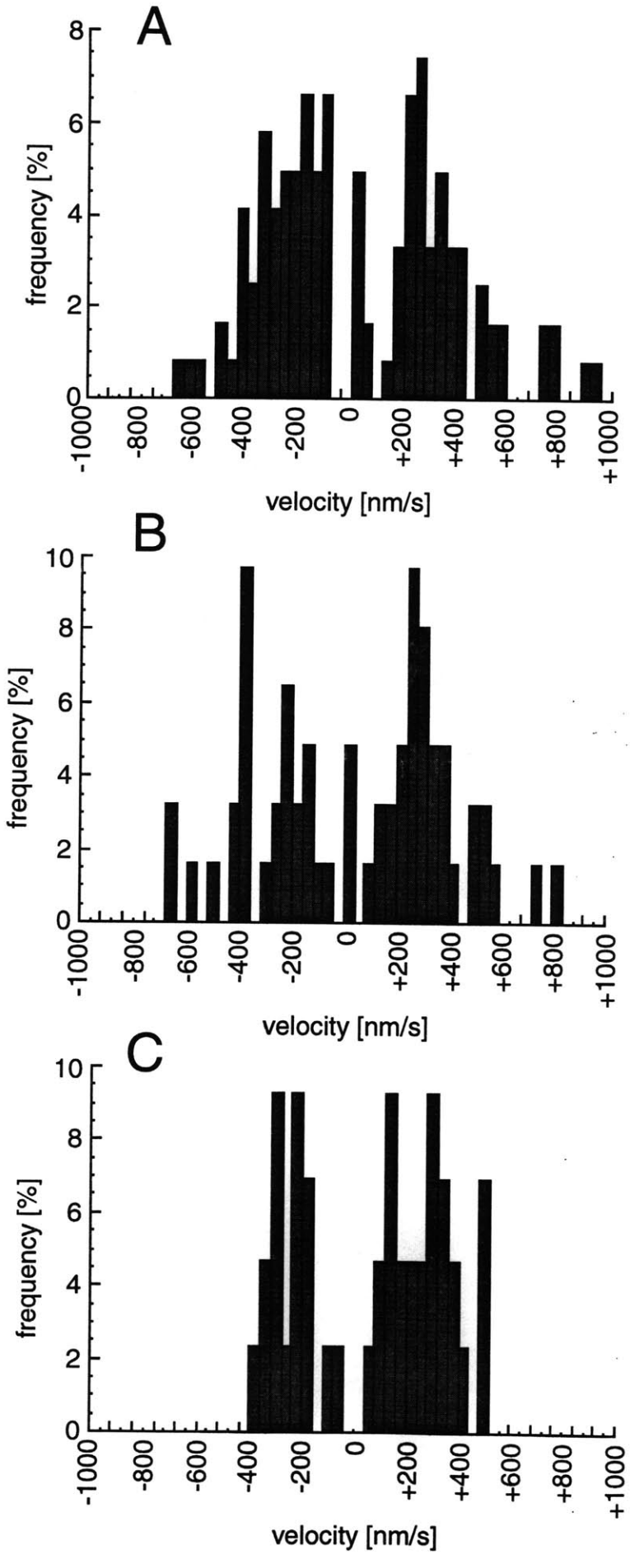

Figure 5-8 : **Velocity histograms in the presence of dynein inhibitors.** Histograms of processed trajectories in the presence of : **A**, a dynein intermediate chain antibody, **B**, 200 μM vanadate and **C**, 1 mM EHNA. When compared to the ATP alone histogram (figure 5-7**B**), these histograms have a decrease in number of minus-ended excursions, especially at high velocity (> 400 nm/s).

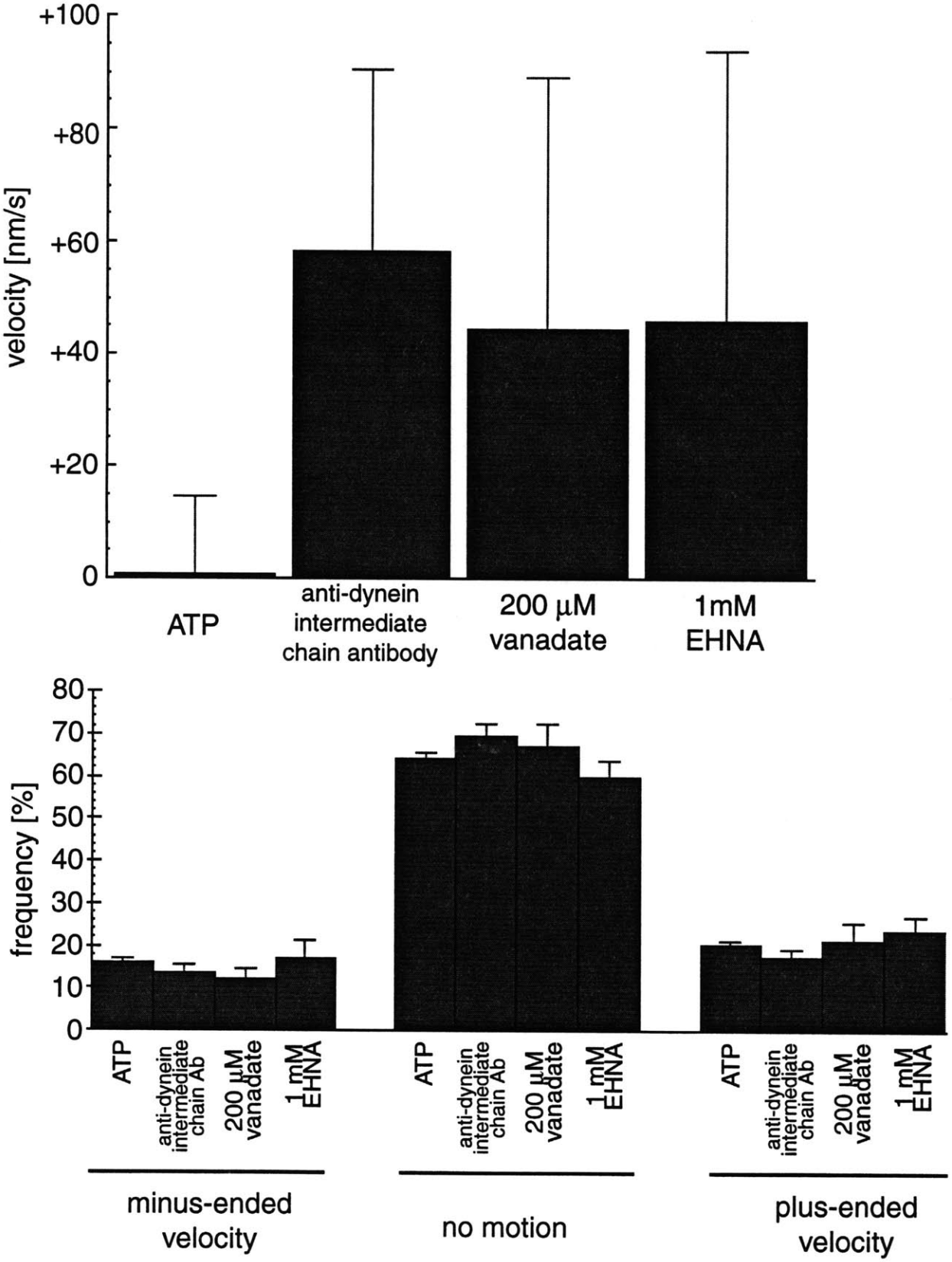

Figure 5-9 : **Net velocities and time histograms in the presence of dynein inhibitors.** **A**, Net velocity in the presence of ATP, a dynein intermediate chain antibody, 200 µM vanadate and 1 mM EHNA demonstrate the plus-ended bias resulting from dynein disruption. **B**, Histograms of time spent in minus, plus or zero velocity states show no significant change in the presence of dynein inhibitors.

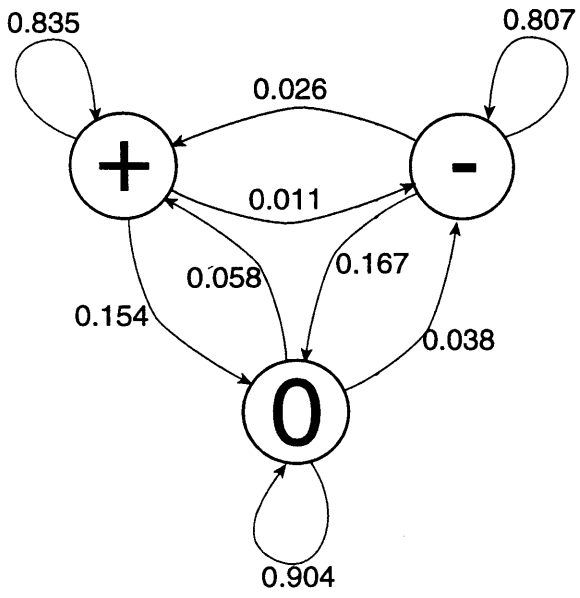

ATP

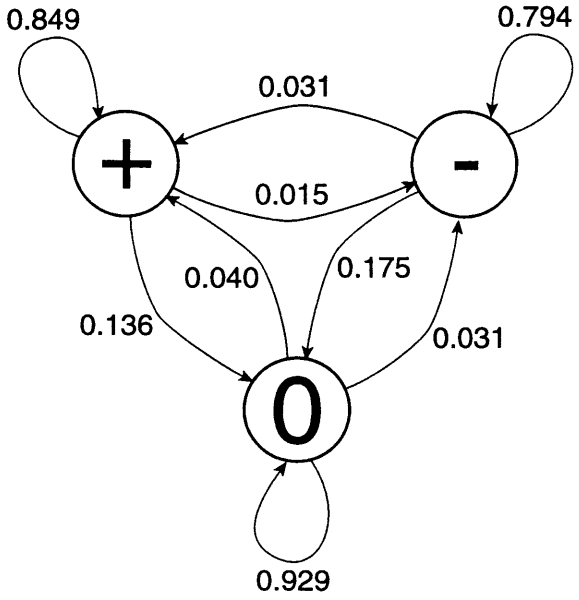

anti-dynein intermediate chain Ab

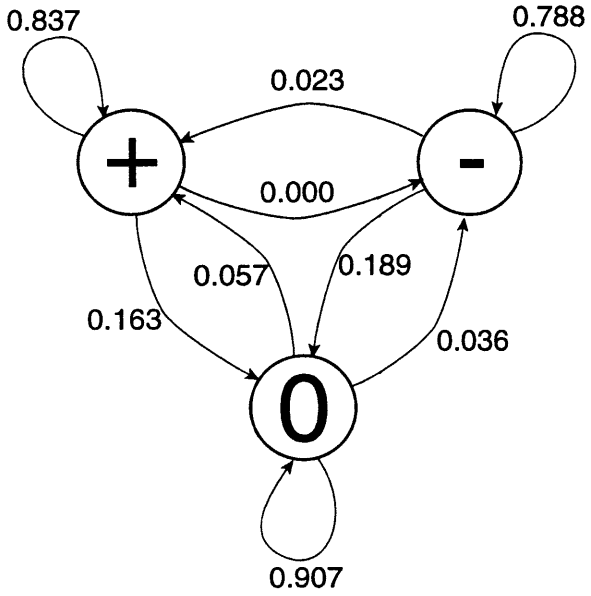

200 μM vanadate

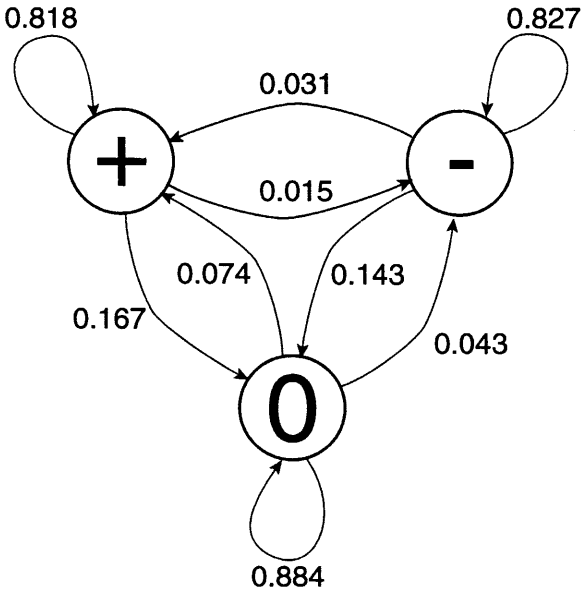

1 mM EHNA

Figure 5-10 : **Transition probabilities in the presence of dynein inhibitors.** The state transition probabilities between motility states : plus-ended, minus-ended and zero velocity, were computed under ATP alone and dynein inhibitors. The transition probabilities are the ratio of A to B transitions to the total number of transitions from state A. Under the dynein inhibitors none of the transition probabilities were significantly different from ATP alone.

5.3.4 Dynein/dynactin are partly responsible for minus-end directed motility

Specific disruption of dynein motility by antibodies, as observed in the motility assay, has been previously interpreted as a disruption of dynein-dynactin interactions(43, 152). In particular, the interaction of dynein intermediate chain with a component of the dynactin complex ($p150^{glued}$) (figure 5-11A) is a potential disruption site (figure 5-11A)(151).

The 74.1 dynein intermediate chain antibody used to block NF motility (see figure 5-6C) recognizes the same epitope(Kevin Pfister, personal communication) as a previously characterized antibody that displaces dynein intermediate chain from its cargo(136). Incubation of NFs with the 74.1 antibody also displaced dynein intermediate chain from the NFs (figure 5-11B). Approximately 50% of the dynein intermediate chain is released from NFs with this treatment. In contrast, $p150^{glued}$ was not removed by treatment with the 74.1 antibody (Lisa A. Flanagan, personal communication), suggesting that members of the dynactin complex remain associated with NFs. The displacement of dynein intermediate chain from the NFs by the 74.1 antibody suggests that the disruption of NF motility was the result of decoupling the dynein motor domain from the NFs, thereby reducing the number of minus end directed motile events.

Fractions from the NF purification were probed with antibodies to dynein and members of the dynactin complex. The multi-protein dynactin complex links dynein to its cargo and regulates its activity(34). An antibody to the intermediate chain of dynein shows strong reactivity in the purified NFs (figure 5-12A) as does an antibody against the dynein heavy chain isoform 1b (figures 5-15 and 5-16). The purified NF fraction also contains the dynactin complex proteins : $p150^{glued}$ (figure 5-12B), p50/dynamitin (figure 5-12C), capZ (figure 5-12D) and arp1 (Lisa A. Flanagan, personal communication). The presence of dynactin complex members in the NF fraction indicates a possible link between NFs and dynein mediated by the dynactin complex.

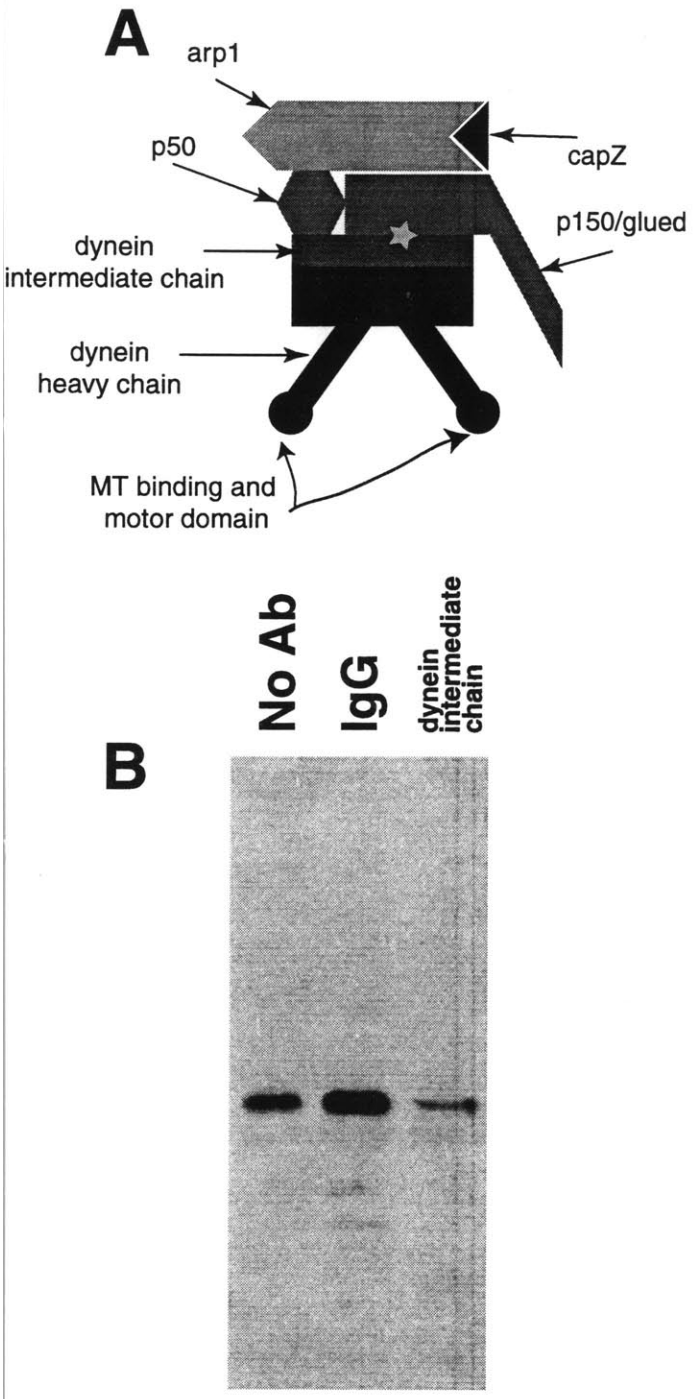

Figure 5-11 : **Disruption of dynein-neurofilament interaction by an anti-dynein antibody.**
A, Cartoon of dynein/dynactin complex. The star indicates the putative site disrupted by the dynein intermediate chain antibody. **B**,The dynein-NF interaction was disrupted with an antibody to the intermediate chain of dynein and the NFs pelleted and analysed by immunoblotting to determine the amount of dynein intermediate chain that remained bound to NFs. Controls without antibody and with an isotype IgG are shown for comparison.

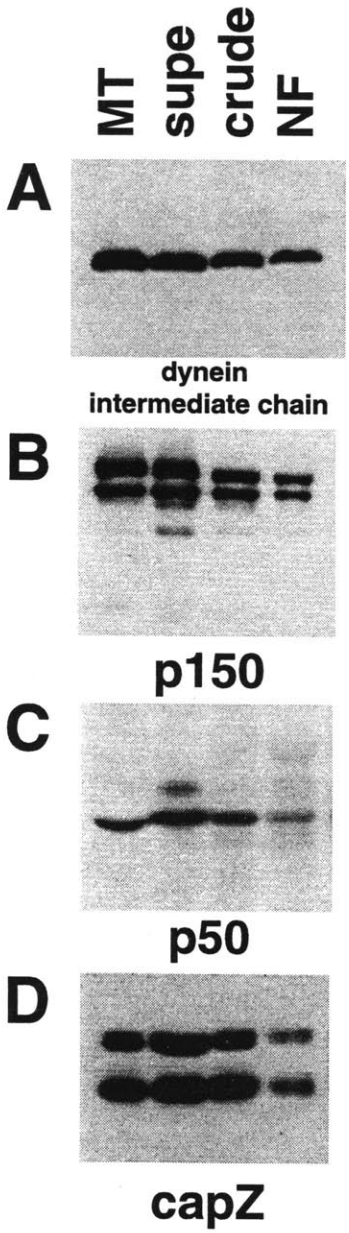

Figure 5-12 : **Dynein and dynactin complex members copurify with neurofilaments.**
Fractions from the NF purification were probed with antibodies to **A**, dynein intermediate chain, **B**, p150glued (showing p150 and the neuronal p135 isoform), **C**, p50 (dynamitin), and **D**, capZ (alpha and beta subunits). Microtubules prepared from bovine brain were used as a positive control, and the NF fractions are those shown in figure 5-2**A**.

5.3.5 Dynein is localized to NFs

NFs were analyzed by immuno-electron microscopy to determine if dynein is localized to NFs. NFs were adsorbed to grids, incubated with an anti-dynein intermediate chain antibody (74.1) and a gold-conjugated secondary antibody, and negatively stained. Figures 5-13A and 5-13B show colocalization of 8 nm gold particles with the NFs and verify that dynein is not bound to MTs or vesicles. Note that the pattern of staining is concentrated to a subset of NF contours. Secondary antibody alone (figure 5-13C) or isotype control antibodies (Lisa A. Flanagan, personal communication) showed no labelling, demonstrating the specific association of dynein with NFs. Similar colocalization of dynein with NFs was obtained with purified NF preparations from rat spinal cord (Lisa A. Flanagan and Jean-François Leterrier, personal commmunication). Approximately 5-10 % of all NFs observed show dense dynein intermediate chain immunoreactivity along the length of the NF indicating that only a subset of the NFs isolated from whole spinal cord have bound dynein. This heterogeneity is also apparent in the motility assay in which a minority of the added NFs bind to and are transported along MTs. This pattern of labelling further implies that the binding of motors to NFs is specific, since a non-specific interaction would result in sparse, homogeneous labelling of the NFs with motor epitopes.

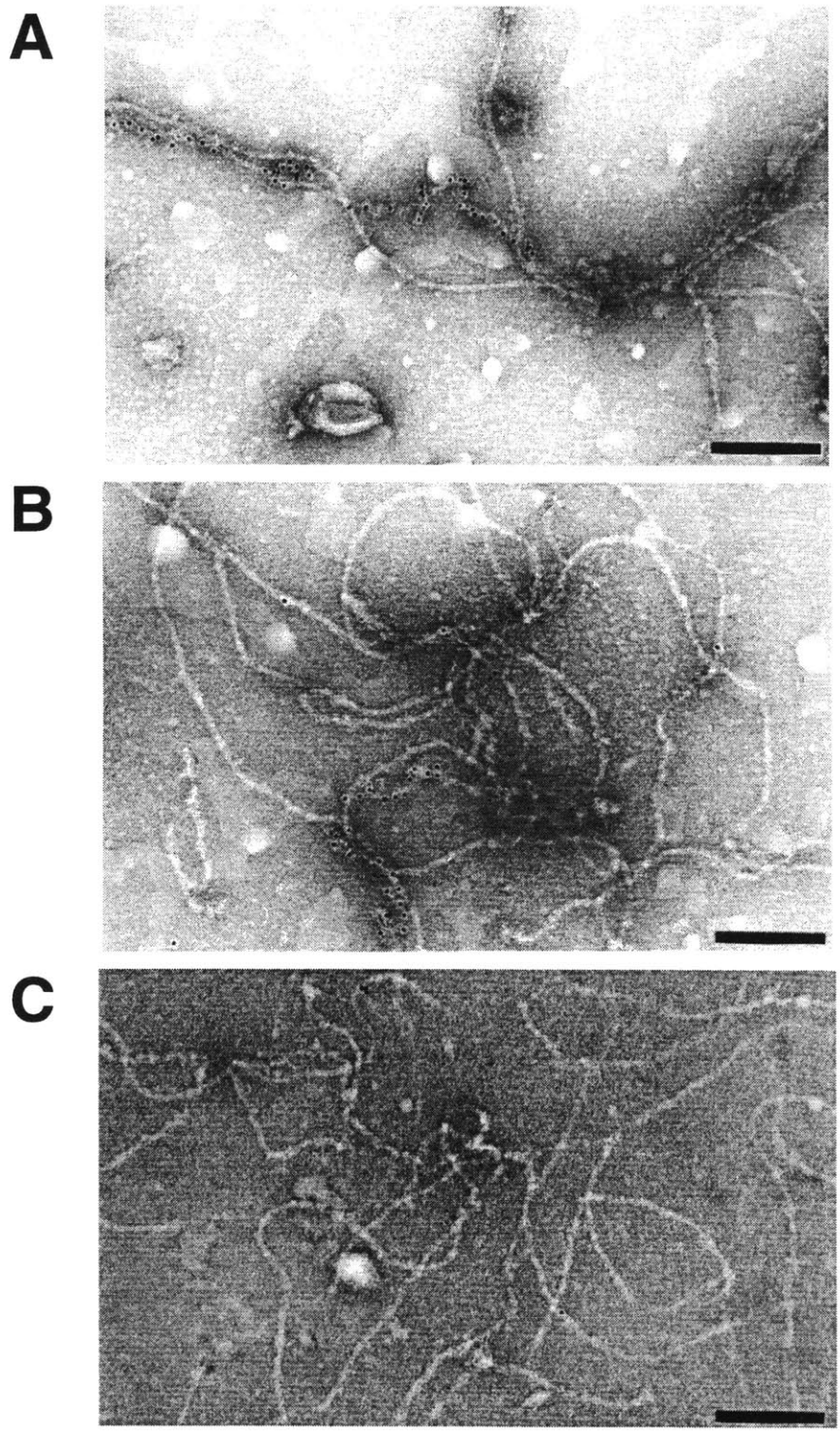

Figure 5-13 : **Dynein intermediate chain localizes to neurofilament contours.** **A**, **B**, Two electron micrographs of NFs showing reactivity with dynein intermediate chain antibody, **C**, Control electron micrograph of NF treated with secondary antibody alone. All scale bars are 200 nm.

5.3.6 Kinesin-like proteins copurify with NFs

An antibody to the heavy chain of conventional kinesin, SUK4(58), showed no reactivity in the NF preparation by immunoblotting (figure 5-14A) or immunoelectron microscopy (Lisa A. Flanagan, personal communication), although it reacted with soluble fractions resulting from the NF preparation (figure 5-14A). The absence of conventional kinesin, a contamination in many motor preparations, in the purified NF fraction decreases the likelihood of significant contamination by motor-bound organelles.

Hirokawa and colleagues have previously reported the identification of sixteen novel kinesin family members(105) and the size of this family is still increasing. Due to the large number of mammalian kinesins, some of which are still uncharacterized, the approach used to study the presence of the kinesins in the NF preparation took advantage of a peptide antibody developed against the MT binding region of Xenopus conventional kinesin heavy chain (CHIPYRESKLT)(128) which recognizes a variety of kinesin family members. The anti-HIPYR antibody consistently revealed a number of HIPYR positive polypeptides, both in rat and bovine preparations (figure 5-14B). The molecular weights of these putative kinesin related proteins were 200 kDa, 160 kDa, 110 kDa, 95 kDa and 85 kDa. Treatment of the NF preparation with alkaline phosphatase increased the electrophoretic mobility of NF-H but not that of the 200 kDa kinesin-like band, demonstrating that the 200 kDa polypeptide is distinct from NF-H (figure 5-14B). A significant problem with using broad specificity antibodies is the possible detection of non-kinesin family members. The HIPYR result was used as a guide to motivate probing the NF preparation with antibodies to other kinesin family members.

Immunoblotting with a variety of kinesin family antibodies was also carried out by Joe Marszalek, a graduate student in Larry Goldstein's laboratory (University of California, San Diego). The results are shown in figures 5-14C through 5-14G. The positive control in these blots was a murine brain homogenate since the antibodies had not been previously tested on bovine material. Blotting both bovine and murine homogenate aided in qualitatively distinguishing between species variability and actual detection of the protein. Two major family members were examined in this set of immunoblots - KIF5 and KIF3 family members. The KIF5 subfamily of kinesins includes conventional kinesin designated KIF5B by the nomenclature and also includes two kinesins, KIF5A and KIF5C which are closely related to KIF5B but are restricted to neuronal tissue. The SUK4 antibody described above is directed against KIF5B but its cross-reactivity for 5A and 5C has not been investigated. The KIF3 subfamily forms a set of proteins which form heterodimeric kinesins, unlike the conventional kinesins which form homodimeric motor complexes. The KIF3 subfamily currently includes three members KIF3A, 3B, and 3C. In vivo KIF3A form heterodimers with 3B or 3C and is thought to play a role in vesicle transport(104, 160). KIF3 family members are particularly interesting in this system since they have been demonstrated to

play a role in ciliary, flagellar assembly(101) which requires transport of non-membranous, cytoskeletal cargoes along oriented microtubules, a process analogous to slow transport in neurons.

Of the kinesins examined, KIF3A (figure 5-14C) and KIF5A (figure 5-14F) showed copurification with NFs. Other kinesins such as KIF3B (figure 5-14D), KIF3C (figure 5-14E), KIF5C (figure 5-14G) and KIF21B (Joe Marszalek, personal communication) were either not bound to the NFs or have sufficiently different bovine epitopes (versus murine) as to be unrecognized by the antibody. Qualitative observations indicate that the antibodies for KIF3B, KIF3C and KIF5C do recognize bovine material and are probably not responsible for the NF motility.

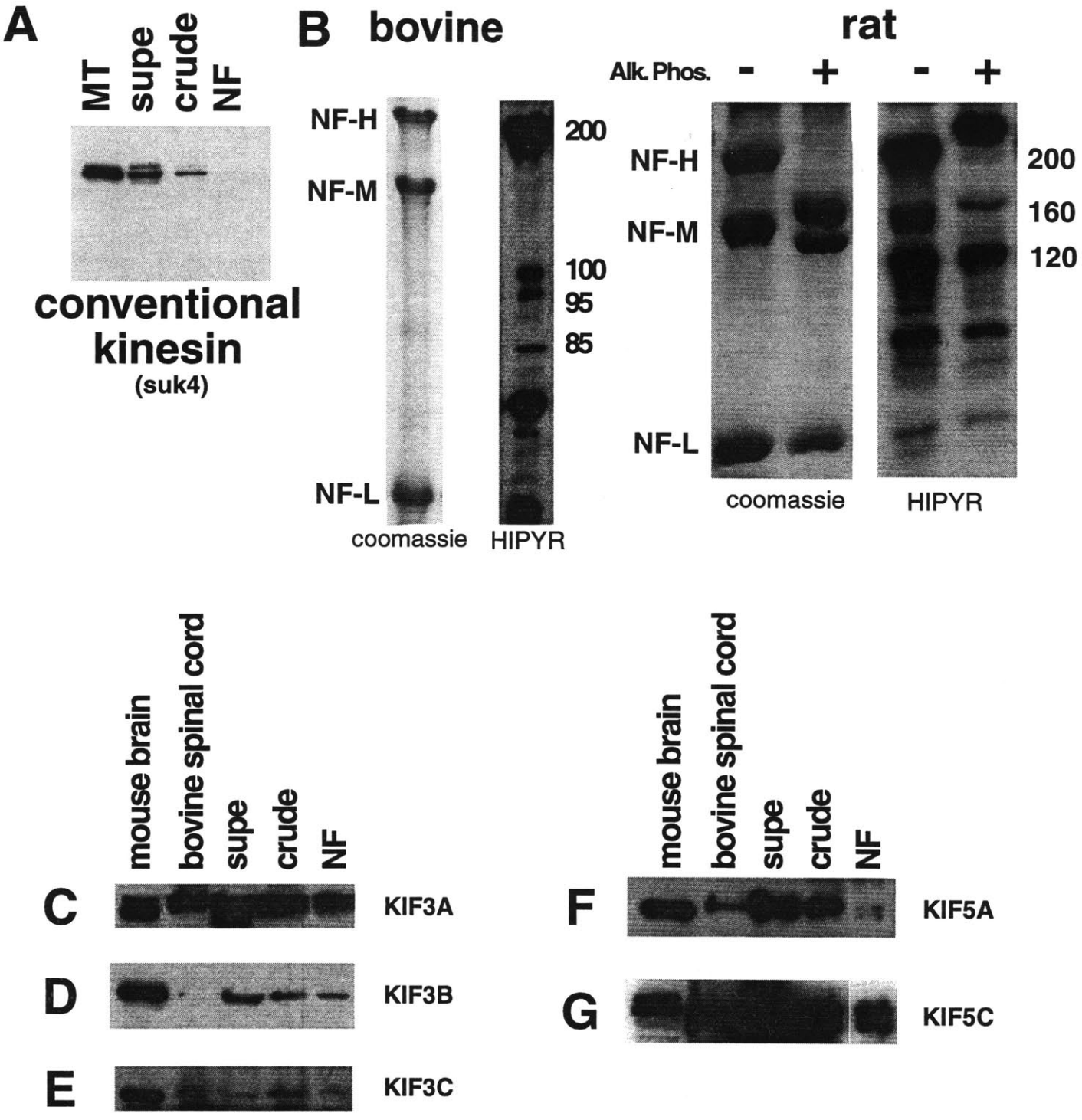

Figure 5-14 : **Kinesin related proteins copurify with neurofilaments.**
A, Fractions from the NF purification were probed with an anti-conventional kinesin heavy chain antibody, SUK4. **B**, HIPYR epitope probed by immunoblotting in both rat and bovine NF preparations. The corresponding coomassie stained gel is included to demonstrate that the 200 kDa immunoreactivity is distinct from NF-H since NF-H migrates faster after treatment with alkaline phosphatase (alk. phos.). The bovine NF preparation was probed with antibodies to : **C**, KIF3A, **D**, KIF3B, **E**, KIF3C, **F**, KIF5A and **G**, KIF5C. The 'mouse brain' lane designates a mouse brain homogenate, and the lane designated 'bovine spinal cord' is a bovine sinal cord homogenate. These lanes were not loaded for equal protein.

5.3.7 Motor binding to NFs is insensitive to detergents, chaotropic agents and NF phosphorylation state

To investigate the nature of the NF-motor interaction, the NFs were passed through a number of biochemical steps and later probed with motor antibodies to assay for the integrity of the NF-motor interaction. Figures 5-15 and 5-16 document a number of attempts to disrupt the NF-motor interactions. For each modification as described in the material and methods section of this chapter, the presence of KIF3A and dynein heavy chain isoform 1b (DHC1b) were examined. Biochemical treatment with 1% Triton X-100 to disrupt membranous associations is shown in figure 5-11. In comparison with mock-treated NFs the binding of the motors, both DHC1b and KIF3A, were unperturbed by detergent treatment. This is also true for 1 M KCl and 0.6 M KI which are also shown in figure 5-15. In the case of KI treated NFs there is migration of the NF bands to the supernatant, as detected by coomassie staining, which is most likely due to direct disruption of the NFs or the dynactin complex. This disruption accounts for a slight increase in motor signal in the supernatant of KI treated NFs. Qualitative assessment of the motility of the treated NFs indicated no change in control, Triton or KCl treated NFs. KI treated NFs were either extremely compacted or had become too short to visualize by light microscopy and thus their motility could not be assessed.

To investigate the possible role of phosphorylation in NF-motor binding, NFs were treated with alkaline phosphatase to directly dephosphorylate NF subunits(85) or okadaic acid, a phosphatase inhibitor. Dephosphorylation can be detected by an increase in electrophoretic mobility as seen in figure 5-16, whereas okadaic acid requires other methods which were not attempted in this study. There does exist evidence for an NF-associated phosphatase(122), although its presence in this preparation has not been documented. In each case, both with alkaline phosphatase and okadaic acid treatment, the motors examined (i.e. DHC1b and KIF3A) remained bound to NFs (figure 5-16).

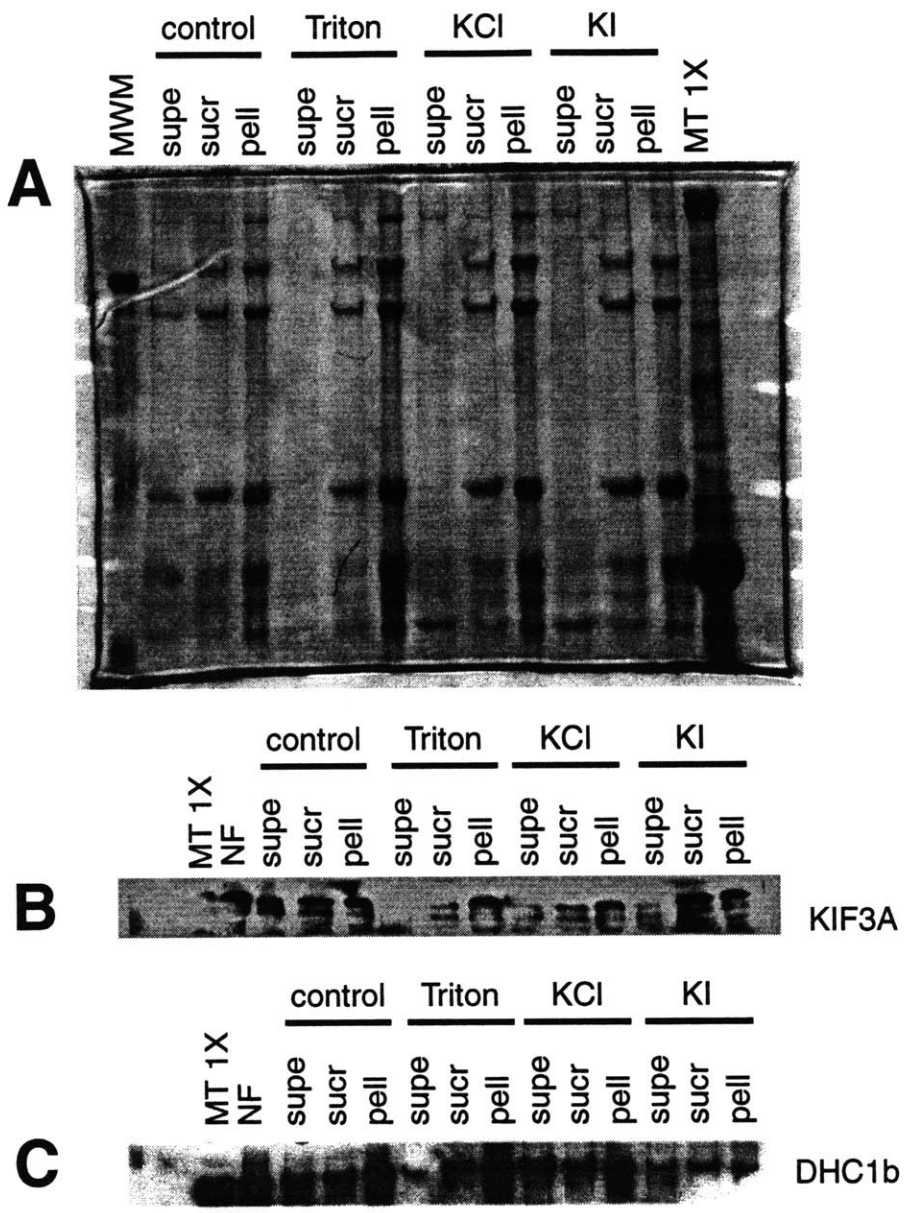

Figure 5-15 : **Biochemical treatment of NFs - effect on motor binding.** **A**, SDS-PAGE analysis of four treatments of the NF preparation : control, 1% Triton X-100, 1 M KCl, 0.6 M KI. For each treatment three fractions were prepared : supernatant (supe), sucrose cushion (sucr) and pellet (pell). **B**, Immunoblot analysis of the biochemical treatments probing for KIF3A. **C**, Immunoblot analysis of the biochemical treatments probing for DHC1b.

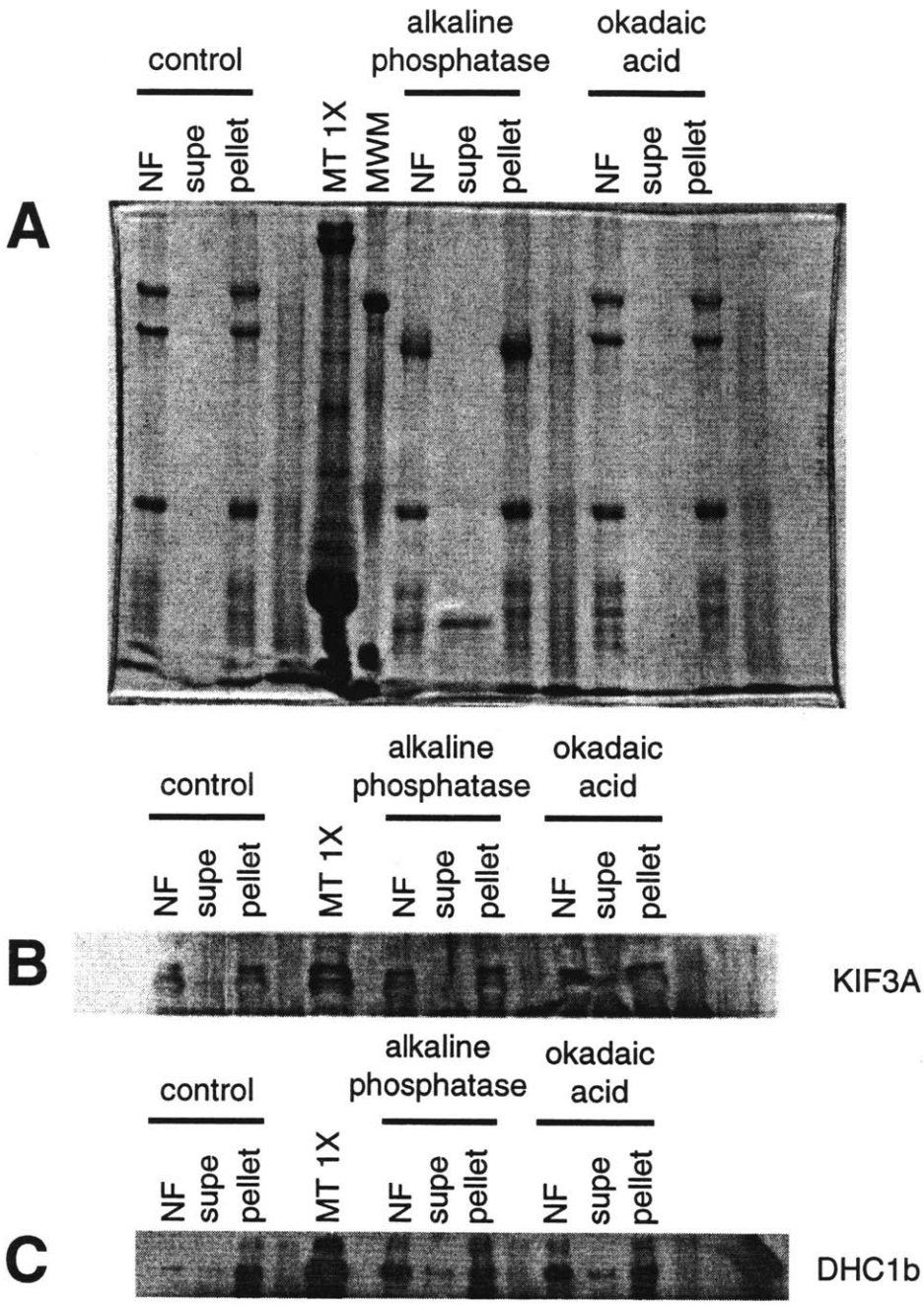

Figure 5-16 : **Modulating the phosphorylation state of NFs - effect on motor binding.** **A**, SDS-PAGE analysis of control, alkaline phosphatase (5 U/ml) and okadaic acid (4 μM) treatments of NF preparation. For each treatment three fractions were prepared : treated NFs, supernatant (supe) and pellet (pell). **B**, Immunoblot analysis of the phosphorylation treatments probing for KIF3A. **C**, Immunoblot analysis of the phosphorylation treatments probing for DHC1b.

5.4 Discussion

The movement of neuronal cytoskeletal proteins down the axon occurs at rates 100 times slower than those observed for identified molecular motors. Currently there exists no evidence for a single molecular motor that is responsible for this process. The data presented indicates that NFs prepared in their native polymerized state bear multiple MT-dependent motors which contribute to the bidirectional translocation of NFs along MTs in vitro. The motility of NFs observed in vitro is not diffusive and is ATP-dependent. The minus end directed component of this motion is shown to be partially due to the dynein/dynactin complex whereas the complement of the motility is due to at least one kinesin-related protein found associated with NFs. The motor-NF interaction is resistant to 1% Triton X-100, 1 M KCl and 0.6 M KCl. The interaction is also not affected by dephosphorylation or okadaic acid treatment.

5.4.1 Biophysical characteristics of NF motility on MTs

NF translocation on MTs was extensively characterized in this study. Initial observations demonstrated the disruption of the motility by NF antibodies, ATP depletion, vanadate, anti-dynein antibodies and a specific kinesin toxin. Together the bulk motility data points to a motor driven process in which both dynein and kinesin are attached to NFs and engage bidirectional motility. This motility may be bidirectional due to some regulation, implying that the dynein and kinesin are complexed together and are engaged in an alternating fashion. Alternatively, the motors may be in a tug-of-war being simultaneously engaged and the direction of motion determined by binding kinetics and number of motors engaged. As yet the nature of the linkage is not clear.

The addition of the anti-dynein intermediate chain antibody or vanadate biased the motility observed toward the plus end, indicating that the motility was motor driven and not completely diffusive (figure 5-9A). However, the residual motility had a significant number of minus ended excursions and the total time spent in minus end directed motion was not significantly different than that of ATP alone (figures 5-7B and 5-9B). In addition, the probability of switching to a minus end directed motion was not different from ATP alone (figure 5-10).

One possible explanation is that there is a minus-ended kinesin present in the preparation and that it is less processive than dynein resulting in short minus ended excursions. This would explain the minus ended excursions and the complete loss of motility in the presence of the kinesin toxin (figure 5-6D). Due to the large number of kinesin like proteins, some of which have yet to be identified, this possibility cannot be readily investigated.

Another possible explanation is the superposition of a non-motor driven process on the motor

driven process. For example, the NFs can bind MTs directly as described previously by Hisanaga and Hirokawa(50) and Leterrier et al(86). If NFs bound MTs during the motor driven process, the molecules may become extended as shown in figure 5-5A and recoil when the motor dissociates from the MT. The resulting recoil may be indistinguishable from a motor driven motility. Such a process could account for the change in net motility but lack of effect on time spent in minus ended motility or switching probability in the presence of dynein inhibitors.

The biophysical interaction of a MT motor and a filamentous cargo presents a unique system which cannot be completely characterized by traditional motor techniques. The system described here is bidirectional, filamentous and complex in composition. The study demonstrated the novel nature of NF motility along MTs and presents a number of interesting problems, such as the role of elastic recoil, for further study.

5.4.2 Role of a dynein-NF interaction

The association of dynein with NFs is surprising since the motor direction is the wrong direction for NF transport. In addition, Dillman and co-workers have documented the presence of dynein in the slow transport wave which does not contain NFs. Nonetheless, the association of dynein with NFs was shown to partially mediate the minus-end directed motility along NFs. In vivo such an interaction would result in either retrograde motion of free NFs on a fixed MTs or anterograde movement of MTs on a fixed NF network.

Previous work by Griffin and colleagues(37, 154) has demonstrated the retrograde flow of NFs in axons using an in vivo transected nerve model. In these investigations, sciatic nerves from mice were transected and both proximal and distal stumps were observed for cytoskeletal redistribution. The mouse strain used for this study had a phenotype of delayed Wallerian degeneration upon nerve transection making the long time points where NF motion was measured accessible. NFs accumulated at both the proximal and distal stumps demonstrating that retrograde transport of NFs occurs in vivo. The data presented above suggest that the retrograde transport of NFs along MTs can occur through the activity of dynein and the dynactin complex.

The binding of dynein to NFs could also support polarized, directed transport of MTs through an NF network. Work by Ahmad and co-workers(1) demonstrate the role of dynein and dynactin in the transport of MTs from the cell body into the axon of neuronal cells. The motor in this case is bound to a fixed substrate and transports the MTs, analogous to a MT gliding assay. The key role played by dynein is that it forces the MTs to enter the axon plus end leading - the polarity that is found throughout the axon. The report by Ahmad and co-workers, however, does not

identify the substrate to which the dynein/dynactin complex is bound. Given the findings in this study, one possible candidate for the substrate is the NF cytoskeleton. The findings reported in this thesis describe a bidirectional motion that has been shown to be due to both dynein and kinesin motor proteins. A regulatory mechanism by which dynein, and not kinesin, binds to cell body NFs is necessary to implicate NFs in MT transport. In addition, the role of NFs in MT transport could be tested directly by observations of neurons from transgenic NF mice, where the selective expression of NF subunits has been altered(33, 74, 97, 148, 159, 163).

5.4.3 Role and identity of NF-bound kinesins

The association of intermediate filaments and kinesins has been described in a non-neuronal system by Prahlad and coworkers(116). In spreading cells, the intermediate filament protein vimentin was transported along microtubule packets that later form filaments at the cell periphery. The transport in these cells is mediated by conventional kinesin. This finding, together with a previous report by Gyoeva and Gelfand(42) showing that injection of anti-kinesin antibodies in cells results in the collapse of the vimentin IF network around the nucleus, points to the existence of dynamic interactions between MTs and vimentin that are required for normal IF distribution.

The role of kinesins in the NF motility is demonstrated by the decrease caused by the AS-2 toxin which has been shown to be specific for kinesins(123). The toxin binds to the kinesin MT binding site and disrupts the MT-kinesin interaction. As a result, the decrease in motility is due both to a lower number of NFs moving and a slight decrease in NFs bound. However, unlike the disruption of dynein-based motility, the disruption of kinesin by AS-2 did not result in any residual minus-end directed motility. One possible interpretation for this is that the effective affinity of the NF for the MT is partly due to the motors bound to the NFs. If the kinesin plays a role in keeping the NF near the MT surface, then disruption of this interaction would result in lower binding. The role of dynein in this process is that it contributes to the motility but has a lower contribution to the effective NF affinity for MTs. It is also possible that the high concentration of toxin used in these experiments could interfere with dynein binding or NF binding to the MTs.

The addition of kinesin antibodies to the motility assay was attempted to distinguish between the kinesin family members that are responsible for the motility. The KIF3A antibody has no previously documented effect on KIF3A mediated motility and as such the negative result does not provide evidence into its role in NF motility. The K2.4 antibody, not yet tested in this system, has been previously utilized in echinoderms to block kinesin II (the echinoderm KIF3 subfamily) mediated motility(101). However, its effect on mammalian KIF3 mediated motility has not been documented. To examine the role of other kinesins such as KIF5 subfamily members, there exist blocking antibodies which perturb vesicle transport in neuronal (H2)(5) and non-neuronal cells

(H1)(89). Further analysis with the H1 and H2 antibodies will aid in identifying the responsible kinesin. The broad immunological analysis performed on the NF preparation (figure 5-14) has identified a number of proteins which correspond to known kinesins (by molecular weight) and some which are novel. The presence of a completely novel kinesin that is responsible for the motility is an intriguing possibility.

The high molecular weight kinesin-like proteins (200 and 160 kDa) detected by the HIPYR antibody do not correspond to any presently documented kinesins. The 110 kDa polypeptide detected by the anti-HIPYR antibody has a molecular weight similar to conventional kinesin isoforms but does not correspond to the conventional kinesin isoform recognized by the SUK4 antibody (i.e. KIF5B)(58) (figure 5-14A). Thus the 110 kDa kinesin-like proteins could represent one of the KIF5 isoforms(105) which are restricted to neural tissue(KIF5A and KIF5C). Figures 5-14F and 5-14G indicate that KIF5A is present in greater quantity than KIF5C, making it a good candidate for kinesin mediated NF motility. The HIPYR positive polypeptides in the 85/95 range probably correspond to heterotrimeric kinesin (KIF3) subfamily members(160). The KIF3A subunit was detected in the NF preparation (figure 5-14C) whereas immunoblotting for KIF3B and KIF3C demonstrated lower protein levels. Since KIF3A is usually thought to be dimerized with KIF3B or KIF3C, the increased level of KIF3A over KIF3B or KIF3C implicates the presence of another KIF3 protein involved with NF motility. In addition, the residual minus end directed motility after dynein inhibition may point to the presence of a minus end directed kinesin.

In total, the lack of conventional kinesin (figure 5-14A) in the NF preparation, a significant contaminant in many motor preparations, suggests that the other kinesin-like molecules identified by the anti-HIPYR and more specific antibodies are specifically bound to NFs and partly responsible for motility observed.

5.4.4 Biochemical treatments of NF preparation and motor binding

NFs were subjected to a number of biochemical treatments to examine the nature of the motor-NF interactions. Due to limited access to antibodies only DHC1b and KIF3A were tested for their interaction with the NFs under the different treatments. In all cases the motors were not dissociated from the NFs. In particular the stability of the interaction under 1% Triton X-100, a non-ionic detergent, indicates that the association is not due to a membranous structure. This evidence eliminates the likelihood that the NFs have become associated with membranous organelles, with bound motors, during the purification process, and that these motors have mediated the motility. The affinity of IFs for lipids has been previously documented(93, 112, 124, 125) and is an important consideration in this system. The resistance to disruption by KCl and KI reveals a strong interaction between the motors and the NFs that is mediated in part by non-ionic

interactions.

Another important aspect of NF-motor binding is the regulatory mechanism of motor binding. The most dramatic post-translational modification of NFs in vivo is their change in phosphorylation state(18, 108, 110) which represents a possible candidate for regulation of ligand binding. To test the hypothesis that the phosphorylation state can change the motor binding, the NFs were treated with alkaline phosphatase and okadaic acid. In both dephosphorylated and okadaic acid treated NFs the motors examined remained bound to the NFs. These experiments do not rule out the role of phosphorylation in the regulation of motor binding but will require a detailed study of specific phosphorylation sites which are not be modified by the treatments used(110). The treatment of NFs with alkaline phosphatase did decrease the motility of the NFs. However, this result is interpreted to be a significant increase in number of bound NFs, as previously documented(49), rather than a change in the motile pool. The treatment of NFs with okadaic acid produced no significant change in percentage of motile NFs. However, the dramatic increase in number of motile NFs implies a role for phosphatases in NF aggregation.

A much more exotic form of regulation could be through the carbohydrate modification of NFs. NFs can be o-glycosylated at a number of residues, often overlapping with potential phosphorylation sites(21). The role of sugars in protein-protein interactions is highly speculative, but may be an alternative form of regulating motor binding.

5.4.5 Bidirectional motion in slow axonal transport

The cytoskeleton of axons is constantly renewed much like the cytoskeleton of non-neuronal cells, but the length of neuronal processes presents a barrier to diffusive transport. The turnover of the axonal cytoskeleton requires the active transport of newly synthesized cytoskeletal proteins from the cell body along the axon. The transport of NF and microtubule (MT) proteins have been observed to take place at rates 100 times slower (0.1-1.0 mm/day or 1.0-10 nm/s) than fast axonal transport (~50-100 mm/day or 500-1000 nm/s) of vesicular cargoes(4, 52, 106).

Since the first reports of a slow phase of axonal transport over 30 years ago(6, 70, 82, 98, 155) the motors responsible for the directed transport of slow components have yet to be identified. The orientation of the axonal microtubules, with minus ends pointing towards the cell body, suggests the action of a slow, plus end directed motor, but no such motor has been identified. An alternative hypothesis is that the rate of the motor in not slow but that the motor-MT or cargo-motor interactions is transient giving rise to an effective on-off scheme with slow net velocity. Finally, the velocity of MT motors have been shown to be load dependent(35) and the interactions between the cytoskeletal cargo and the surrounding stationary cytoskeleton can

impose a load which results in a slow velocity from a motor with fast velocity when unloaded.

The observed bidirectional motion of purified NFs along MTs in vitro suggests a slow transport mechanism by which the net, long time scale velocity of motion is slow, but the short time scale velocity is consistent with reported MT motor velocities (figure 5-7). Observations made using radiolabeled protein transport(107) are sensitive to the long time scale motions but would be unable to discern short time scale motions. This form of motion is similar to that seen for axonal mitochondria, which translocate by saltatory bidirectional motions, but achieve a net plus-ended velocity which is on the order of slow transport rates(100).

The data presented here suggest the hypothesis in which neurofilaments are transported along the axon in a saltatory bidirectional fashion requiring multiple MT motors. Further investigation of this reconstituted system may elucidate the enigmatic nature of slow axonal transport.

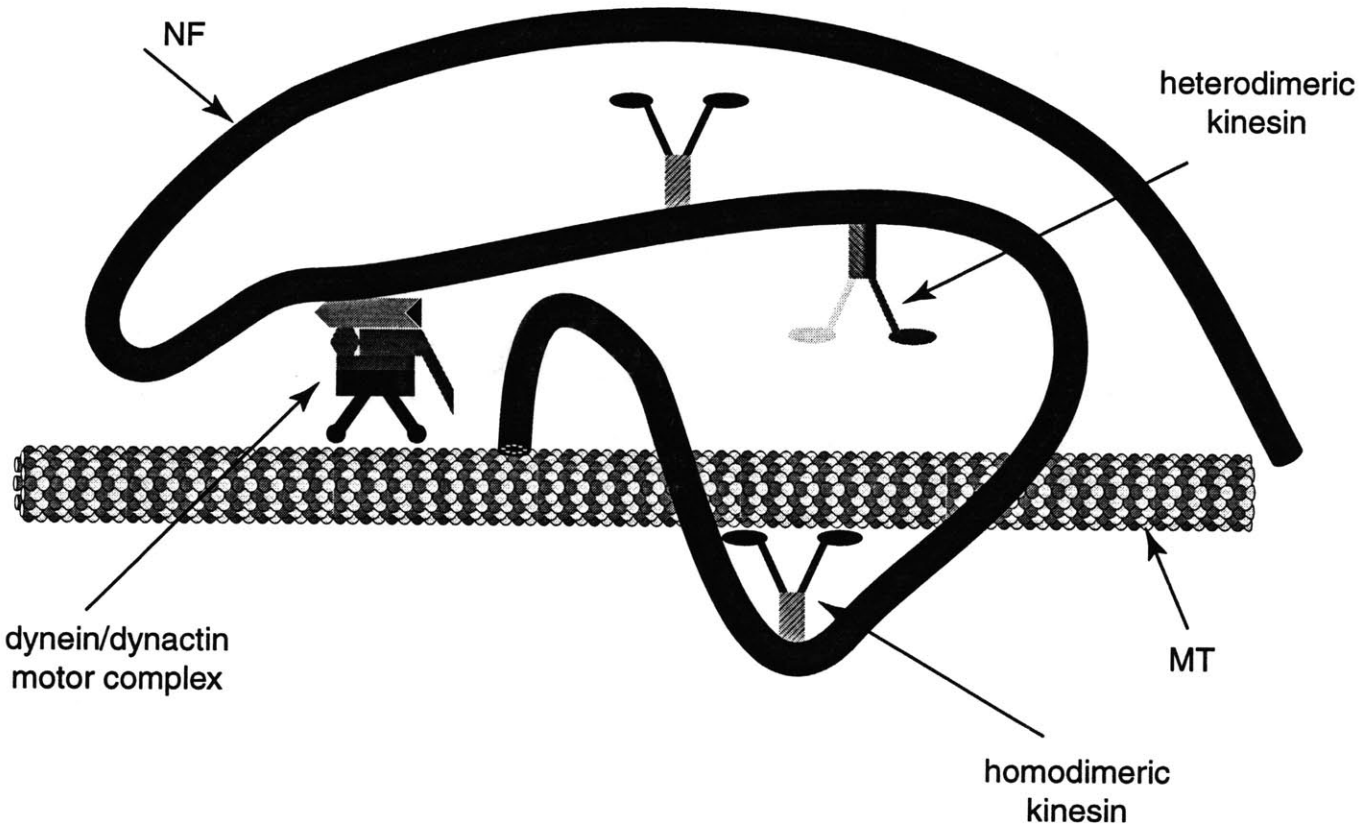

Figure 5-17 : **Model of filamentous NF transport by dynein and kinesin motors.**

5.4.6 Alternative hypotheses for NF-MT motor interactions

In addition to the role of transport, an active interfilament interaction could also be important in mechanics. The active contraction within a crosslinked network is expected to increase the stiffness of the network. The NF-MT lattice present in the axonal compartment can take advantage of the MT-motors bound to the NFs to generate a stiff axoplasmic matrix which is constantly under pre-stress.

The active interaction between NFs and MTs can also serve to localize the elements in the neuron much like for vimentin(42, 116) and provide the unique spatial organization found in the axon. Currently, the observed interaction between NFs and MTs is consistent with a role in slow axonal transport, further in vivo and biochemical studies will test the validity of this hypothesis.

Chapter 6

Discussion and Summary

The previous chapters have identified a novel set of interactions between cytoskeleton filaments. These interfilament interactions add to an already rich variety of interactions in the cytoskeleton within each filament system. The role of these interfilament interactions were discussed in the context of well-documented functions of the cytoskeleton - mechanics, transport and organization.

The approach used in this thesis was to vary the nature of the interfilament interaction, i.e. steric, passive or active, and study the resulting change in a physical parameter, e.g. diffusion, mechanics, transport. Chapter 3 demonstrated the role of simple steric interactions in limiting MT diffusion through an f-actin network, a possible mechanism for maintaining spatial organization between MTs and f-actin within the cell. Chapter 4 showed a direct interaction between f-actin and the c-terminus of vimentin through a variety of techniques. The role of a passive f-actin-vimentin interaction was seen in the mechanical properties of vimentin-f-actin mixtures which have material properties unlike each system in isolation. Chapter 5 illustrated one possible role of active, motor driven interactions between cytoskeletal filaments. The bidirectional motion of NFs along MTs provided a hypothesis for the in vivo slow transport of NFs in neurons, a long-standing problem in axonal transport. These studies represent a few examples of how the cytoskeleton has adapted to perform many functions, many of which are redundant, from a set of simple filamentous constituents and soluble crosslinker and motor proteins.

6.1 Steric constraints - a role in cellular organization

In understanding the role of steric constraints as described in chapter 3, a system was developed to analyse the motions of fluorescent filament and was extensively outlined in chapter 2. Using this system, the motions of fluorescent MTs within an f-actin network were analysed. The simple steric constraints imposed by the f-actin network are a significant barrier to diffusion for long MTs and provide hydrodynamic screening for short MTs. At a length of 15 μm there is a transition between the low diffusive and length-independent diffusive states. The molecular nature of the transition and plateau states is conjectured in chapter 3 but further experimentation is required to test these hypotheses. The addition of crosslinking agents to the f-actin network in the form of biotin-avidin links produced a similar pattern of MT diffusivity but strict interpretation is difficult due to a large degree of scatter in the data which may have been brought about by inherent inhomogeneities in the f-actin network introduced by crosslinking. MTs within the crosslinked MT-f-actin network exhibited no diffusive motions as would be expected.

One possible utility of steric constraints is to maintain the spatial organization of MT and f-actin. In many cells, the MT system has a low degree of overlap with the f-actin network indicating a mechanism for spatial organization. In motile cells few MTs can penetrate the actin-rich leading edge although they are present at the border of the edge(153). The simple steric interaction could represent the first level of interaction preventing MTs from entering the leading edge of the motile cell. Within the cell this barrier is probably reinforced by other molecules which directly bind the cytoskeletal filaments together to maintain a specific spatial arrangement.(16, 31, 38, 40, 81).

6.2 Passive interactions - role for mechanics

The role of passive interactions in the cytoskeleton has been well-described by the many f-actin binding proteins that change the elasticity of f-actin networks(66, 67). The role of mechanics in cellular integrity has also been documented in a number of transgenic systems for both f-actin(15) and IFs(29, 32).

In chapter 4 the direct interaction of the vimentin c-terminus and f-actin are an example of a connection between cytoskeletal filaments with possible mechanical consequences. The c-terminal peptide had been previously shown to colocalize to f-actin rich structures in vivo. In vitro experiments indicated its direct interaction with f-actin and an ability to bundle f-actin. Previous experiments conducted by Janmey and colleagues(69) (figure 4-9) indicate novel mechanical properties for vimentin-f-actin mixtures when compared to the single component networks. The direct interaction of the c-terminus of vimentin with f-actin could be responsible for these composite mechanical properties.

The role of the c-terminus of vimentin has also been shown to affect its localization in cells(120), preventing its accumulation in the nucleus. Given its interaction with f-actin, the c-terminus may also be important in the organization of vimentin by attaching vimentin to the cytoplasmic f-actin network and preventing its translocation to the nucleus.

Further studies with other cytoskeletal mixtures and passive crosslinkers may reveal other unique composite materials. Obtaining the mechanical properties of these composite materials is essential in developing an integrated model of cellular mechanics.

6.3 Active interactions - role for transport

The role of active, or motor mediated, interactions between cytoskeletal elements represent an interesting mechanism for a variety of cytoskeletal functions including transport, mechanics and spatial organization. In chapter 5 the role of MT motors in the translocation of NFs along MTs has

been demonstrated. In the context of slow transport mechanisms, this finding could be an important molecular clue as to the transport of NFs in axons both in health and disease states. An active interaction between cytoskeletal polymers being utilized for transport represents just one possible function for motor driven interactions.

A previously documented cellular example of a motor based interfilament interaction is kinesin mediating vimentin-MT interactions. Kinesin transports vimentin IFs from a perinuclear location to the periphery of the cell(116). This type of interaction clearly demonstrates the role of motor driven interactions in maintaining the spatial organization of vimentin IFs. In fact, if kinesin antibodies are injected into the cell, the vimentin IFs collapse to a perinuclear distribution, indicating a role for the motor in maintenance of vimentin at the periphery of the cell(42).

Active motor interactions can also be responsible for novel mechanical properties. Myosin in the actin cortex has been speculated to play an important role in cell mechanics as have stress fibres which are contractile bundles of actin and myosin. The effect of active elements within a polymer network has been tested in a system with a similar structure to the cytoskeleton - platelets in a fibrin network(132). Here the fibrin network assumes the role of the cytoskeleton and the platelets are the active elements which contract and crosslink the polymers together. The contraction of the platelets acted to significantly increase the elasticity of the network. The mechanism by which this occurred was speculated to be a straightening of the fibrin strands thereby reducing the excess contour length available to the polymers upon deformation. Observation of platelets in fibrin networks are consistent with this hypothesis.

In the cytoskeleton, the role of the motor driven interaction could provide a similar polymer straightening mechanism by which the cell can modulate a variety of its mechanical properties. The active nature of cytoskeletal connections would be an additional interaction in models of cell mechanics. In synthetic polymer systems the active crosslinking elements ia analogous to a 'smart' material in which individual chains undergo conformation changes in response to a local environment change and as such, biopolymer-motor networks would be an ideal substrate for designing smart materials.

The studies presented here represent three paradigms for classifying interfilament interactions in the cytoskeleton and generally apply to both intersystem and intrasystem interactions. Steric constraints represent the interaction resulting from filaments not being able to occupy the same space. Passive interactions represent connections between the filaments provided by a molecule which can bind each filament independently. Active interactions are provided by mechanoenzymes which bind two filaments together and transduce chemical energy into the mechanical translocation of one filament along the other. In classifying the physical nature of the interaction, it is essential to keep the possible intracellular function in mind. In this study, three

possible roles of the cytoskeleton have been discussed : mechanics, transport and spatial organization. In principle, each physical mechanism can correspond to an intracellular process giving rise to a rich variety cellular functions provided by very few cellular components.

Literature cited

1. Ahmad, F. J., C. J. Echeverri, R. B. Vallee, and P. W. Baas. 1998. Cytoplasmic dynein and dynactin are required for the transport of microtubules into the axon. *Journal of Cell Biology.* 140:391-401.

2. Bassell, G. J., C. M. Powers, K. L. Taneja, and R. H. Singer. 1994. Single mRNAs visualized by ultrastructural in situ hybridization are principally localized at actin filament intersections in fibroblasts. *Journal of Cell Biology.* 126:863-76.

3. Beuttenmuller, M., M. Chen, A. Janetzko, S. Kuhn, and P. Traub. 1994. Structural elements of the amino-terminal head domain of vimentin essential for intermediate filament formation in vivo and in vitro. *Experimental Cell Research.* 213:128-42.

4. Black, M. M., and R. J. Lasek. 1980. Slow components of axonal transport: two cytoskeletal networks. *Journal of Cell Biology.* 86:616-23.

5. Brady, S. T., K. K. Pfister, and G. S. Bloom. 1990. A monoclonal antibody against kinesin inhibits both anterograde and retrograde fast axonal transport in squid axoplasm. *Proceedings of the National Academy of Sciences of the United States of America.* 87:1061-5.

6. Bray, J. J., and L. Austin. 1969. Axoplasmic transport of 14C proteins at two rates in chicken sciatic nerve. *Brain Research.* 12:230-3.

7. Brown, K. D., and L. I. Binder. 1992. Identification of the intermediate filament-associated protein gyronemin as filamin. Implications for a novel mechanism of cytoskeletal interaction. *Journal of Cell Science.* 102:19-30.

8. Capote, C., and R. B. Maccioni. 1998. The association of tau-like proteins with vimentin filaments in cultured cells. *Experimental Cell Research.* 239:202-13.

9. Carlier, M. F., V. Laurent, J. Santolini, R. Melki, D. Didry, G. X. Xia, Y. Hong, N. H. Chua, and D. Pantaloni. 1997. Actin depolymerizing factor (ADF/cofilin) enhances the rate of filament turnover: implication in actin-based motility. *Journal of Cell Biology.* 136:1307-22.

10. Cary, R. B., M. W. Klymkowsky, R. M. Evans, A. Domingo, J. A. Dent, and L. E. Backhus. 1994. Vimentin's tail interacts with actin-containing structures in vivo. *Journal of Cell Science.* 107:1609-22.

11. Caspi, A., M. Elbaum, R. Granek, A. Lachish, and D. Zbaida. 1998. Semiflexible polymer network - a view from inside. *Physical Review Letters.* 80:1106-1109.

12. Chou, Y. H., K. L. Ngai, and R. Goldman. 1991. The regulation of intermediate filament

reorganization in mitosis. p34cdc2 phosphorylates vimentin at a unique N-terminal site. *Journal of Biological Chemistry*. 266:7325-8.

13. Colucci-Guyon, E., Y. R. M. Gimenez, T. Maurice, C. Babinet, and A. Privat. 1998. Cerebellar defect and impaired motor coordination in mice lacking vimentin. *GLIA*. 25:33-43.

14. Colucci-Guyon, E., M. M. Portier, I. Dunia, D. Paulin, S. Pournin, and C. Babinet. 1994. Mice lacking vimentin develop and reproduce without an obvious phenotype. *Cell*. 79:679-94.

15. Cunningham, C. C., J. B. Gorlin, D. J. Kwiatkowski, J. H. Hartwig, P. A. Janmey, H. R. Byers, and T. P. Stossel. 1992. Actin-binding protein requirement for cortical stability and efficient locomotion. *Science*. 255:325-7.

16. Cunningham, C. C., N. Leclerc, L. A. Flanagan, M. Lu, P. A. Janmey, and K. S. Kosik. 1997. Microtubule-associated protein 2c reorganizes both microtubules and microfilaments into distinct cytological structures in an actin-binding protein-280-deficient melanoma cell line. *Journal of Cell Biology*. 136:845-857.

17. de Gennes, P. G. 1971. Reptation of a polymer chain in the presence of fixed obstacles. *Journal of Chemical Physics*. 55:572-79.

18. de Waegh, S. M., and S. T. Brady. 1991. Local control of axonal properties by Schwann cells: neurofilaments and axonal transport in homologous and heterologous nerve grafts. *Journal of Neuroscience Research*. 30:201-12.

19. Dillman 3rd, J. F., L. P. Dabney, and K. K. Pfister. 1996. Cytoplasmic dynein is associated with slow axonal transport. *Proceedings of the National Academy of Sciences of the United States of America*. 93:141-4.

20. Doi, M., and S. F. Edwards. 1986. The Theory of Polymer Dynamics. *In* The International Series of Monographs on Physics. Vol. 73. J. Birman, S. F. Edwards, C. H. L. Smith, and M. Rees, editors. Oxford University Press, Oxford. 391.

21. Dong, D. L. Y., Z. S. Xu, G. W. Hart, and D. W. Cleveland. 1996. Cytoplasmic o-glcnac modification of the head domain and the KSP repeat motif of the neurofilament protein neurofilament-H. *Journal of Biological Chemistry*. 271:20845-20852.

22. Dye, R. B., S. P. Fink, and R. C. Williams, Jr. 1993. Taxol-induced flexibility of microtubules and its reversal by MAP-2 and tau. *Journal of Biological Chemistry*. 268:6847-50.

23. Edwards, S. F. 1967. The statistical mechanics of polymerized material. *Proc. Phys. Soc.* 92:9-16.

24. Eichinger, L., B. Koppel, A. A. Noegel, M. Schleicher, M. Schliwa, K. Weijer, W. Witke, and P. A. Janmey. 1996. Mechanical perturbation elicits a phenotypic difference between Dictyostelium wild-type cells and cytoskeletal mutants. *Biophysical Journal.* 70:1054-60.

25. Evans, R. M. 1998. Vimentin: the conundrum of the intermediate filament gene family. *Bioessays.* 20:79-86.

26. Eyer, J., W. G. McLean, and J. F. Leterrier. 1989. Effect of a single dose of beta,beta'-iminodipropionitrile in vivo on the properties of neurofilaments in vitro: comparison with the effect of iminodipropionitrile added directly to neurofilaments in vitro. *Journal of Neurochemistry.* 52:1759-65.

27. Ferry, J. 1980. Viscoelastic Properties of Polymers. John Wiley, New York.

28. Flory, P. J. 1953. Principles of Polymer Chemistry. Cornell University Press, Ithaca, NY.

29. Fuchs, E. 1994. Intermediate filaments and disease: mutations that cripple cell strength. *Journal of Cell Biology.* 125:511-6.

30. Fuchs, E., and K. Weber. 1994. Intermediate filaments: structure, dynamics, function, and disease. *Annual Review of Biochemistry.* 63:345-82.

31. Fujii, T., T. Hiromori, M. Hamamoto, and T. Suzuki. 1997. Interaction of chicken gizzard smooth muscle calponin with brain microtubules. *Journal of Biochemistry.* 122:344-51.

32. Galou, M., J. Gao, J. Humbert, M. Mericskay, Z. L. Li, D. Paulin, and P. Vicart. 1997. The importance of intermediate filaments in the adaptation of tissues to mechanical stress - evidence from gene knockout studies. *Biology of the Cell.* 89:85-97.

33. Gibb, B. J. M., J. P. Brion, J. Brownlees, B. H. Anderton, and C. C. J. Miller. 1998. Neuropathological abnormalities in transgenic mice harbouring a phosphorylation mutant neurofilament transgene. *Journal of Neurochemistry.* 70:492-500.

34. Gill, S. R., T. A. Schroer, I. Szilak, E. R. Steuer, M. P. Sheetz, and D. W. Cleveland. 1991. Dynactin, a conserved, ubiquitously expressed component of an activator of vesicle motility mediated by cytoplasmic dynein. *Journal of Cell Biology.* 115:1639-50.

35. Gittes, F., E. Meyhofer, S. Baek, and J. Howard. 1996. Directional loading of the kinesin motor molecule as it buckles a microtubule. *Biophysical Journal.* 70:418-29.

36. Gittes, F., B. Mickey, J. Nettleton, and J. Howard. 1993. Flexural rigidity of microtubules and actin filaments measured from thermal fluctuations in shape. *Journal of Cell Biology.* 120:923-34.

37. Glass, J. D., and J. W. Griffin. 1991. Neurofilament redistribution in transected nerves:

evidence for bidirectional transport of neurofilaments. *Journal of Neuroscience*. 11:3146-54.

38. Gonzalez, M., V. Cambiazo, and R. B. Maccioni. 1998. The interaction of Mip-90 with microtubules and actin filaments in human fibroblasts. *Experimental Cell Research*. 239:243-253.

39. Gorlin, J. B., R. Yamin, S. Egan, M. Stewart, T. P. Stossel, D. J. Kwiatkowski, and J. H. Hartwig. 1990. Human endothelial actin-binding protein (ABP-280, nonmuscle filamin): a molecular leaf spring. *Journal of Cell Biology*. 111:1089-105.

40. Griffith, L. M., and T. D. Pollard. 1978. Evidence for actin filament-microtubule interaction mediated by microtubule-associated proteins. *Journal of Cell Biology*. 78:958-65.

41. Griffith, L. M., and T. D. Pollard. 1982. The interaction of actin filaments with microtubules and microtubule-associated proteins. *Journal of Biological Chemistry*. 257:9143-51.

42. Gyoeva, F. K., and V. I. Gelfand. 1991. Coalignment of vimentin intermediate filaments with microtubules depends on kinesin. *Nature*. 353:445-8.

43. Heald, R., R. Tournebize, A. Habermann, E. Karsenti, and A. Hyman. 1997. Spindle assembly in Xenopus egg extracts: respective roles of centrosomes and microtubule self-organization. *Journal of Cell Biology*. 138:615-28.

44. Heimann, R., M. L. Shelanski, and R. K. Liem. 1985. Microtubule-associated proteins bind specifically to the 70-kDa neurofilament protein. *Journal of Biological Chemistry*. 260:12160-6.

45. Henrion, D., F. Terzi, K. Matrougui, M. Duriez, C. M. Boulanger, E. Colucci-Guyon, C. Babinet, P. Briand, G. Friedlander, P. Poitevin, and B. I. Levy. 1997. Impaired flow-induced dilation in mesenteric resistance arteries from mice lacking vimentin. *Journal of Clinical Investigation*. 100:2909-14.

46. Herrmann, H., and U. Aebi. 1998. Intermediate Filament Assembly - Fibrillogenesis Is Driven By Decisive Dimer-Dimer Interactions. *Current Opinion in Structural Biology*. 8:177-185.

47. Herrmann, H., M. Haner, M. Brettel, S. A. Muller, K. N. Goldie, B. Fedtke, A. Lustig, W. W. Franke, and U. Aebi. 1996. Structure and assembly properties of the intermediate filament protein vimentin: the role of its head, rod and tail domains. *Journal of Molecular Biology*. 264:933-53.

48. Hirokawa, N., S. Hisanaga, and Y. Shiomura. 1988. MAP2 is a component of crossbridges between microtubules and neurofilaments in the neuronal cytoskeleton: quick-freeze, deep-etch immunoelectron microscopy and reconstitution studies. *Journal of Neuroscience*. 8:2769-79.

49. Hisanaga, S., and N. Hirokawa. 1989. The effects of dephosphorylation on the structure of the projections of neurofilament. *Journal of Neuroscience*. 9:959-66.

50. Hisanaga, S., and N. Hirokawa. 1990. Dephosphorylation-induced interactions of neurofilaments with microtubules. *Journal of Biological Chemistry.* 265:21852-8.

51. Hoffman, P. N., D. W. Cleveland, J. W. Griffin, P. W. Landes, N. J. Cowan, and D. L. Price. 1987. Neurofilament gene expression: a major determinant of axonal caliber. *Proceedings of the National Academy of Sciences of the United States of America.* 84:3472-6.

52. Hoffman, P. N., and R. J. Lasek. 1975. The slow component of axonal transport. Identification of major structural polypeptides of the axon and their generality among mammalian neurons. *Journal of Cell Biology.* 66:351-66.

53. Houseweart, M. K., and D. W. Cleveland. 1998. Intermediate filaments and their associated proteins - multiple dynamic personalities. *Current Opinion in Cell Biology.* 10:93-101.

54. Hubbard, B. D., and E. Lazarides. 1979. Copurification of actin and desmin from chicken smooth muscle and their copolymerization in vitro to intermediate filaments. *Journal of Cell Biology.* 80:166-82.

55. Hyman, A., D. Drechsel, D. Kellogg, S. Salser, K. Sawin, P. Steffen, L. Wordeman, and T. Mitchison. 1991. Preparation of modified tubulins. *Methods in Enzymology.* 196:478-85.

56. Hyman, A. A. 1991. Preparation of marked microtubules for the assay of the polarity of microtubule-based motors by fluorescence. *Journal of Cell Science - Supplement.* 14:125-7.

57. Inagaki, M., Y. Nakamura, M. Takeda, T. Nishimura, and N. Inagaki. 1994. Glial fibrillary acidic protein: dynamic property and regulation by phosphorylation. *Brain Pathology.* 4:239-43.

58. Ingold, A. L., S. A. Cohn, and J. M. Scholey. 1988. Inhibition of kinesin-driven microtubule motility by monoclonal antibodies to kinesin heavy chains. *Journal of Cell Biology.* 107:2657-67.

59. Isambert, H., and A. C. Maggs. 1996. Dynamics and rheology of actin solutions. *Macromolecules.* 29:1036-1040.

60. Ito, J., M. Masudaisobe, Z. L. Yong, and R. Tanaka. 1996. Promotion of microfilament polymerization by depolymerized glia filament preparation through interaction of vimentin with actin. *Neurochemistry International.* 29:383-389.

61. Ito, T., A. Suzuki, and T. P. Stossel. 1992. Regulation of water flow by actin-binding protein-induced actin gelation. *Biophysical Journal.* 61:1301-5.

62. Janmey, P., E. Amis, and J. Ferry. 1983. Rheology of fibrin clots. VI. Stress relaxation, creep, and differential dynamic modulus of fine clots in large shearing deformations. *J Rheol.* 27:135-153.

63. Janmey, P. A. 1991. A torsion pendulum for measurement of the viscoelasticity of

biopolymers and its application to actin networks. *Journal of Biochemical and Biophysical Methods*. 22:41-53.

64. Janmey, P. A., U. Euteneuer, P. Traub, and M. Schliwa. 1991. Viscoelastic properties of vimentin compared with other filamentous biopolymer networks. *Journal of Cell Biology*. 113:155-60.

65. Janmey, P. A., S. Hvidt, J. Käs, D. Lerche, A. Maggs, E. Sackmann, M. Schliwa, and T. P. Stossel. 1994. The mechanical properties of actin gels. *Journal of Biological Chemistry*. 269:32503-32513.

66. Janmey, P. A., S. Hvidt, J. Lamb, and T. P. Stossel. 1990. Resemblance of actin-binding protein/actin gels to covalently crosslinked networks. *Nature*. 345:89-92.

67. Janmey, P. A., S. Hvidt, J. Peetermans, J. Lamb, J. D. Ferry, and T. P. Stossel. 1988. Viscoelasticity of F-actin and F-actin/gelsolin complexes. *Biochemistry*. 27:8218-27.

68. Janmey, P. A., J. Peetermans, K. S. Zaner, T. P. Stossel, and T. Tanaka. 1986. Structure and mobility of actin filaments as measured by quasielastic light scattering, viscometry, and electron microscopy. *Journal of Biological Chemistry*. 261:8357-62.

69. Janmey, P. A., J. V. Shah, K. P. Janssen, and M. Schliwa. 1998. Viscoelasticity of intermediate filament networks. *In* Intermediate filaments. H. Herrmann and R. Harris, editors. Plenum Press, New York. 381-397.

70. Karlsson, J. O., and J. Sjostrand. 1968. Transport of labelled proteins in the optic nerve and tract of the rabbit. *Brain Research*. 11:431-9.

71. Käs, J., H. Strey, and E. Sackmann. 1994. Direct imaging of reptation for semiflexible actin filaments. *Nature*. 368:226-229.

72. Käs, J., H. Strey, J. X. Tang, D. Finger, R. Ezzell, E. Sackmann, and P. A. Janmey. 1996. F-actin, a model polymer for semiflexible chains in dilute, semidilute, and liquid crystalline solutions. *Biophysical Journal*. 70:609-25.

73. Kishino, A., and T. Yanagida. 1988. Force measurements by micromanipulation of a single actin filament by glass needles. *Nature*. 334:74-6.

74. Kong, J. M., V. W. Y. Tung, J. Aghajanian, and Z. S. Xu. 1998. Antagonistic roles of neurofilament subunits NF-H and NF-M against NF-L in shaping dendritic arborization in spinal motor neurons. *Journal of Cell Biology*. 140:1167-1176.

75. Kouyama, T., and K. Mihashi. 1980. Pulse-fluorometry study on actin and heavy meromyosin

using F-actin labelled with N-(1-pyrene)maleimide. *European Journal of Biochemistry*. 105:279-87.

76. Kreitzer, G., G. Liao, and G. G. Gundersen. 1999. Detyrosination of tubulin regulates the interaction of intermediate filaments with microtubules in vivo via a kinesin dependent mechanism. *Molecular Biology of the Cell*. 10:1105-1118.

77. Kroy, K., and E. Frey. 1996. Force-extension relation and plateau modulus for wormlike chains. *Physical Review Letters*. 77:306-309.

78. Kuznetsov, S. A., G. M. Langford, and D. G. Weiss. 1992. Actin-dependent organelle movement in squid axoplasm. *Nature*. 356:722-5.

79. Laemmli, U. K. 1970. Cleavage of structural proteins during the assembly of the head of bacteriophage T4. *Nature*. 227:680-5.

80. Langford, G. M. 1995. Actin- and microtubule-dependent organelle motors: interrelationships between the two motility systems. *Current Opinion in Cell Biology*. 7:82-8.

81. Lantz, V. A., and K. G. Miller. 1998. A class VI unconventional myosin is associated with a homologue of a microtubule-binding protein, cytoplasmic linker protein-170, in neurons and at the posterior pole of Drosophila embryos. *Journal of Cell Biology*. 140:897-910.

82. Lasek, R. J. 1967. Bidirectional transport of radioactively labelled axoplasmic components. *Nature*. 216:1212-4.

83. Leterrier, J. F., and J. Eyer. 1987. Properties of highly viscous gels formed by neurofilaments in vitro. A possible consequence of a specific inter-filament cross-bridging. *Biochemical Journal*. 245:93-101.

84. Leterrier, J. F., J. Eyer, D. G. Weiss, and L. M. 1991. In vitro studies of the physical interactions between neurofilaments, microtubules and mitochondria isolated from the central nervous system. *In* The Living Cell in Four Dimensions. Vol. 226. G. Paillotin, editor. American Institute for Physics, Gif Sur Yvette. 91-105.

85. Leterrier, J. F., J. Kas, J. Hartwig, R. Vegners, and P. A. Janmey. 1996. Mechanical effects of neurofilament cross-bridges. Modulation by phosphorylation, lipids, and interactions with F-actin. *Journal of Biological Chemistry*. 271:15687-94.

86. Leterrier, J. F., R. K. Liem, and M. L. Shelanski. 1982. Interactions between neurofilaments and microtubule-associated proteins: a possible mechanism for intraorganellar bridging. *Journal of Cell Biology*. 95:982-6.

87. Leterrier, J. F., J. Wong, R. K. Liem, and M. L. Shelanski. 1984. Promotion of microtubule assembly by neurofilament-associated microtubule-associated proteins. *Journal of Neurochemistry*. 43:1385-91.

88. Liao, G., and G. G. Gundersen. 1998. Kinesin is a candidate for cross-bridging microtubules and intermediate filaments. Selective binding of kinesin to detyrosinated tubulin and vimentin. *Journal of Biological Chemistry*. 273:9797-803.

89. Lippincott-Schwartz, J., N. B. Cole, A. Marotta, P. A. Conrad, and G. S. Bloom. 1995. Kinesin is the motor for microtubule-mediated Golgi-to-ER membrane traffic. *Journal of Cell Biology*. 128:293-306.

90. Mabuchi, K., B. Li, W. Ip, and T. Tao. 1997. Association of calponin with desmin intermediate filaments. *Journal of Biological Chemistry*. 272:22662-6.

91. MacKintosh, F., J. Käs, and P. Janmey. 1995. Elasticity of semiflexible biopolymer networks. *Physical Review Letters*. 75:4425-4428.

92. MacLean-Fletcher, S., and T. D. Pollard. 1980. Identification of a factor in conventional muscle actin preparations which inhibits actin filament self-association. *Biochemical & Biophysical Research Communications*. 96:18-27.

93. Maison, C., H. Horstmann, and S. D. Georgatos. 1993. Regulated docking of nuclear membrane vesicles to vimentin filaments during mitosis. *Journal of Cell Biology*. 123:1491-1505.

94. Makarova, I., D. Carpenter, S. Khan, and W. Ip. 1994. A conserved region in the tail domain of vimentin is involved in its assembly into intermediate filaments. *Cell Motility and the Cytoskeleton*. 28:265-77.

95. Malekzadeh-Hemmat, K., P. Gendry, and J. F. Launay. 1993. Rat pancreas kinesin: identification and potential binding to microtubules. *Cellular & Molecular Biology*. 39:279-85.

96. Maniotis, A. J., C. S. Chen, and D. E. Ingber. 1997. Demonstration of mechanical connections between integrins, cytoskeletal filaments, and nucleoplasm that stabilize nuclear structure. *Proceedings of the National Academy of Sciences of the United States of America*. 94:849-54.

97. Marszalek, J. R., T. L. Williamson, M. K. Lee, Z. Xu, P. N. Hoffman, M. W. Becher, T. O. Crawford, and D. W. Cleveland. 1996. Neurofilament subunit NF-H modulates axonal diameter by selectively slowing neurofilament transport. *Journal of Cell Biology*. 135:711-24.

98. McEwen, B. S., and B. Grafstein. 1968. Fast and slow components in axonal transport of protein. *Journal of Cell Biology*. 38:494-508.

99. McNally, F. J., and R. D. Vale. 1993. Identification of katanin, an ATPase that severs and disassembles stable microtubules. *Cell.* 75:419-29.

100. Morris, R. L., and P. J. Hollenbeck. 1995. Axonal transport of mitochondria along microtubules and F-actin in living vertebrate neurons. *Journal of Cell Biology.* 131:1315-26.

101. Morris, R. L., and J. M. Scholey. 1997. Heterotrimeric kinesin-II is required for the assembly of motile 9+2 ciliary axonemes on sea urchin embryos. *Journal of Cell Biology.* 138:1009-22.

102. Morse, D. C. 1998. Viscoelasticity of tightly entangled solutions of semiflexible polymers. *Physical Review E (Statistical Physics, Plasmas, Fluids, and Related Interdisciplinary Topics).* 58:R1237-40.

103. Muller, O., H. E. Gaub, M. Barmann, and E. Sackmann. 1991. Viscoelastic moduli of sterically and chemically cross-linked actin networks in the dilute to semidilute regime - measurements by an oscillating disk rheometer. *Macromolecules.* 24:3111-3120.

104. Muresan, V., T. Abramson, A. Lyass, D. Winter, E. Porro, F. Hong, N. L. Chamberlin, and B. J. Schnapp. 1998. KIF3C and KIF3A form a novel neuronal heteromeric kinesin that associates with membrane vesicles. *Molecular Biology of the Cell.* 9:637-52.

105. Nakagawa, T., Y. Tanaka, E. Matsuoka, S. Kondo, Y. Okada, Y. Noda, Y. Kanai, and N. Hirokawa. 1997. Identification and classification of 16 new kinesin superfamily (KIF) proteins in mouse genome. *Proceedings of the National Academy of Sciences of the United States of America.* 94:9654-9.

106. Nixon, R. A. 1998. The slow axonal transport of cytoskeletal proteins. *Current Opinion in Cell Biology.* 10:87-92.

107. Nixon, R. A., and K. B. Logvinenko. 1986. Multiple fates of newly synthesized neurofilament proteins: evidence for a stationary neurofilament network distributed nonuniformly along axons of retinal ganglion cell neurons. *Journal of Cell Biology.* 102:647-59.

108. Nixon, R. A., P. A. Paskevich, R. K. Sihag, and C. Y. Thayer. 1994. Phosphorylation on carboxyl terminus domains of neurofilament proteins in retinal ganglion cell neurons in vivo: influences on regional neurofilament accumulation, interneurofilament spacing, and axon caliber. *Journal of Cell Biology.* 126:1031-46.

109. Odijk, T. 1983. On the statistics and dynamics of confined or entangled stiff polymers. *Macromolecules.* 16:1340-1344.

110. Pant, H. C., and Veeranna. 1995. Neurofilament phosphorylation. *Biochemistry & Cell Biology.* 73:575-592.

111. Penningroth, S. M. 1986. Erythro-9-[3-(2-hydroxynonyl)]adenine and vanadate as probes for microtubule-based cytoskeletal mechanochemistry. *Methods in Enzymology*. 134.

112. Perides, G., A. Scherbarth, and P. Traub. 1986. Influence of phospholipids on the formation and stability of vimentin-type intermediate filaments. *European Journal of Cell Biology*. 42:268-80.

113. Perkins, T. T., D. E. Smith, and S. Chu. 1994. Direct observation of tube-like motion of a single polymer chain. *Science*. 264:819-22.

114. Pluta, M. 1988. Advanced light microscopy. Vol. 1. Elsevier, New York. 464.

115. Pokrywka, N. J., and E. C. Stephenson. 1991. Microtubules mediate the localization of bicoid RNA during Drosophila oogenesis. *Development*. 113:55-66.

116. Prahlad, V., M. Yoon, R. D. Moir, R. D. Vale, and R. D. Goldman. 1998. Rapid movements of vimentin on microtubule tracks - kinesin-dependent assembly of intermediate filament networks. *Journal of Cell Biology*. 143:159-170.

117. Pryer, N. K., P. Wadsworth, and E. D. Salmon. 1986. Polarized microtubule gliding and particle saltations produced by soluble factors from sea urchin eggs and embryos. *Cell Motility & the Cytoskeleton*. 6:537-48.

118. Riveline, D., C. H. Wiggins, R. E. Goldstein, and A. Ott. 1997. Elastohydrodynamic study of actin filaments using fluorescence microscopy. *Physical Review A*. 56:R1330-R1333.

119. Rodionov, V. I., A. J. Hope, T. M. Svitkina, and G. G. Borisy. 1998. Functional coordination of microtubule-based and actin-based motility in melanophores. *Current Biology*. 8:165-168.

120. Rogers, K. R., A. Eckelt, V. Nimmrich, K. P. Janssen, M. Schliwa, H. Herrmann, and W. W. Franke. 1995. Truncation mutagenesis of the non-alpha-helical carboxyterminal tail domain of vimentin reveals contributions to cellular localization but not to filament assembly. *European Journal of Cell Biology*. 66:136-50.

121. Rosette, C., and M. Karin. 1995. Cytoskeletal control of gene expression: depolymerization of microtubules activates NF-kappa B. *Journal of Cell Biology*. 128:1111-9.

122. Saito, T., H. Shima, Y. Osawa, M. Nagao, B. A. Hemmings, T. Kishimoto, and S. Hisanaga. 1995. Neurofilament-associated protein phosphatase 2A: its possible role in preserving neurofilaments in filamentous states. *Biochemistry*. 34:7376-84.

123. Sakowicz, R., M. S. Berdelis, K. Ray, C. L. Blackburn, C. Hopmann, D. J. Faulkner, and L. S. Goldstein. 1998. A marine natural product inhibitor of kinesin motors. *Science*. 280:292-5.

124. Sarria, A. J., J. G. Lieber, S. K. Nordeen, and R. M. Evans. 1994. The presence or absence of a vimentin-type intermediate filament network affects the shape of the nucleus in human SW-13 cells. *Journal of Cell Science*. 107:1593-607.

125. Sarria, A. J., S. R. Panini, and R. M. Evans. 1992. A functional role for vimentin intermediate filaments in the metabolism of lipoprotein-derived cholesterol in human SW-13 cells. *Journal of Biological Chemistry*. 267:19455-63.

126. Satcher, R. L., and C. F. Dewey. 1996. Theoretical estimates of mechanical properties of the endothelial cell cytoskeleton. *Biophysical Journal*. 71:109-118.

127. Sato, M., W. H. Schwarz, and T. D. Pollard. 1987. Dependence of the mechanical properties of actin/alpha-actinin gels on deformation rate. *Nature*. 325:828-30.

128. Sawin, K. E., T. J. Mitchison, and L. G. Wordeman. 1992. Evidence for kinesin-related proteins in the mitotic apparatus using peptide antibodies. *Journal of Cell Science*. 101:303-13.

129. Schmidt, C. F., M. Bärmann, G. Isenberg, and E. Sackmann. 1989. Chain dynamics, mesh size and diffusive transport in networks of polymerized actin. A quasi-elastic light scattering and microfluoresence study. *Macromolecules*. 22:3638-3649.

130. Schnapp, B. J. 1997. Retroactive motors. *Neuron*. 18:523-526.

131. Semenov, A. N. 1986. Dynamics of concentrated solutions of rigid-chain polymer part 1 - Brownian motion of persistent macromolecules in isotropic solution. *J. Chem. Soc., Faraday Trans. 2*. 82:317-329.

132. Shah, J. V., and P. A. Janmey. 1997. Strain hardening of fibrin gels and plasma clots. *Rheologica Acta*. 36:262-268.

133. Shah, J. V., L. Z. Wang, P. Traub, and P. A. Janmey. 1998. Interaction of vimentin with actin and phospholipids. *Biological Bulletin*. 194:402-405.

134. Shojaee, N., W. F. Patton, N. Chung-Welch, Q. Su, H. B. Hechtman, and D. Shepro. 1998. Expression and subcellular distribution of filamin isotypes in endothelial cells and pericytes. *Electrophoresis*. 19:323-32.

135. Spudich, J. A., and S. Watt. 1971. The regulation of rabbit skeletal muscle contraction. I. Biochemical studies of the interaction of the tropomyosin-troponin complex with actin and the proteolytic fragments of myosin. *Journal of Biological Chemistry*. 246:4866-71.

136. Steffen, W., S. Karki, K. T. Vaughan, R. B. Vallee, E. L. F. Holzbaur, D. G. Weiss, and S. A. Kuznetsov. 1997. The involvement of the intermediate chain of cytoplasmic dynein in binding the

motor complex to membranous organelles of xenopus oocytes. *Molecular Biology of the Cell.* 8:2077-2088.

137. Sternberger, L. A., and N. H. Sternberger. 1983. Monoclonal antibodies distinguish phosphorylated and nonphosphorylated forms of neurofilaments in situ. *Proceedings of the National Academy of Sciences of the United States of America.* 80:6126-30.

138. Steuer, E. R., L. Wordeman, T. A. Schroer, and M. P. Sheetz. 1990. Localization of cytoplasmic dynein to mitotic spindles and kinetochores. *Nature.* 345:266-8.

139. Struik, L. C. E. 1967. Free damped vibrations of linear viscoelastic materials. *Rheologica Acta.* 6:119-129.

140. Svitkina, T. M., A. B. Verkhovsky, and G. G. Borisy. 1996. Plectin sidearms mediate interaction of intermediate filaments with microtubules and other components of the cytoskeleton. *Journal of Cell Biology.* 135:991-1007.

141. Takafuta, T., G. Wu, G. F. Murphy, and S. S. Shapiro. 1998. Human beta-filamin is a new protein that interacts with the cytoplasmic tail of glycoprotein Ibalpha. *Journal of Biological Chemistry.* 273:17531-8.

142. Tang, J. X., T. Ito, T. Tao, P. Traub, and P. A. Janmey. 1997. Opposite effects of electrostatics and steric exclusion on bundle formation by f-Actin and other filamentous polyelectrolytes. *Biochemistry.* 36:12600-12607.

143. Tang, J. X., and P. A. Janmey. 1996. The polyelectrolyte nature of F-actin and the mechanism of actin bundle formation. *Journal of Biological Chemistry.* 271:8556-63.

144. Terzi, F., D. Henrion, E. Colucci-Guyon, P. Federici, C. Babinet, B. I. Levy, P. Briand, and G. Friedlander. 1997. Reduction of renal mass is lethal in mice lacking vimentin. Role of endothelin-nitric oxide imbalance. *Journal of Clinical Investigation.* 100:1520-8.

145. Tint, I. S., P. J. Hollenbeck, A. B. Verkhovsky, I. G. Surgucheva, and A. D. Bershadsky. 1991. Evidence that intermediate filament reorganization is induced by ATP-dependent contraction of the actomyosin cortex in permeabilized fibroblasts. *Journal of Cell Science.* 98:375-84.

146. Towbin, H., T. Staehelin, and J. Gordon. 1979. Electrophoretic transfer of proteins from polyacrylamide gels to nitrocellulose sheets: procedure and some applications. *Proceedings of the National Academy of Sciences of the United States of America.* 76:4350-4.

147. Traub, P., A. Scherbarth, J. Willingale-Theune, and U. Traub. 1988. Large scale co-isiolation of vimentin and nuclear Lamins from Erhlich ascites tumour cells cultured in vitro. *Preparative Biochemistry.* 18:381-404.

148. Tu, P. H., G. Elder, R. A. Lazzarini, D. Nelson, J. Q. Trojanowski, and V. M. Lee. 1995. Overexpression of the human NFM subunit in transgenic mice modifies the level of endogenous NFL and the phosphorylation state of NFH subunits. *Journal of Cell Biology*. 129:1629-40.

149. Vale, R. D., B. J. Schnapp, T. Mitchison, E. Steuer, T. S. Reese, and M. P. Sheetz. 1985. Different axoplasmic proteins generate movement in opposite directions along microtubules in vitro. *Cell*. 43:623-32.

150. Vallee, R. B. 1986. Reversible assembly purification of microtubules without assembly-promoting agents and further purification of tubulin, microtubule-associated proteins, and MAP fragments. *Methods in Enzymology*. 134:89-104.

151. Vaughan, K. T., and R. B. Vallee. 1995. Cytoplasmic dynein binds dynactin through a direct interaction between the intermediate chains and p150Glued. *Journal of Cell Biology*. 131:1507-16.

152. Waterman-Storer, C. M., S. B. Karki, S. A. Kuznetsov, J. S. Tabb, D. G. Weiss, G. M. Langford, and E. L. Holzbaur. 1997. The interaction between cytoplasmic dynein and dynactin is required for fast axonal transport. *Proceedings of the National Academy of Sciences of the United States of America*. 94:12180-5.

153. Waterman-Storer, C. M., and E. D. Salmon. 1997. Actomyosin-based retrograde flow of microtubules in the lamella of migrating epithelial cells influences microtubule dynamic instability and turnover and is associated with microtubule breakage and treadmilling. *Journal of Cell Biology*. 139:417-434.

154. Watson, D. F., J. D. Glass, and J. W. Griffin. 1993. Redistribution of cytoskeletal proteins in mammalian axons disconnected from their cell bodies. *Journal of Neuroscience*. 13:4354-60.

155. Weiss, P. A., and H. B. Hiscoe. 1948. Experiments on the mechanism of nerve growth. *Journal of Experimental Zoology*. 107:315-396.

156. Wiche, G., R. Krepler, U. Artlieb, R. Pytela, and H. Denk. 1983. Occurrence and immunolocalization of plectin in tissues. *Journal of Cell Biology*. 97:887-901.

157. Wiemer, E. A., T. Wenzel, T. J. Deerinck, M. H. Ellisman, and S. Subramani. 1997. Visualization of the peroxisomal compartment in living mammalian cells: dynamic behavior and association with microtubules. *Journal of Cell Biology*. 136:71-80.

158. Wilhelm, J., A. Chiang, J. V. Shah, and J. Käs. 1999. Measuring filament stiffness from flickering actin filaments. *in preparation*.

159. Xu, Z., L. C. Cork, J. W. Griffin, and D. W. Cleveland. 1993. Increased expression of

neurofilament subunit NF-L produces morphological alterations that resemble the pathology of human motor neuron disease. *Cell.* 73:23-33.

160. Yamazaki, H., T. Nakata, Y. Okada, and N. Hirokawa. 1995. KIF3A/B: a heterodimeric kinesin superfamily protein that works as a microtubule plus end-directed motor for membrane organelle transport. *Journal of Cell Biology.* 130:1387-99.

161. Yang, Y., J. Dowling, Q. C. Yu, P. Kouklis, D. W. Cleveland, and E. Fuchs. 1996. An essential cytoskeletal linker protein connecting actin microfilaments to intermediate filaments. *Cell.* 86:655-65.

162. Yin, H. L., and T. P. Stossel. 1979. Control of cytoplasmic actin gel-sol transformation by gelsolin, a calcium-dependent regulatory protein. *Nature.* 281:583-6.

163. Zhu, Q. Z., M. Lindenbaum, F. Levavasseur, H. Jacomy, and J. P. Julien. 1998. Disruption of the NF-H gene increases axonal microtubule content and velocity of neurofilament transport - relief of axonopathy resulting from the toxin beta,beta'-iminodipropionitrile. *Journal of Cell Biology.* 143:183-193.